Diss. ETH No. 21573

STEERING OF SEMI-TRAILERS

A dissertation submitted to
ETH ZURICH

for the degree of
Doctor of Sciences

presented by
Matthäus Bernhard Alberding

Dipl.-Ing., University of Stuttgart
born May 21, 1982
citizen of Germany

accepted on the recommendation of
Prof. Dr. Lino Guzzella, examiner
Prof. Dr.-Ing. Christoph Glocker, co-examiner
Dr.-Ing. Frank Sager, co-examiner

2013

Für Martina und meine Familie

In it he set a mast and a yard-arm, fitted to it, and further-more made him a steering-oar, wherewith to steer.

Homer, The Odyssey 5.254-255

Acknowledgements

Contents

Contents

Abstract

The objective of this work is to contribute to two aspects of the steering of semi-trailers. First, the steering mechanism, second, the steering control.

The first part of this work addresses the steering mechanism. To date, trailer steering offers two uncompromising choices. Self-steering does not require an actuation, but has a limited performance and cannot be controlled. Command steer allows to control the steering and to improve the performance, but requires an expensive high-power actuation. This work presents a novel approach that strikes a balance between these extremes.

In this approach, the steering is influenced by introducing a variable steering geometry into a self-steering system. The steering geometry defines the lever arm of the tyre forces in relation to the kingpin axis. Changing the steering geometry thus changes the steering angle. It is shown that the caster angle is the best choice for this degree of freedom.

The load torque in the variable geometry is compensated by a torsional spring. Without any actuation, the resulting force balance amplifies the steering angle compared to a conventional self-steering. As a result, the passive steering behaviour can be designed to resemble that of an active command steer system and to improve the low-speed performance of the vehicle. In addition, the variable caster angle can be used to steer during reverse travel. Using a locking mechanism allows to switch between conventional and amplified self-steering.

Optionally, a low-power actuation can be used to introduce a limited controllability. Both electric and pneumatic actuations are feasible.

A complete controllability can be obtained without any further actuation by a torsional spring with adjustable stiffness.

The approach can be implemented in different mechanical designs. The scope of this work is limited to a preliminary steering mechanism to discuss the technical feasibility.

The approach is tested in simulation experiments using a detailed multi-body model

of the vehicle. The technical feasibility is investigated in vehicle experiments using a simple demonstrator based on a standard production self-steering axle.

In its present form, the approach has three limitations. First, as for conventional self-steering, the high-speed performance is limited. Second, braking forces are a disturbance that increases the steering angle. Third, if the spring stiffness is not adjustable, the steering amplitude decreases with the vehicle load.

The second part of this work addresses the steering control. It presents a novel approach for the steering control of a semi-trailer in reverse travel. The objective is to optimally assist a human driver.

Based on the driver's steering actions on the tractor, the control system operates in two modes, one to stabilize the articulation angle, the other to change it.

As a result, both the off-tracking of the vehicle and the steering effort of the driver are reduced substantially. The vehicle shows a fast response to a change of direction as well as a good stability during straight-ahead travel and constant cornering.

The control algorithm is computationally efficient and is suitable for low-cost automotive electronic control units.

The system requires information on the articulation angle, the tractor steering angle, the time derivative of the tractor steering, the vehicle speed, the reversing light, and the semi-trailer suspension pressure.

A state estimator in the form of a discrete-time Kalman filter is introduced to estimate the tractor steering and the articulation angle. The estimation is evaluated at various speeds using measurement data obtained from vehicle experiments. At medium and high speeds, the estimation provides good results. At walking speeds, the experiments show that a reliable estimation is not feasible. For the controller developed in this work, the need for measurements of the tractor steering and the articulation angle thus cannot be avoided.

The linear model derived for the control design is validated using measurement data obtained from vehicle experiments. The control system is tested using a validated multi-body simulation model.

Zusammenfassung

Das Ziel dieser Arbeit sind Beiträge zu zwei Aspekten der Lenkung von Sattelaufliegern. Erstens zu dem Lenkmechanismus, zweitens zu der Regelung des Lenksystems.

Der erste Teil der Arbeit beschäftigt sich mit dem Lenkmechanismus. Der Stand der Technik von Anhängerlenksystemen lässt sich in zwei Gruppen zusammenfassen. Nachlauflenksysteme arbeiten passiv, sind jedoch in ihrem Nutzen begrenzt und bieten keine Möglichkeit, den Lenkwinkel direkt zu steuern. Zwangslenkungen erlauben eine solche Steuerung, erfordern hierzu jedoch eine leistungsstarke und entsprechend kostenintensive Aktorik. Die vorliegende Arbeit entwickelt einen neuen Ansatz, der einen Mittelweg zwischen Nachlauf- und Zwangslenkung eröffnet.

In diesem Ansatz wird der Lenkwinkel durch die Erweiterung einer Nachlauflenkung um eine variable Lenkgeometrie beeinflusst. Die Lenkgeometrie bestimmt den Hebelarm der Reifenkräfte in Bezug auf die geometrische Lenkachse. Eine Änderung der Lenkgeometrie bewirkt somit eine Änderung des Lenkwinkels. Als Freiheitsgrad der Lenkgeometrie wird der Nachlaufwinkel gewählt.

Das Lastmoment in der verstellbaren Lenkgeometrie wird durch eine Torsionsfeder kompensiert. Durch das entstehende Kräftegleichgewicht wird der Lenkwinkel gegenüber einer konventionellen Nachlauflenkung verstärkt. Diese Verstärkung erfolgt ohne den Einsatz von Stellkräften. Im Ergebnis lässt sich ein passives Lenkverhalten vorgeben, welches dem Verhalten einer aktiven Zwangslenkung entspricht und die Kurvenlaufeigenschaften des Fahrzeug bei langsamer Fahrt optimiert. Darüber hinaus erlaubt der veränderliche Nachlaufwinkel den Einsatz der Lenkung während der Rückwärtsfahrt. Ein Sperrmechanismus ermöglicht, zwischen konventioneller und verstärkter Nachlauflenkung umzuschalten.

Optional kann eine Aktorik zum Zweck einer begrenzten Steuerbarkeit des Systems vorgesehen werden. Im Vergleich zur Zwangslenkung sind wesentlich geringere Stellkräfte erforderlich, woraus sich Vorteile für Kosten und Bauraum ergeben. Der Einsatz sowohl von elektrischen als auch von pneumatischen Komponenten ist möglich.

Eine vollständige Steuerbarkeit des Lenkwinkels kann ohne jegliche weitere Aktorik

durch den Einsatz einer Torsionsfeder mit veränderlicher Steifigkeit erreicht werden.

Der Lenkmechanismus lässt sich konstruktiv in verschiedenen Varianten umsetzen. Die vorliegende Arbeit beschränkt sich auf einen einfachen konstruktiven Ansatz zur Erörterung der technischen Machbarkeit.

Das Lenksystem wird in einer detaillierten Mehrkörpersimulation des Gesamtfahrzeugs erprobt. Die technische Machbarkeit wird im Fahrversuch untersucht. Hierzu wird ein einfaches Funktionsmodell verwendet, welches auf einer kommerziell verfügbaren Nachlauflenkung basiert.

Der vorgestellte Ansatz hat in seiner jetzigen Form drei Schwächen. Erstens ist wie bei der konventionellen Nachlauflenkung der Nutzen im hohen Geschwindigkeitsbereich eingeschränkt. Zweitens wirken Bremskräfte als eine Störgrösse, welche eine Vergrösserung des Lenkwinkels zur Folge hat. Drittens verkleinert sich beim Einsatz einer Torsionsfeder ohne variable Steifigkeit die Lenkverstärkung mit abnehmender Fahrzeugbeladung.

Der zweite Teil der Arbeit beschäftigt sich mit der Regelung der Lenkung eines Sattelaufliegers. Das Ergebnis ist ein neuer Ansatz zur Regelung während der Rückwärtsfahrt. Das Ziel ist die optimale Unterstützung eines menschlichen Fahrers.

Auf Basis der Lenkeingriffe des Fahrers am Zugfahrzeug arbeitet das Regelsystem in zwei Modi. Einer zur Stabilisierung des Knickwinkels zwischen Zug- und Anhängerfahrzeug, einer zur Veränderung desselben.

Im Ergebnis werden sowohl die Spurabweichung des Fahrzeugs als auch der Lenkaufwand des Fahrers deutlich reduziert. Das Fahrzeug zeigt sowohl eine forcierte Reaktion auf Richtungsänderungen als auch eine verbesserte Stabilität während Geradeausfahrten und Kreisfahrten mit konstantem Radius.

Der Regelalgorithmus stellt geringe Anforderungen an die Rechenleistung und kann in Echtzeit im Fahrzeugsteuergerät umgesetzt werden.

Das System benötigt Informationen über den Knickwinkel, den Lenkwinkel des Zugfahrzeugs, die Zeitableitung desselben, die Fahrzeuggeschwindigkeit, die Aktivität der Rückfahrleuchte und den Luftdruck in der Luftfederung des Aufliegers.

Zur Beobachtung von Fahrerlenkwinkel und Knickwinkel wird ein Zustandsbeobachter in Form eines zeitdiskreten Kalman-Filters entworfen. Die Beobachtung wird unter Verwendung realer Messdaten in verschiedenen Geschwindigkeitsbereichen erprobt. Bei mittleren und hohen Geschwindigkeiten zeigt die Beobachtung gute Ergebnisse. Unter Schrittgeschwindigkeiten ist eine zuverlässige Beobachtung nicht möglich. Für das entwickelte Regelsystem sind somit die Messungen von Fahrerlenkwinkel und Knickwinkel unumgänglich.

Das für den Reglerentwurf entwickelte lineare Modell der Fahrdynamik wird mit Messdaten eines Versuchsfahrzeugs validiert. Das Regelsystem wird in einem detaillierten und validierten Mehrkörpersimulationsmodell des Gesamtfahrzeugs erprobt.

Nomenclature

$\Delta\delta$	[rad]	deviation of δ from δ_o
$\Delta\tau$	[rad]	joint angle
Δh	[m]	height change due to the steering
Γ	[rad]	articulation angle (Γ_o at δ_o)
α	[rad]	side-slip angle of the semi-trailer steering axle
α_F	[rad]	side-slip angle of the tractor front axle
α_R	[rad]	side-slip angle of the tractor rear axle
α_1	[rad]	side-slip angle of the semi-trailer foremost axle
α_2	[rad]	side-slip angle of the semi-trailer middle axle
β	[rad]	semi-trailer side-slip angle
β_T	[rad]	tractor side-slip angle
γ	[rad]	camber angle
δ	[rad]	semi-trailer steering angle (defined about the kingpin)
δ_T	[rad]	tractor steering angle
δ_s	[rad]	semi-trailer steering angle defined about the contact patch
δ_o	[rad]	semi-trailer steering angle associated with zero side-slip
μ	[-]	tyre-road friction coefficient
ρ	[m]	tyre radius
ρ_e	[m]	effective rolling radius
σ	[rad]	kingpin inclination
σ_o	[rad]	kingpin inclination in the joint initial position
τ	[rad]	caster angle
τ_o	[rad]	caster angle in the joint initial position
ψ	[rad]	semi-trailer yaw angle

Nomenclature

$\dot{\psi}$	$[\text{rad s}^{-1}]$	semi-trailer yaw rate
ψ_T	$[\text{rad}]$	tractor yaw angle
$\dot{\psi}_T$	$[\text{rad s}^{-1}]$	tractor yaw rate
ω	$[\text{rad s}^{-1}]$	wheel angular velocity
C	$[\text{-}]$	Pacejka shape factor
C_α	$[\text{N rad}^{-1}]$	cornering stiffness of a tyre at the semi-trailer steering axle
$C_{\alpha,F}$	$[\text{N rad}^{-1}]$	cornering stiffness of a tyre at the tractor front axle
$C_{\alpha,R}$	$[\text{N rad}^{-1}]$	cornering stiffness of a tyre at the tractor rear axle
$C_{\alpha,o}$	$[\text{rad}^{-1}]$	normalized cornering stiffness
$C_{\alpha,1}$	$[\text{N rad}^{-1}]$	cornering stiffness of a tyre at the semi-trailer foremost axle
$C_{\alpha,2}$	$[\text{N rad}^{-1}]$	cornering stiffness of a tyre at the semi-trailer middle axle
C_γ	$[\text{N rad}^{-1}]$	camber stiffness of a tyre at the steering axle
C_s	$[\text{N}]$	longitudinal slip stiffness
D	$[\text{N m s rad}^{-1}]$	damping coefficient of the revolute joint
E	$[\text{-}]$	Pacejka shape factor
E_pot	$[\text{J}]$	potential energy related to height change ($E_{\text{pot},2}$ total potential energy for both wheels)
F_y	$[\text{N}]$	lateral force of a tyre at the semi-trailer steering axle
$F_{y,\alpha}$	$[\text{N}]$	cornering force
$F_{y,\gamma}$	$[\text{N}]$	camber thrust
$F_{y,C}$	$[\text{N}]$	lateral force at the fifth wheel
$F_{y,F}$	$[\text{N}]$	lateral force of a tyre at the tractor front axle
$F_{y,R}$	$[\text{N}]$	lateral force of a tyre at the tractor rear axle
$F_{y,1}$	$[\text{N}]$	lateral force of a tyre at the semi-trailer foremost axle
$F_{y,2}$	$[\text{N}]$	lateral force of a tyre at the semi-trailer middle axle
F_z	$[\text{N}]$	load of a semi-trailer tyre
$F_{z,F}$	$[\text{N}]$	load of a tyre at the tractor rear axle
$F_{z,R}$	$[\text{N}]$	load of a tyre at the tractor front axle
$F_{z,o}$	$[\text{N}]$	rated wheel load
J	$[\text{kg m}^2]$	moment of inertia of the revolute joint
J_z	$[\text{kgm}^2]$	yaw inertia semi-trailer
$J_{z,T}$	$[\text{kgm}^2]$	yaw inertia tractor
L	$[\text{m}]$	distance from the semi-trailer rear to the fifth wheel
M_δ	$[\text{N m}]$	kingpin torque ($M_{\delta,F}$ due to tyre forces)
M_τ	$[\text{N m}]$	joint torque ($M_{\tau,F}$ due to tyre forces)
R	$[\text{m}]$	radius of curvature

X	[m]	semi-trailer length
X_T	[m]	tractor length
Y	[m]	semi-trailer width
Y_T	[m]	tractor width
a	[m]	distance from the fifth wheel to the semi-trailer steering axle
a_F	[m]	distance from the fifth wheel to the tractor front axle
a_R	[m]	distance from the fifth wheel to the tractor rear axle
a_y	[m s^{-2}]	lateral acceleration at the semi-trailer centre of gravity
a_1	[m]	distance from the fifth wheel to the semi-trailer foremost axle
a_2	[m]	distance from the fifth wheel to the semi-trailer middle axle
b	[m]	tyre width
b_c	[m]	width of the partial tyre contact
c_δ	[m rad^{-1}]	load-dependent stiffness of the kingpin spring
c_τ	[m rad^{-1}]	load-dependent stiffness of the joint spring
c_y	[N m^{-1}]	lateral tyre stiffness
c_z	[N m^{-1}]	vertical tyre stiffness
c_1	[N rad^{-1}]	maximum cornering stiffness
c_2	[N]	load at the maximum cornering stiffness
d	[m]	distance from the semi-trailer centre of gravity to the semi-trailer steering axle
d_F	[m]	distance from the tractor centre of gravity to the tractor front axle
d_R	[m]	distance from the tractor centre of gravity to the tractor rear axle
d_1	[m]	distance from the semi-trailer centre of gravity to the semi-trailer foremost axle
d_2	[m]	distance from the semi-trailer centre of gravity to the semi-trailer middle axle
g	[m s^{-2}]	gravitational acceleration
k_α	[-]	proportionality factor between α and $\Delta\delta$
k_δ	[-]	desired ratio between δ_o and $\Delta\delta$
k_γ	[-]	proportionality factor between camber stiffness and cornering stiffness
k_a	[-]	desired steering amplification factor
k_b	[-]	feedback gain

Nomenclature

k_f	[-]	feedforward gain
k_r	[-]	steady-state factor
l	[m]	distance from the semi-trailer centre of gravity to the fifth wheel
l_T	[m]	distance from the tractor centre of gravity to the fifth wheel
m	[kg]	semi-trailer mass
m_A	[kg]	total load of the semi-trailer axles
m_T	[kg]	tractor mass
n	[m]	geometric caster offset
n_τ	[m]	wheel-centre caster offset
n_R	[m]	pneumatic trail
n_o	[m]	wheel-centre caster offset in the joint initial position
r	[m]	geometric kingpin offset
r_σ	[m]	wheel-centre kingpin offset
r_R	[m]	lateral displacement of the tyre forces ($r_{R,\alpha}$ due to cornering, $r_{R,\gamma}$ due to cambering)
r_o	[m]	wheel-centre kingpin offset in the joint initial position
s	[-]	longitudinal tyre slip
t_s	[s]	sampling time of the electronic control unit
v_x	[m s^{-1}]	vehicle speed (negative during reverse travel)

1

Introduction

Modern commercial vehicles are facing increasingly demanding challenges in a highly competitive market. The global economy depends on reliable, cost-effective, and ecologically sustainable logistics to master the continuously rising commodity flow. Major challenges for the design of future vehicles are to further cut down costs and emissions to cope with these demands.

One factor in these efforts are the vehicle dimensions. Longer or heavier vehicles are generally associated with an increased productivity. This economic view is constrained by requirements on the manoeuvrability and safety as defined by legislative regulations.

Another factor is a considerate use of the tyres of the vehicle. Preserving those from unnecessary stress pays off both economically and ecologically: the tyre life time is increased, the fuel economy is improved, and the service costs can be reduced.

These two factors are the major motivation to use trailer steering systems.

Articulated commercial vehicles are commonly equipped with multiple axles on the trailer. To date, in the majority of vehicles these axles are non-steering. Com-

pared to steering trailer suspensions, the benefits of this design are a moderate capital investment, a low weight, and mechanical simplicity.

On the downside, multiple non-steering axles significantly limit the manoeuvrability and put a high stress on both the tyres and the road, especially in tight low-speed turns (Fancher & Winkler 2007). To address these problems, the use of trailer steering systems has shown a remarkable potential. Field tests quantify tyre cost savings of up to 50 % (Coleman & Sweatman 2002) and fuel savings of up to 4 % (Provencher 1989). The gain in manoeuvrability enables vehicles with extended dimensions to show a competitive performance, promising substantial economic benefits (Coleman & Sweatman 2002).

The most common form of trailer steering are self-steering systems (Jujnovich & Cebon 2002). As shown in Fig. 1.1, such systems utilize a considerable caster in the steering geometry to obtain a steering motion (LeBlanc, El-Gindy & Woodrooffe 1989). The caster introduces a feedback for the lateral tyre forces, seeking the steering angle of zero side-slip. Most self-steering axles are equipped with a centring device to assist and stabilize the return to straight-ahead travel and to absorb any negative effects of unbalanced braking (LeBlanc et al. 1989). Current designs of the centring device vary greatly among manufacturers (LeBlanc et al. 1989), but they mostly show a spring-damper-like behaviour (Jujnovich & Cebon 2002). This approach prevents the steering from reaching zero side-slip and allows a certain level of lateral tyre forces. When the vehicle travels in reverse, the caster introduces a positive feedback that leads to an unstable steering motion. Therefore, self-steering systems need to be locked during reverse travel (LeBlanc et al. 1989). For steering a three-axle semi-trailer, usually the rear-most axle is designed to be self-steering (Fancher & Winkler 2007). Despite the two leading axles remaining non-steering, the tyre wear of all three axles is reduced (Jujnovich & Cebon 2002). Generally, the steering improves the performance of the vehicle at low speeds, but it shows a negative impact at higher speeds (Jujnovich & Cebon 2002). The latter can be avoided by locking the steering beyond a predefined speed threshold.

Another common form of trailer steering are command steer systems (Jujnovich & Cebon 2002). These are steered by an actuation mechanism, such as a hydraulic unit or a mechanical linkage (Fancher & Winkler 2007). For a three-axle semi-trailer, usually the rear two axles are steered (Jujnovich & Cebon 2002). The steering angles are typically maintained proportional to the articulation angle (Jujnovich & Cebon 2002). Analogously to the self-steering, this approach provides benefits in terms of low-speed performance, but is unfavourable at higher speeds and often locked above a certain speed limit (Fancher & Winkler 2007). Modern command steer systems are controlled electronically and allow more advanced control algorithms, optimizing both low-speed and high-speed performance (Odhams, Roebuck, Jujnovich & Cebon 2011). Given sufficiently good dynamical properties of the actuation, the steering can even be used for active safety (Cheng & Cebon 2008, Imine, Fridman & Madani 2012).
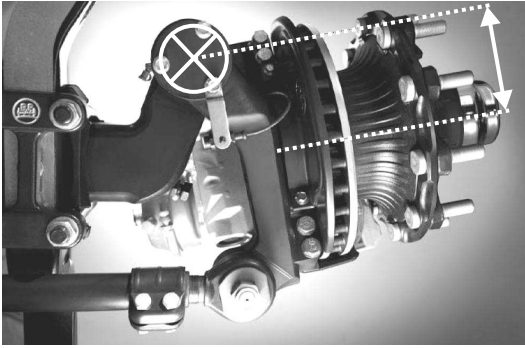
Figure 1.1: State-of-the-art self-steering system for commercial vehicle semi-trailers. The white arrow highlights the caster. *Image courtesy BPW Bergische Achsen KG. Source: Alberding et al. (in press), ©IEEE.*

1.1 Scope

The objective of this work is to contribute to two aspects of the steering of semi-trailers.

The first aspect is the steering mechanism. As introduced previously, trailer steering offers two uncompromising choices. Self-steering does not require an actuation, but has a limited performance, cannot be controlled, and cannot be used during reverse travel. Command steer allows the steering to be controlled and can be used in both directions of travel, but requires a high-power actuation that is expensive in terms of both cost and weight. This work presents a novel approach that strikes a balance between these extremes. The approach is tested in simulation experiments using a detailed multi-body model of the vehicle. The technical feasibility is investigated in vehicle experiments using a functional demonstrator based on a standard production self-steering axle.

The second aspect is the steering control. Any electronically controllable steering mechanism requires a controller that provides a reference for the steering angle. The majority of commercial command-steer systems control the steering angle proportionally to the articulation angle, both during forward and reverse travel (Jujnovich & Cebon 2002). For forward travel, advanced controllers optimize both the low- and high-speed performance (Odhams et al. 2011). For reverse travel, advanced systems provide a remote control for the trailer steering to the driver. This work takes a novel approach to the steering control during reverse travel. The objective is to optimally assist a human driver to reverse a tractor semi-trailer combination. The trailer steering is to be based on the driver's steering actions on the tractor, without a remote control or any other additional driver input. The linear model derived for the control design is validated using measurement data obtained from vehicle experiments. The control system is tested using a validated multi-body simulation model.

1.2 Contributions

The results of the research within the scope of this work have been summarized in the following papers.

- Alberding, M., Onder, C., Sager, F. & Guzzella, L. (in press), 'Variable caster steering', *IEEE Transactions on Vehicular Technology*. ©IEEE

- Alberding, M., Vivaldelli, M., Sager, F. & Onder, C. (2013), Steering control of a semi-trailer in reverse travel, Manuscript submitted for publication.

With extensions and minor modifications, this dissertation is a reprint of the author's manuscripts for these papers.

The first paper, Alberding et al. (in press), presents the research on the steering mechanism. The second paper, Alberding, Vivaldelli, Sager & Onder (2013), presents the research on steering control.

1.3 Student Projects

The following student projects have been supervised as part of the author's doctoral studies and contributed to the research.

- Böhl, S. (2011), Lenkstrategie für einen aktiv gelenkten Sattelauflieger, Semester project, ETH Zurich, Switzerland.

- van der Velden, B. (2011), Steering Control of Semi-Trailers: Model-Based Vehicle Dynamics Control for Rollover Prevention, Internship, Eindhoven University of Technology, The Netherlands.

- Vivaldelli, M. (2012), Semi-Trailer Steering Strategies: Model-Based Vehicle Dynamics Controllers for Reversing Manoeuvres, Master's thesis, Politecnico di Milano, Italy.

- Gacka, S. (2013), Receding Horizon Semi-Trailer Steering Control Implementation, Semester project, ETH Zurich, Switzerland.

- Störkle, J. (2013), Lateral Dynamics of Multiaxle Vehicles, Diploma thesis, University of Stuttgart, Germany.

- Gacka, S. (2013), Formula 1 Vertical Dynamics: Model-Based Tools for Vehicle Dynamics Development, Master's thesis, ETH Zurich, Switzerland.

1.4 Outline

Chapter 2 presents the research on the steering mechanism, based on the author's manuscript for the paper Alberding et al. (in press). Sections 2.1 and 2.2 derive a simplified mathematical model of the interaction between steering kinematics and tyre behaviour. Section 2.3 analyses a variable steering geometry and investigates how it can be used to control the steering angle. Section 2.4 addresses the minimization of actuation energy. Section 2.5 presents simulation results, and Section 2.6 discusses the experimental validation.

Chapter 3 presents the steering control research, based on the author's manuscript for the paper Alberding et al. (2013). Section 3.1 derives a time-variant linear model of the system dynamics. The model is validated using measurement data from vehicle experiments. Based on the model, a state estimator in the form of a discrete-time Kalman filter is designed. The feasibility of estimating the tractor steering and the articulation angle at various speeds is investigated. Section 3.2 presents the control system, which is the main result of this chapter. In Section 3.3, the controller is tested using a validated multi-body simulation model. The system is compared to a conventional controller design that steers proportionally to the articulation angle.

Chapter 4 provides concluding remarks.

2

Variable Caster Steering

Compared to command steer, the key benefits of self-steering are low cost and weight, mainly owing to the absence of an actuation unit. On the downside, self-steering cannot be used during reverse travel, and its steering angle cannot be controlled. This makes trailer steering a choice between Scylla and Charybdis: the limited performance of self-steering or the high cost and weight of command steer. Being constrained by these factors, steering suspensions are far from being competitive with the cost-benefit ratio of their non-steering counterparts, and their market penetration remains modest. Still, steering has appealing benefits. If a next generation steering system succeeds in overcoming the conflict between cost and performance, it can be expected to find an interested market.

One approach towards such new steering system is to advance self-steering, overcoming its performance limitations. The incapability of reverse-travel steering can be considered the major weakness. In general, there are two approaches conceivable to address this problem.

One approach is to stabilize the steering by the use of external forces. The required magnitude of these forces has to be higher than for command steer systems, since the caster provides a lever arm to the lateral tyre forces. The stabilization imposes
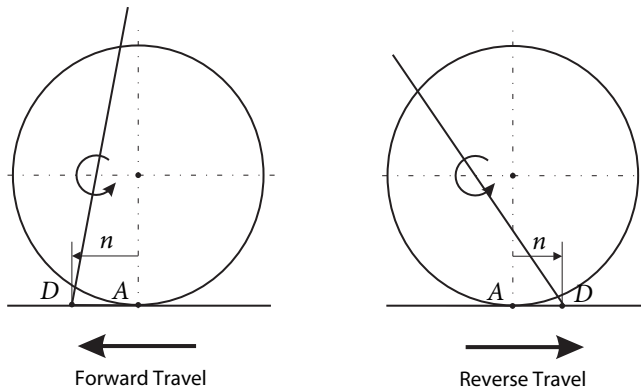
Figure 2.1: Variation of the caster to stabilize the self-steering during reverse travel. *Source: Alberding et al. (in press), ©IEEE.*

high requirements on the dynamic properties of the actuation or the ability to hold the steering in the desired position. An advantage of this approach is the possibility to further use the external forces to overcome the second limitation of self-steering, namely the incapability to control the steering angle. Due to the large actuation forces, this approach inevitably requires a high-power actuation hardware. Installing command steer actuation such as a hydraulic unit, the cost of the complete steering system can be estimated to be at least equal to command steer. A prospect to fulfil the ambition of significantly improving the cost-benefit ratio must be doubted. An interesting alternative could be the use of single-sided braking, even if the challenges of this approach, e.g. the limited precision and dynamics of braking, can be expected to limit the performance and/or require additional hardware.

The second approach is to directly eliminate the source of the instability, which is the negative caster. This approach requires the capability to change the steering geometry. An example for such a variable geometry approach is shown in Fig. 2.1, where the caster angle is manipulated on the axle level, influencing the caster offset such that it is positive for reverse travel. A number of solutions have been proposed to implement this approach in a mechanical design (Chalin 2001, Gottschalk & Jablonski 2001). Its appeal is that it can be realized using a small low-power actuation. The downside is an increased mechanical complexity while only the problem of reverse-travel self-steering is solved, leaving the cost-benefit ratio unsatisfactory. Compared to command steer, the performance is still limited since the steering angle cannot be controlled. The idea to actively change the suspension geometry is also known from passenger vehicles (Watanabe & Sharp 1999, Lee, Lee, Han, Hedrick & Català 2008, Jazar, Subic & Zhang 2012), where it is motivated by the optimization of vehicle

dynamics, rather than by the intention to influence the behaviour of a self-steering system.

Based on these considerations, the starting points that might lead to a next generation steering system are manifold. The variable geometry approach seems particularly elegant since it aims at affecting the steering behaviour without a high-power, cost- and weight-intensive actuation. To evolve its state of the art, the objective is clearly to either decrease the mechanical complexity or to increase the benefit. At present, a variable geometry only solves the problem of reverse-travel self-steering. The benefit could be clearly increased if it could be used to control the steering angle as well. The final objective would be to realize a system with a small low-cost actuation that reaches the same performance levels as command steer, including the capability of reverse-travel steering and the controllability of the steering angle. In other words, command steer properties without command steer hardware. If this would be feasible under modest additional design requirements, it might justify the mechanical complexity of a variable geometry, possibly in the end providing a competitive cost-benefit ratio.

This work analyses the feasibility of this novel approach. The objective is a description of the resulting system structure and a comprehensive assessment of its properties and limitations using simulation experiments. The technical feasibility is investigated in vehicle experiments.

The chapter is organized as follows. Sections 2.1 and 2.2 derive a simplified mathematical model of the interaction between steering kinematics and tyre behaviour. Section 2.3 analyses a variable steering geometry and investigates how it can be used to control the steering angle. Section 2.4 addresses the minimization of actuation energy. Section 2.5 presents simulation results and Section 2.6 discusses the experimental validation.

2.1 The Steering Geometry

The steering geometry is the source for both the capabilities and limitations of conventional self-steering. A comprehensive understanding of the underlying physics is important for the design of any new steering concept with self-steering properties and is essential to study a variable steering geometry.

2.1.1 Characterization of the Steering Geometry

This section briefly introduces the characterization of the steering geometry based on Matschinsky (2007).

Figure 2.2 shows a conventional steering geometry of a rigid axle with a fixed king-pin axis. The geometry is characterized by the orientation and the position of the kingpin axis in relation to the wheel carrier.

The position can be described at road level. For a steering angle of zero, the kingpin axis intersects the road at point D. The geometrical tyre contact point A is the contact point of the road and a simplified representation of the tyre as a disc in the rim centre plane of tyre radius ρ. For a pneumatic tyre, the tyre forces attack displaced towards A; this displacement will be discussed in Section 2.2. The distance between D and A in longitudinal direction is the geometric caster offset n, the distance in lateral direction is the geometric kingpin offset r. The caster offset is mainly important in its role as a lever arm for the lateral tyre forces, the kingpin offset as a lever arm for the longitudinal forces.

Alternatively, the position can be described at axle level. The longitudinal distance of the wheel centre M to the kingpin is called wheel-centre caster offset n_τ, the lateral distance wheel-centre kingpin offset r_σ.

In the longitudinal direction, the kingpin axis is inclined by the caster angle τ, in the lateral direction by the kingpin inclination σ. In suspension design, these angles are used to obtain effects like a self-centring torque and a camber change that stabilizes the vehicle during cornering.

In their role as a lever arm of the tyre forces, caster and kingpin offset can change as a function of the steering angle. In this work, all parameters of the steering geometry previously introduced are related to a steering angle of zero.

The inclination of the rim centre plane in the lateral direction is the camber angle γ. It is defined positive for the upper end of the wheel directing outwards with respect to the chassis. The camber can be used to obtain lateral tyre forces and to improve the cornering behaviour. It is a function of the steering angle. To improve the readability of the following equations and without loss of generality, in this work it is assumed that for straight-ahead travel the camber is designed to be zero.

The steering angle is denoted δ. It is defined about the kingpin, throughout this work the difference towards the steering angle about the contact patch δ_s is generally neglected. The only exception is the exact representation of the kinematics in Section 2.1.3.
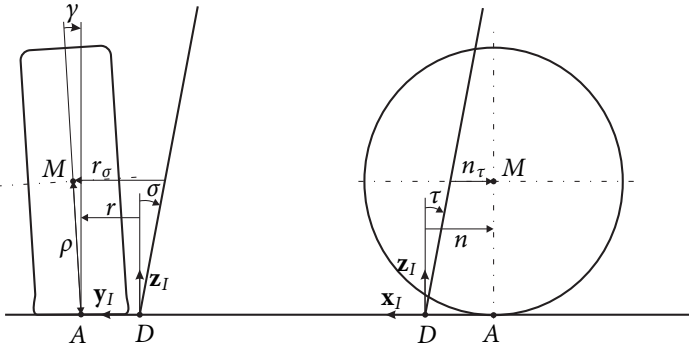
Figure 2.2: Parameters of the steering geometry, based on Matschinsky (2007). *Source: Alberding et al. (in press), ©IEEE.*
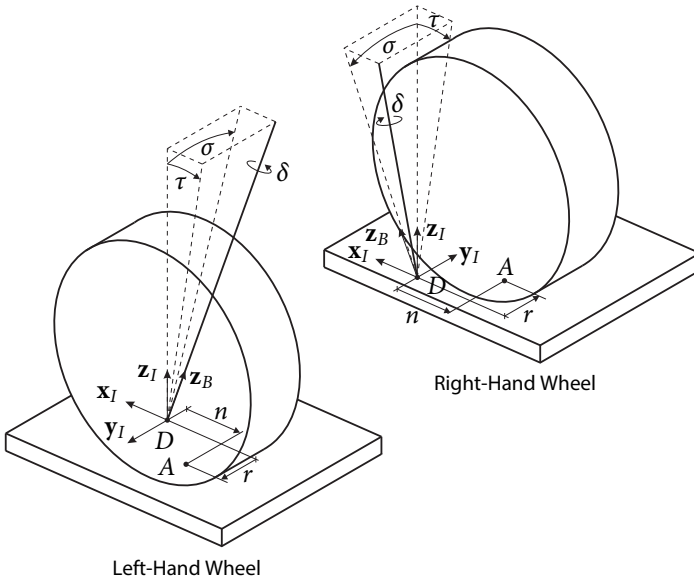
Left-Hand Wheel

Figure 2.3: Sign convention for the left-hand and the right-hand wheel. *Source: Alberding et al. (in press), ©IEEE.*

2.1.2 Sign Convention

The signs are defined as shown in Fig. 2.3.

The longitudinal axis $\mathbf{x}_I$ is defined positive in the direction of travel, i.e. towards the front during forward and towards the rear during reverse travel. Accordingly, left and right are defined with respect to the direction of travel.

The left-hand wheel is described using a right-handed coordinate system, the right-hand wheel using a left-handed coordinate system. This convention leads to a generalization of the direction of the steering angle and the lateral coordinate: these are positive when directed to the outside of the wheel and negative when directed to the inside.

In an exception from the mathematical convention, the caster angle is defined positive for a negative rotation about $\mathbf{y}_I$, associated to a positive caster offset.

When describing the state of the vehicle or axle instead of a single wheel, it is necessary to use a mutual sign convention for both wheels. In this case, the respective variables are marked by an asterisk, e.g. δ^*, and are defined according to a right-handed system. If it is necessary to distinguish variables between the two wheels, an index l refers to the left-hand wheel and an index r to the right-hand wheel.

2.1.3 Kinematics

A kinematic analysis of the steering geometry enables the position and orientation of the wheel to be determined for a given steering angle trajectory. The following derivation briefly introduces both an exact and a simplified mathematical model of the kinematics. The exact representation is described by Eqs. (2.3a), (2.5a) and (2.5b), the simplified one by Eqs. (2.3b), (2.5c) and (2.5d). The model error resulting from the simplifications is shown in Figs. 2.4 and 2.12. The analysis in the following sections uses the simplified representation.

Throughout the model, the superscript of a vector refers to its coordinate system, e.g. $\mathbf{v}^S$. The axes of a three-dimensional Cartesian coordinate system S are denoted by $\mathbf{x}_S$, $\mathbf{y}_S$, and $\mathbf{z}_S$. The matrix $\mathbf{R}_{AB}$ describes the transformation between the coordinate systems A and B. A rotation matrix of angle α about an axis i is denoted by $\mathbf{R}_{i,\alpha}$.

To describe the motion of the wheel relative to the kingpin, the kingpin is assumed to be fixed. As shown in Fig. 2.3, the fixed inertial frame I is chosen as a Cartesian coordinate system with its origin in the intersection D of the kingpin axis with the road surface. As mentioned above, this system is chosen right-handed for the left-hand wheel and left-handed for the right-hand wheel. The z-axis $\mathbf{z}_I$ is defined normal to the road surface, the x-axis $\mathbf{x}_I$ in direction of travel for a steering angle of zero.

A second, kingpin-fixed frame B is defined in the same origin and $\mathbf{z}_B$ in the kingpin axis. The transformation is expressed in terms of a yaw angle δ, pitch angle τ', and roll

angle σ,

$$\mathbf{R}_{IB} = \begin{pmatrix} \mathbf{x}_B^I & \mathbf{y}_B^I & \mathbf{z}_B^I \end{pmatrix} = \mathbf{R}_{x,\sigma}\, \mathbf{R}_{y,-\tau'}\, \mathbf{R}_{z,\delta}, \quad \mathbf{R}_{z,\delta} = \begin{pmatrix} \cos\delta & -\sin\delta & 0 \\ \sin\delta & \cos\delta & 0 \\ 0 & 0 & 1 \end{pmatrix}, \quad (2.1)$$

where

$$\tan\tau' = \tan\tau \cdot \cos\sigma. \quad (2.2)$$

For convenience, the first two rotations in the following are expressed by a single matrix, yielding the exact representation

$$\mathbf{R} = \mathbf{R}_{x,\sigma}\, \mathbf{R}_{y,-\tau'} = \begin{pmatrix} \dfrac{1}{\sqrt{\cos^2\sigma\tan^2\tau + 1}} & 0 & -\dfrac{\cos\sigma\tan\tau}{\sqrt{\cos^2\sigma\tan^2\tau + 1}} \\[2mm] -\dfrac{\cos\sigma\sin\sigma\tan\tau}{\sqrt{\cos^2\sigma\tan^2\tau + 1}} & \cos\sigma & -\dfrac{\sin\sigma}{\sqrt{\cos^2\sigma\tan^2\tau + 1}} \\[2mm] \dfrac{\cos^2\sigma\tan\tau}{\sqrt{\cos^2\sigma\tan^2\tau + 1}} & \sin\sigma & \dfrac{\cos\sigma}{\sqrt{\cos^2\sigma\tan^2\tau + 1}} \end{pmatrix}. \quad (2.3a)$$

Neglecting the non-commutativity of the first two rotations by the assumption of a small kingpin inclination implies that $\tau' \approx \tau$ and yields the approximation used for the simplified model

$$\mathbf{R} \approx \mathbf{R}_{x,\sigma}\, \mathbf{R}_{y,-\tau} = \begin{pmatrix} \cos\tau & 0 & -\sin\tau \\ -\sin\sigma\sin\tau & \cos\sigma & -\cos\tau\sin\sigma \\ \cos\sigma\sin\tau & \sin\sigma & \cos\sigma\cos\tau \end{pmatrix}. \quad (2.3b)$$

Using the camber angle γ and the steering angle about the contact patch δ_s, the vector $\mathbf{w}$ normal to the wheel centre plane can be expressed by

$$\mathbf{w}^I = \mathbf{R}_{z,\delta_s} \begin{pmatrix} 0 \\ \cos\gamma \\ -\sin\gamma \end{pmatrix} = \begin{pmatrix} -\sin\delta_s\cos\gamma \\ \cos\delta_s\cos\gamma \\ -\sin\gamma \end{pmatrix}. \quad (2.4a)$$

The alternative formulation

$$\mathbf{w}^B = \mathbf{R}^{\mathsf{T}}\mathbf{y}_I^I, \quad \mathbf{w}^I = \mathbf{R}_{IB}\,\mathbf{w}^B = \begin{pmatrix} w_1^I \\ w_2^I \\ w_3^I \end{pmatrix} \quad (2.4b)$$

can be used to determine γ and δ_s through

$$\sin\gamma = -w_3^I, \qquad \cos\gamma = \sqrt{1 - w_3^{I\,2}}, \qquad (2.5a)$$

$$\sin\delta_s = -\dfrac{w_1^I}{\sqrt{1 - w_3^{I\,2}}}, \quad \cos\delta_s = \dfrac{w_2^I}{\sqrt{1 - w_3^{I\,2}}}. \qquad (2.5b)$$
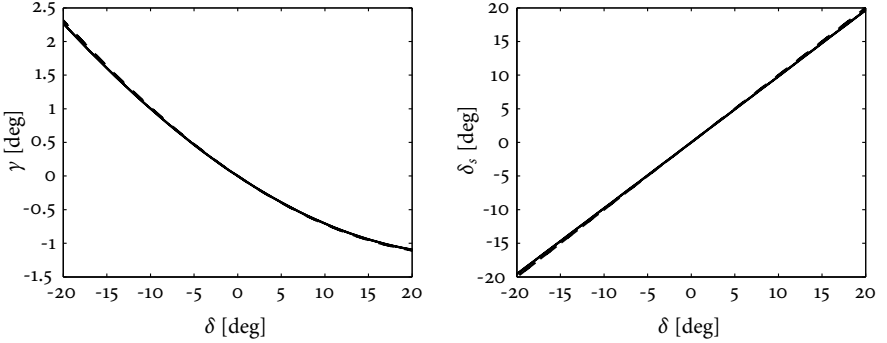
Figure 2.4: Model error of camber and steering angle for a steering geometry $n = 100$ mm, $r = 200$ mm, $\tau = -5°$, $\sigma = 10°$. The solid line shows the exact representation of the kinematics, the dashed line the simplified model.

For the simplified model, assuming small angles τ and σ, the camber can be approximated via linearization

$$\gamma \approx \tau \sin \delta + \sigma(1 - \cos \delta) \tag{2.5c}$$

and the difference between δ_s and δ can be neglected

$$\delta_s \approx \delta. \tag{2.5d}$$

Figure 2.4 shows the error of these approximations.

A third, wheel-fixed coordinate frame R is defined with $\mathbf{x}_R$ in the longitudinal and $\mathbf{y}_R$ in the lateral direction of the wheel, i.e., $\mathbf{y}_R$ is the normal vector of the rim centre plane $\mathbf{w}$, which yields the transformation matrix

$$\mathbf{R}_{IR} = \begin{pmatrix} \mathbf{x}_R^I & \mathbf{y}_R^I & \mathbf{z}_R^I \end{pmatrix} = \mathbf{R}_{z,\delta_s} \, \mathbf{R}_{x,-\gamma} = \begin{pmatrix} \cos \delta_s & -\sin \delta_s \cos \gamma & -\sin \delta_s \sin \gamma \\ \sin \delta_s & \cos \delta_s \cos \gamma & \cos \delta_s \sin \gamma \\ 0 & -\sin \gamma & \cos \gamma \end{pmatrix}. \tag{2.6}$$

A fourth coordinate frame F is introduced to describe the wheel forces. The vector $\mathbf{x}_F$ is defined in the longitudinal direction and $\mathbf{y}_F$ in the lateral direction of the wheel, but in contrast to the wheel-fixed frame both lie on the road plane.

$$\mathbf{R}_{IF} = \begin{pmatrix} \mathbf{x}_F^I & \mathbf{y}_F^I & \mathbf{z}_F^I \end{pmatrix} = \mathbf{R}_{z,\delta_s} = \begin{pmatrix} \cos \delta_s & -\sin \delta_s & 0 \\ \sin \delta_s & \cos \delta_s & 0 \\ 0 & 0 & 1 \end{pmatrix}. \tag{2.7}$$

Using the defined frames and transformations, the position vector of the wheel

centre $\mathbf{r}_M$ can described by

$$\mathbf{r}_M^I = \mathbf{R}_{IB}\,\mathbf{r}_M^B, \quad \mathbf{r}_M^B = \mathbf{R}^{\mathrm{T}} \begin{pmatrix} -n \\ r \\ \rho \end{pmatrix}, \tag{2.8}$$

and the position vector of the geometrical tyre contact point $\mathbf{r}_A$ by

$$\mathbf{r}_A^I = \mathbf{r}_M^I - \rho\mathbf{z}_R^I. \tag{2.9}$$

2.2 Tyre Model

The self-steering motion is caused by the interaction of the steering geometry and the tyre forces. The steering geometry serves the tyre forces as a lever arm, leading to the resultant steering torque about the kingpin.

For a pneumatic tyre, the contact points of the forces that develop in the tyre-road interaction are generally displaced from the geometric contact point. This affects the steering geometry. Therefore, besides the magnitude of the resultant forces, their location in the contact patch is of interest.

This section provides a brief introduction to the physics of pneumatic tyres. It discusses the development of forces in the tyre-road interaction and summarizes common mathematical models. The following discussion and the data presented are mainly based on Clark (1981), Pacejka (2006), Wong (2008), Fancher, Ervin, Winkler & Gillespie (1986), and Segel, Ervin & Fancher (1981).

2.2.1 Longitudinal Forces

Longitudinal forces are developed during braking and traction and due to the rolling resistance. Since the wheels on a trailer are not connected to the drive-train, the driven case is of minor relevance for this work.

Braking and Traction

A braking torque acting on the wheel causes a stretch of the tyre tread before the contact patch and a compression after the contact (Clark 1981). This phenomenon is connected to a braking force developing in the contact patch. A driving torque shows the inverted behaviour, where the tread is compressed before and stretched after the contact patch, associated to a driving force.

The phenomenon affects the ratio between longitudinal speed v_x and the angular velocity ω, which can be used to quantify the braking or the traction, respectively. For that purpose, the effective rolling radius ρ_e can be defined by the ratio between v_x
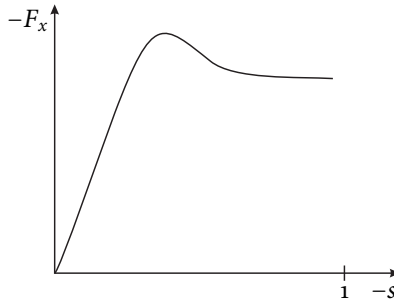
Figure 2.5: Typical brake force characteristics according to Pacejka (2006).

and ω for a free rolling tyre (Pacejka 2006). While the value ρ_e is defined for the free rolling tyre and always remains constant, the ratio $\frac{v_x}{\omega}$ changes when the wheel is being braked or driven. In such a case, the longitudinal slip s defined by

$$s = \frac{\rho_e \omega - v_x}{v_x} \tag{2.10a}$$

becomes non-zero. It takes positive values, i.e. $\rho_e \omega > v_x$, for a driven wheel, negative values, i.e. $\rho_e \omega < v_x$, for a braked wheel, and $s = -1$ for a locked wheel. To limit the slip to $s = 1$, the longitudinal slip for a driven wheel is sometimes redefined to

$$s = \frac{\rho_e \omega - v_x}{\rho_e \omega}, \tag{2.10b}$$

as for instance used by Kiencke & Nielsen (2000). Since the driven case is not relevant for this work, this distinction is not applied.

Figure 2.5 shows typical brake force characteristics according to Pacejka (2006). For small longitudinal slips, the relationship is almost linear and can be approximated by

$$F_x(s, F_z) = C_s(F_z)\, s, \quad \mathbf{F}_x(s, F_z) = F_x(s, F_z)\, \mathbf{x}_F, \tag{2.11}$$

where $C_s > 0$ is the longitudinal slip stiffness for braking. The stiffness increases with the wheel load (Segel et al. 1981). The brake force saturates for higher slips due to the limits imposed by the tyre-road friction. It shows its maximum in the beginning of the nonlinear region and a monotonic decrease for slips beyond that value. This behaviour is commonly characterized by the peak and slide values and of the braking force coefficient $-\frac{F_x}{F_z}$. The characteristics are influenced by the tyre-road friction, speed, and wheel load (Fancher et al. 1986, Clark 1981, Wong 2008).

The characteristics of the driven case are similar to braking and can be approached analogously (Clark 1981).

Rolling Resistance

Internal friction losses related to the deformation of the carcass are the primary cause for the rolling resistance of a tyre (Clark 1981). Due to this hysteresis, the centroid of the normal force distribution in a free rolling tyre lies ahead of the geometric centre of the contact patch; i.e., it is shifted in the direction opposite to that of the cornering force. The resulting torque around the wheel centre is balanced by a longitudinal braking force. The term rolling resistance generally refers to this force.

The rolling resistance of a tyre is characterized by the coefficient of rolling resistance, which is defined by the ratio between the rolling resistance force and the wheel load. It is smaller for truck tyres than for car tyres, according to Clark (1981) it ranges from 0.5 % to 1.2 %. Related to the tyre radius, the coefficient of rolling resistance determines the longitudinal shift of the normal force. Since the force is small in relation to the range of typical cornering forces and the shift is small in relation to the geometric caster offset, both are neglected in this work.

The rolling resistance is influenced by a number of factors such as tyre structure, wheel load, braking and traction, cornering, inflation pressure, temperature, surface conditions, and vehicle speed (Clark 1981, Wong 2008).

2.2.2 Lateral Forces

The cornering properties of a tyre are of fundamental importance to the dynamical behaviour of the vehicle. For an analysis of the steering geometry, the effect of cambering needs to be addressed as well.

Cornering

As shown in Fig. 2.6, cornering is generally specified by the side-slip angle α between the longitudinal axis of the wheel $\mathbf{x}_F$ and its velocity vector $\mathbf{v}_w$. This induces a cornering force $\mathbf{F}_{y,\alpha}$ in the opposite direction of α. This force is usually attacking behind the centre of the contact patch. This longitudinal displacement is known as the pneumatic trail n_R and the related torque as the self-aligning torque of the wheel.

For small side-slip angles, the contact patch adheres to the road and is directed parallel to the velocity vector of the wheel (Clark 1981). Within the adhesion zone, the lateral deflection of the tyre increases approximately linearly along the contact line. For increasing side-slip angles, the rear end of the contact patch starts to slide towards the rim centre plane. The cornering force is mainly related to this adhesion of the tyre to the road and the resulting deflection. The deformation is also a source of the pneumatic trail and a lateral shift of the tyre forces.
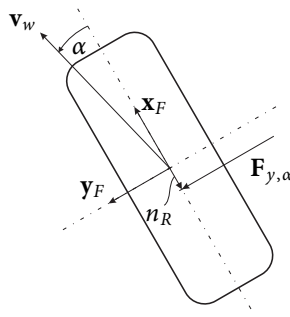
Figure 2.6: Cornering force $\mathbf{F}_{y,\alpha}$, side-slip angle α, and pneumatic trail n_R. *Source: Alberding et al. (in press), ©IEEE.*
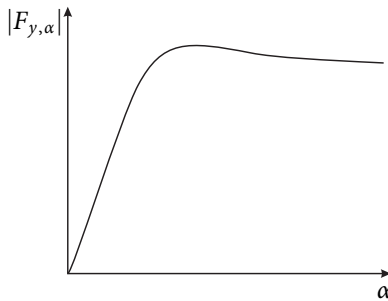
Figure 2.7: Typical cornering force characteristics according to Pacejka (2006).

Characteristics Figure 2.7 shows the typical relationship between cornering force and side-slip angle according to Pacejka (2006). For small angles, the force grows almost linearly until being saturated at the limits of adhesion. The slope near the origin is known as the cornering stiffness $C_\alpha > 0$, determining the force in the linear region by

$$F_{y,\alpha}(\alpha, F_z) = -C_\alpha(F_z)\,\alpha, \quad \mathbf{F}_{y,\alpha}(\alpha, F_z) = F_{y,\alpha}(\alpha, F_z)\,\mathbf{y}_F. \tag{2.12}$$

The sign of the side-slip angle α is defined as illustrated in Fig. 2.6.

As shown in Fig. 2.8, the cornering stiffness is strongly influenced by the vertical force (Pacejka 2006). In this diagram, the vertical force F_z is normalized by the rated load $F_{z,0}$. Car tyres show nonlinear characteristics, reaching the maximum at the rated load. The nonlinearity causes a decrease of the combined cornering stiffness of an axle due to the load transfer during cornering. For truck tyres, the nonlinearity is much smaller and the cornering stiffness continues to increase for higher loads, though at a lower rate. The influence of a load varying in the vicinity of the rated load can be
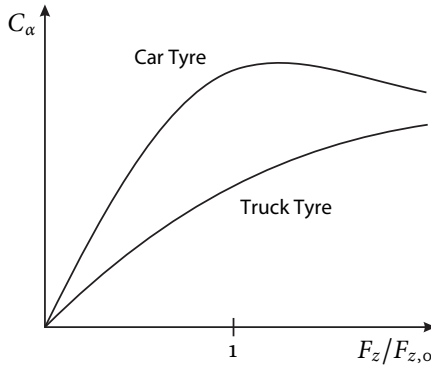
Figure 2.8: Influence of the wheel load on the cornering stiffness according to Pacejka (2006).

estimated by the linear approximation

$$C_\alpha(F_z) = C_{\alpha,0} F_z, \tag{2.13}$$

where $C_{\alpha,0} > 0$, the slope of the curve evaluated at the rated load, is the cornering coefficient. For new radial truck tyres, Fancher et al. (1986) specify a typical cornering coefficient of 7.45 rad^{-1} at a rated load of 2740 kg. They further show that tyres with high cornering coefficients generally also show a higher nonlinearity in the stiffness-load relationship and that the cornering coefficient of a truck tyre is not predictably influenced by the inflation pressure.

The linear approximation Eq. (2.12) of the cornering characteristics is sufficiently accurate for small side-slip angles. For higher side-slip angles, more sophisticated models have to be used. Such models have been subject to intense research over the past decades; one well-established empirical example is known as Pacejka's *magic formula* (Pacejka 2006)

$$\begin{aligned} F_{y,\alpha}(\alpha, F_z) = &- D_\alpha(F_z) \sin[C \arctan\{B_\alpha(F_z)\, \alpha \\ &- E(B_\alpha(F_z)\, \alpha - \arctan(B_\alpha(F_z)\, \alpha))\}], \end{aligned} \tag{2.14}$$

where

$$B_\alpha(F_z) = \frac{C_\alpha(F_z)}{C\, D_\alpha(F_z)}$$

$$D_\alpha(F_z) = \mu F_z$$

$$C_\alpha(F_z) = c_1 \sin\left(2 \arctan \frac{F_z}{c_2}\right).$$

The variables C and E denote shape factors, c_1 the maximum cornering stiffness, c_2 the load at the maximum cornering stiffness, and μ the tyre-road friction coefficient.
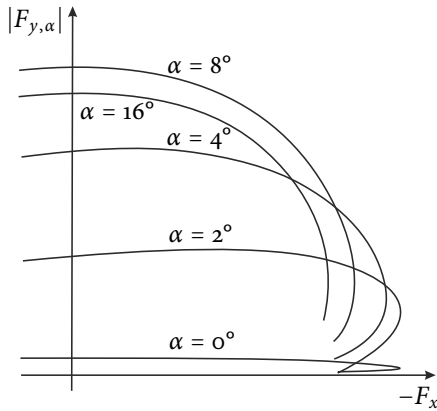
Figure 2.9: Typical combined cornering and brake force characteristics according to Pacejka (2006).
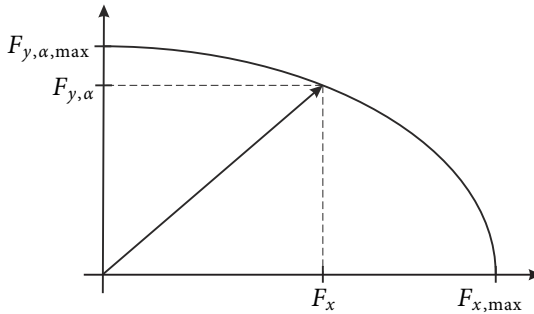
Figure 2.10: The friction ellipse concept.

Combined Slip   The presence of longitudinal slip affects the lateral force character-istics. Vice versa, lateral slip has an influence on the longitudinal force. The total frictional force in the contact patch is limited by the tyre-road friction coefficient and the wheel load. Therefore, the lateral and longitudinal force generally decrease when the other slip component rises. Figure 2.9 shows the resulting characteristics for com-bined cornering and braking force according to Pacejka (2006).

A common model of this behaviour is the friction ellipse (Wong 2008). As shown in Fig. 2.10, it assumes that the combined force lies on an ellipse with the axes defined by the maximum values of the cornering and braking force for pure slip, i.e.

$$\left(\frac{F_x}{F_{x,\text{max}}}\right)^2 + \left(\frac{F_{y,\alpha}}{F_{y,\alpha,\text{max}}}\right)^2 = 1. \tag{2.15}$$

The friction ellipse can be used to find the cornering force in the presence of a given
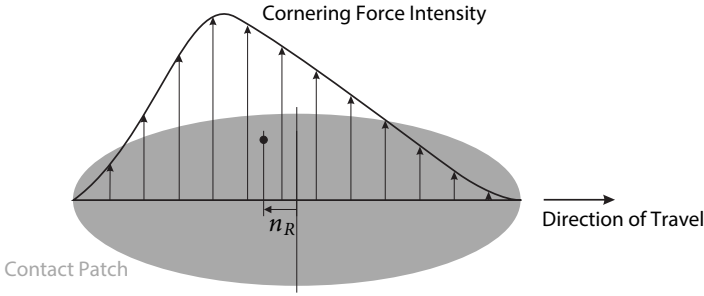
Figure 2.11: Cornering force distribution along the tyre contact patch according to Clark (1981).

braking force via the relationship

$$F_{y,\alpha}(\alpha, F_z, F_x) = F_{y,\alpha,\max}(\alpha, F_z)\sqrt{1 - \left(\frac{F_x}{\mu F_z}\right)^2}. \qquad (2.16)$$

The maximum cornering force $F_{y,\alpha,\max}(\alpha, F_z)$ is the cornering force for pure side-slip as for instance determined by Eq. (2.12) or Eq. (2.14). The maximum braking force is given by the product of the tyre-road friction coefficient μ and the normal force F_z.

Pneumatic Trail   As illustrated in Fig. 2.11, the lateral force intensity during cornering is distributed asymmetrically along the tyre contact patch (Clark 1981). This distribution is related to the lateral deflection of the tyre that increases along the contact line until the adhesion limits are reached. The resultant force attacks at the centroid of the area under the intensity distribution. The longitudinal distance from the geometric centre of the contact patch to this point is the pneumatic trail n_R.

During normal cornering, the asymmetry is in favour of the rearward half of the contact patch and the lateral force is displaced behind the geometric contact point. Due to the smaller adhesion zone, higher side slip angles cause more symmetric distributions of the lateral force and decrease the pneumatic trail. The pneumatic trail is further influenced by the wheel load, inflation pressure, braking and traction, and tread wear (Fancher et al. 1986, Clark 1981, Wong 2008).

The pneumatic trail can be assumed at a quarter of the contact patch length (Pacejka 2006). Fancher et al. (1986) specify 5.3 cm as a typical value for new radial truck tyres at rated load. The pneumatic trail is thus a substantial extension of the caster offset.

Lateral Displacement of the Tyre Forces   The lateral deflection of the tyre due to the adhesion displaces the tyre forces from the geometric contact point. While this effect obviously is not important for the lateral forces themselves, it can be of interest for the normal and longitudinal forces. This lateral displacement $r_{R,\alpha}$ can generally be determined via the lateral stiffness parameter c_y (Clark 1981). For small side-slip angles, it can be approximated by

$$r_{R,\alpha}(\alpha, F_z) = -\frac{C_\alpha(F_z)}{c_y}\alpha. \tag{2.17}$$

The lateral stiffness is generally in the order of 50 % of the vertical stiffness, which relates the vertical deflection to the wheel load (Clark 1981). Naturally, the stiffness properties are strongly influenced by the inflation pressure (Fancher et al. 1986).

According to Segel et al. (1981), the variable $r_{R,\alpha}$ can take values of approximately 10 mm per degree side-slip. In relation to the kingpin offset, such values can become significant. The difference between the deflection of the centre of the contact patch and the deflection of the point where the cornering force attacks is neglected.

Cambering

A camber angle causes a deformation of the wheel in the contact area. This causes a lateral force, the camber thrust (Clark 1981). The phenomenon can be understood on the background that a free rolling cambered wheel would not follow a straight line (Wong 2008). Instead, it would revolve about the point where a line through the wheel centre and normal to the wheel plane intersects the road. Since the vehicle does not allow this movement, a lateral force in the direction of the camber is the consequence.

The relationship between camber angle γ and camber thrust $F_{y,\gamma}$ is almost linear (Clark 1981). It is commonly characterized using the camber stiffness $C_\gamma > 0$ by

$$F_{y,\gamma}(\gamma, F_z) = C_\gamma(F_z)\,\gamma, \quad \mathbf{F}_{y,\gamma}(\gamma, F_z) = F_{y,\gamma}(\gamma, F_z)\,\mathbf{y}_F. \tag{2.18}$$

The influence of cambering is generally smaller than that of cornering. Segel et al. (1981) state that for truck tyres the camber stiffness is typically about 10 % to 20 % of the cornering stiffness. It is strongly influenced by the wheel load (Segel et al. 1981). This relationship can be represented in a simplified form if the camber stiffness is assumed to be proportional to the cornering stiffness

$$C_\gamma(F_z) = k_\gamma C_\alpha(F_z), \tag{2.19}$$

where $k_\gamma > 0$.

In contrast to the cornering force, the camber thrust generally attacks ahead of the geometric contact point (Clark 1981). This longitudinal distance, known as pneumatic lead, is usually small and may be neglected. But since they do not attack in the same point, cornering and cambering forces should be distinguished.

For combined cornering and cambering, the camber thrust decreases for higher side-slip angles due to the sliding in the contact area (Clark 1981).

Cambering causes a lateral shift of the tyre forces. According to Hirschberg, Rill & Weinfurter (2007), for a cambered tyre with full road contact this shift can be modelled by

$$r_{R,y}(\gamma, F_z) = \frac{b^2 c_z \tan\gamma}{12 F_z \cos\gamma}, \tag{2.20a}$$

assuming a trapezoidal shape of the pressure distribution in the contact area. Assuming a small camber and small angles τ and σ, it can be approximated using Eq. (2.5c)

$$r_{R,y} \approx \frac{b^2 c_z}{12 F_z} \left(\tau \sin\delta + \sigma(1 - \cos\delta)\right). \tag{2.20b}$$

Under the assumption of a triangular pressure distribution, the deflection for a tyre with only partial road contact is determined by

$$r_{R,y}(\gamma) = \text{sign}(\gamma) \left(\frac{b_c}{3} - \frac{b}{2\cos\gamma}\right). \tag{2.20c}$$

In these equations, the tyre width is denoted by b, the width of the partial contact by b_c, and the vertical stiffness of the tyre by c_z. This latter parameter relates the vertical deflection of the tyre to the wheel load. For radial truck tyres, Fancher et al. (1986) specify a typical vertical stiffness of $800 \, \text{N} \, \text{mm}^{-1}$, a value that naturally is strongly influenced by the inflation pressure.

2.2.3 Interaction with the Steering Geometry

In theory, the force distribution in the contact patch could be resolved into three forces and torques attacking in a single contact point (Clark 1981). For the kinematics of the steering geometry, it seems reasonable to consider only those displacements that are significant in relation to caster and kingpin offset, namely the the longitudinal displacement n_R of the cornering force by the pneumatic trail and the lateral displacement

$$r_R = r_{R,\alpha} + r_{R,\gamma} \tag{2.21}$$

of the normal and longitudinal forces during cornering and cambering.

Following this approach, two contact points are defined. One, denoted C, for the cornering force $\mathbf{F}_{y,\alpha}$ and the other, denoted N, for the normal force $\mathbf{F}_z$, braking force $\mathbf{F}_x$, and camber thrust $\mathbf{F}_{y,\gamma}$. The vectors to these points are given by

$$\mathbf{r}_C^I = \mathbf{r}_A^I - n_R \mathbf{x}_F^I, \quad \mathbf{r}_C^B = \mathbf{R}_{IB}^T \mathbf{r}_C^I, \tag{2.22a}$$

$$\mathbf{r}_N^I = \mathbf{r}_A^I + r_R \mathbf{y}_F^I, \quad \mathbf{r}_N^B = \mathbf{R}_{IB}^T \mathbf{r}_N^I. \tag{2.22b}$$

The vector $\mathbf{r}_A^I$ to the geometric contact point was given in Eq. (2.9) and the vectors $\mathbf{x}_F^I$ and $\mathbf{y}_F^I$ in Eq. (2.7).

The physics of pneumatic tyres and the interaction between the phenomena that were introduced in the previous discussion are complex. Throughout this chapter, a simplified model of the tyre will be used, intended to be confined to the effects most relevant for the scope of this work. The longitudinal force is restricted to braking and assumed to be given by the braking system. Cornering is limited to moderate side-slip angles, the cornering force for pure side-slip hence is given by Eq. (2.12). For combined slip, braking is taken into account via the friction ellipse Eq. (2.16). The effect of braking on other phenomena is not taken into account. The wheel load is assumed to be in the vicinity of the rated load, allowing the cornering stiffness to be determined via Eq. (2.13). The previous assumptions allow the pneumatic trail to be assumed to be constant. The camber thrust is determined by Eq. (2.18) and the camber stiffness is assumed to be proportional to the cornering stiffness, Eq. (2.19). The lateral displacement of the forces during cornering and cambering is given by the sum of Eqs. (2.17) and (2.20). In Eq. (2.20), the tyre is assumed to have full road contact.

2.3 Analysis of a Variable Steering Geometry

As mentioned above, the objective of this work is to analyse the feasibility of improving the steering behaviour of a trailer self-steering system using a variable steering geometry. The present section analyses a variable geometry and investigates the way it can be used to control the steering angle.

2.3.1 Self-Centring

Controlling the steering angle using a variable geometry requires the existence of a steering torque that depends on the geometry. For the design of static geometries, it is a well-known practice to obtain a self-centring of the steering based on the vertical tyre forces. Before examining a possible extension to the variable geometry and an arbitrary steering angle, this approach is briefly introduced and analysed in the following.

Steering creates a motion of the wheel relative to the kingpin. For an inclined kingpin, this motion has a vertical component, and vertical wheel forces are allowed to create a steering torque. Since the wheel is constrained to remain at road level, the vertical movement is transferred to the kingpin and the attached vehicle body. Thus, potential energy is gained or lost, respectively. Tending towards the state of minimum potential energy, the torque of the vertical wheel forces is always directed to lowering the vehicle.
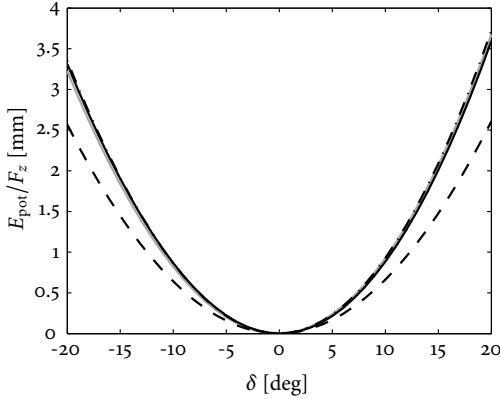
Figure 2.12: Potential energy as a function of the steering angle for a steering geometry $n = 100\,\mathrm{mm}$, $r = 200\,\mathrm{mm}$, $\tau = -5°$, $\sigma = 10°$. The solid line shows the simplified model introduced in Section 2.1.3, the light solid line the exact representation of the kinematics, the dashed line the first-order Taylor approximation with respect to τ, σ, and the dash-dotted line the second-order Taylor approximation. *Source: Alberding et al. (in press), ©IEEE.*

The kinematics of the steering motion and hence the potential energy as a function of the steering angle are determined by the steering geometry. In suspension design, this relationship is commonly used to obtain a self-centring of the steering (Matschinsky 2007). Basically, this effect can be obtained by choosing a steering geometry that has the minimal potential energy at a steering angle of zero.

The kinematics derived in Section 2.1.3 can be used to analyse the relationship between steering geometry and potential energy and to find conditions for the geometry that under the assumptions given guarantee self-centring. For one wheel, the potential energy E_{pot} can be defined as a function of the steering angle by

$$E_{\mathrm{pot}}(\delta) = \Delta h(\delta) F_z, \qquad (2.23)$$

where Δh denotes the difference in height towards the position at a steering angle of zero. As described in Section 2.1.3, a fixed kingpin was assumed. The difference in height thus can be determined via the vertical coordinate of the contact point of the vertical wheel forces

$$\Delta h(\delta) = -\mathbf{z}_I^{I\mathrm{T}} \mathbf{r}_N^I(\delta), \qquad (2.24)$$

which is given in Eq. (2.22b). Figure 2.12 shows such a function for an exemplary set of parameters. Section 2.1.3 introduces both a simplified and an exact representation of the kinematics. The present analysis uses the simplified model. Figure 2.12 additionally includes a function based on the exact representation to evaluate the model error.

Self-centring behaviour is guaranteed if and only if the potential energy function is convex and has a minimum in the origin, as the example in Fig. 2.12 shows. Using the model of Section 2.1.3, this function is highly nonlinear. To identify the key factors for self-centring, it can be simplified by first- or second-order Taylor approximations with respect to τ, σ. Figure 2.12 includes the resulting error for the example function.

A first-order approximation with respect to τ, σ

$$E_{\text{pot}}(\delta) = \left[\sigma\left(n\sin\delta + r(1 - \cos\delta)\right) + \tau\left(r\sin\delta - n(1 - \cos\delta)\right)\right] F_z \qquad (2.25\text{a})$$

leads to the derivatives

$$\frac{\mathrm{d}E_{\text{pot}}}{\mathrm{d}\delta}(\delta) = \left[\sigma\left(n\cos\delta + r\sin\delta\right) + \tau\left(r\cos\delta - n\sin\delta\right)\right] F_z, \qquad (2.25\text{b})$$

$$\frac{\mathrm{d}^2 E_{\text{pot}}}{\mathrm{d}\delta^2}(\delta) = \left[\sigma\left(r\cos\delta - n\sin\delta\right) - \tau\left(n\cos\delta + r\sin\delta\right)\right] F_z. \qquad (2.25\text{c})$$

For a local minimum in the origin, the first and second derivative conditions yield

$$\sigma n = -\tau r, \qquad (2.26\text{a})$$

$$\tau n < \sigma r. \qquad (2.26\text{b})$$

These conditions imply a convexity of the approximated potential energy function, according to Eq. (2.25c) the second derivative is positive for any steering angle.

A second-order approximation for larger caster angles and kingpin inclinations extends the conditions stated in Eq. (2.26) to

$$\sigma n = -\tau r, \qquad (2.27\text{a})$$

$$\tau n < \sigma r + \sigma^2 \rho. \qquad (2.27\text{b})$$

Since $\sigma^2 \rho > 0$, these conditions are less strict and are always satisfied when Eq. (2.26) holds.

In case the parameters n, r, τ, σ are all non-zero, the first condition Eq. (2.26a) is satisfied if and only if $|\sigma n| = |\tau r|$ and the sign of one of the four parameters is different from the others. For stable self-steering, the caster offset n has to be positive. Kingpin offset r and inclination σ cannot both be negative, since this would place the kingpin on the outer side of the wheel. Hence, one of the parameters r, τ, σ has to be negative while the other two are positive. Among these alternatives, only a negative caster angle τ satisfies the second condition stated in Eq. (2.26b). Extending these considerations to the case where the parameters are allowed to take a value of zero, the conditions can only be satisfied for $n = \tau = 0$ while $r > 0$ and $\sigma > 0$ or $r = \sigma = 0$ while $n > 0$ and $\tau < 0$. In the outcome, under consideration of the design constraints the conditions, Eq. (2.26) are equivalent to

$$|\sigma n| = |\tau r|, \quad n \geq 0, r \geq 0, \sigma \geq 0, \tau \leq 0. \qquad (2.28)$$

According to Eq. (2.5c), for a rear axle the negative caster angle leads to a camber directed to the inside of a turn during cornering, thus improving the cornering stability.

In commercial vehicles, a pressure change in the pneumatic suspension tilts the axle including the attached kingpins. As a result, the caster angle can vary considerably, displacing the minimum of the potential energy. It is further possible that design constraints oppose the implementation of Eq. (2.26a). Still, the interaction between both wheels via a track rod can sustain a self-centring action. The first-order Taylor approximation of the total potential energy of such a system is given by

$$
\begin{aligned}
E_{\text{pot},2}(\delta^*) = &\left[\sigma_l \left(n_l \sin \delta^* + r_l (1 - \cos \delta^*) \right) \right. \\
&\left. + \tau_l \left(r_l \sin \delta^* - n_l (1 - \cos \delta^*) \right) \right] F_{z,l} \\
&- \left[\sigma_r \left(n_r \sin \delta^* + r_r (\cos \delta^* - 1) \right) \right. \\
&\left. + \tau_r \left(r_r \sin \delta^* - n_r (\cos \delta^* - 1) \right) \right] F_{z,r}.
\end{aligned}
\tag{2.29}
$$

As defined in Section 2.1.2, the asterisk refers to the mutual sign convention and the indices l and r refer to the left- and right-hand wheel, respectively. Assuming an identical geometry and wheel load on both sides, the total potential energy of both suspensions always has a stationary point at a steering angle of zero. Since the sum of two convex functions is convex, this point is a minimum if Eq. (2.26b) holds. Depending on its direction, the load transfer during cornering can limit the robustness of this effect.

2.3.2 Steering Control

As introduced in Section 2.3.1, potential energy in the suspension can be gained or lost as a function of the steering angle. The shape of this function is determined by the steering geometry. Section 2.3.1 discussed the utilization of this effect for a self-centring of the steering. For this purpose, a static geometry was designed such that the minimum of the potential energy occurs at a steering angle of zero.

Obviously, a variable geometry could be used to modify the potential energy function. A steering torque in the desired direction could be obtained and used to control the steering angle. This torque would only depend on the geometry and the wheel load. No external forces acting at the kingpin would be needed. The self-steering properties would persist, such that a geometry change would only be required if the desired steering angle differs from the self-steering behaviour.

The downside of this approach is obvious: If potential energy is lost during steering, it must be gained when returning to the initial position. The following Section 2.4 discusses a possible conservation of this energy, such that the actuation energy is minimized. The present section addresses the fundamental question of how a variable ge-

ometry can be used to control the steering angle, based on the preliminary assumption that the parameters of the steering geometry can be influenced arbitrarily.

To obtain a steering torque of the vertical wheel forces, the potential energy must show a negative gradient in the desired steering direction. Using the theoretical basis established in Section 2.3.1, Eq. (2.25b) leads to the conditions for a single wheel

$$\text{Steering to the outside:} \quad \sigma n < -\tau r \qquad\qquad (2.30\text{a})$$

$$\text{Steering to the inside:} \quad \sigma n > -\tau r \qquad\qquad (2.30\text{b})$$

For these conditions, all high-order terms are neglected and the gradient is evaluated at a steering angle of zero. Due to the nonlinearity of the potential energy function, the inequality must be sufficiently large to maintain the sign of the gradient over the complete range of steering. Using the generalized sign convention defined in Section 2.1.2, Eq. (2.30) divides the direction into outside and inside instead of left and right. For the left-hand wheel, steering to the outside is steering to the left, while steering to the inside is steering to the right. The condition for steering to the left for the left-hand wheel is the condition for steering to the right for the right-hand wheel and vice versa. For a parallel steering of both wheels, the geometry of one wheel needs to be changed opposite to the other.

If both wheels of an axle are connected by a track rod, the steering is determined by the total potential energy of left- and right-hand wheel, Eq. (2.29). Analogously to the derivation for the single wheel, conditions for the steering of the axle can be obtained from the first derivative of the total potential energy. This process extends Eq. (2.30) to

$$\text{Steering to the left:} \quad \sigma_l n_l - \sigma_r n_r < \tau_r r_r - \tau_l r_l, \qquad (2.31\text{a})$$

$$\text{Steering to the right:} \quad \sigma_r n_r - \sigma_l n_l < \tau_l r_l - \tau_r r_r, \qquad (2.31\text{b})$$

where the index l refers to the left-hand wheel and r to the right-hand wheel. In these simplified conditions, the load on both wheels is assumed to be equal. Whether the load shift supports or reduces the steering depends on the speed and the steering angle.

These conditions hold for both forward and reverse travel. However, in the initial geometry the signs of n and τ change with the direction of travel.

One advantage of the steering approach is its relation to the wheel load. The torque due to the vertical wheel forces is proportional to the load. As discussed in Section 2.2, the cornering forces of a truck tyre and the related torque also increase almost linearly with the load. The steering mainly results from the sum of these two torques. Since their dependence on the load is similar, the steering behaviour can be expected to show a small sensitivity towards the vehicle load.

From the point of view of mechanical design, a rotary degree of freedom intended to influence the caster or kingpin angle is clearly more feasible than a linear one related

to caster or kingpin offset. The direction in which these angles have to be changed to obtain the desired steering direction can be seen from Eq. (2.30) or Eq. (2.31). For the caster angle, the direction depends on the sign of the kingpin offset, while for the kingpin angle it depends on the sign of the caster offset. For both positive caster and kingpin offset, steering to the left, for instance, can be obtained by changing the caster and/or the kingpin angle of the left-hand wheel into the negative direction.

It seems reasonable to place the degree of freedom approximately at axle level. However, any tilt of the kingpin with a centre of rotation above road level has an impact on the caster or kingpin offset as well, as illustrated in Fig. 2.1. A change of the caster angle in the positive or negative direction influences the caster offset in the same direction. In contrast, the kingpin offset changes against the kingpin inclination. Whether these interrelations support or oppose the steering depends on the signs of the parameters and is determined by Eq. (2.30) or Eq. (2.31). Thus, a geometry should be chosen that exploits these effects to improve the steering. This benefit is given for a self-centring geometry in compliance with Eq. (2.28), for instance.

Depending on the design selected, the interrelation between the parameters may be more complex. For instance, a rotation of the kingpin around the main axis of the axle primarily changes the caster angle and offset. However, in the case of a non-zero kingpin inclination, it further has a minor effect on the kingpin inclination and offset that counteracts the steering. Still, such undesired effects can be accepted in favour of mechanical simplicity.

A change of kingpin and caster offset influences the lever arm of the longitudinal and lateral wheel forces. The latter is of particular importance. The torque due to caster and lateral force steers towards the angle of zero side-slip. If a different steering angle is desired, this torque acts against the torque of the vertical forces. Hence, a decrease of the caster offset supports the desired steering, whereas an increase opposes it. As mentioned above, for a parallel steering of both wheels, the geometry of one wheel needs to be changed opposite to the other. Hence, the caster of one wheel needs to be decreased, while the caster of the other wheel needs to be increased. Due to the relation to the lateral forces, rotating the kingpin with a decreasing caster has a much greater effect on the steering than rotating the kingpin with the increasing caster. Therefore, if both wheels are connected by a track rod, rotating only the kingpin with a decreasing caster is more efficient than rotating both. Even more, if the caster offset of the rotated kingpin is decreased beyond zero, the sign of the lateral force torque of that wheel changes. The feedback becomes positive, such that instead of opposing the desired steering, it starts to support it. Since the second wheel still has a positive caster offset that creates an opposing torque, the stability of the steering can be maintained. This effect has a key impact. Under idealized assumptions, it allows arbitrarily large steering angles to be obtained and makes the caster angle a much more powerful input than the kingpin angle.

The steering behaviour is affected by numerous further effects, such as the change

of caster and camber during steering or the load transfer. Though they are far less fundamental for the design than the effects mentioned above, their existence should not be ignored.

Depending on design constraints and priorities, the approach proposed can be translated into many different designs. The key points are the conditions Eqs. (2.30) and (2.31). The resulting steering system can be more or less effective, depending on the extent to which the interrelations of the parameters and the effect on the lever arm of the tyre forces are to be exploited. Without excluding any alternative solutions, the considerations listed above on these issues can be summarized in the suggestion of a steering system with the following properties:

1. A degree of freedom that rotates the kingpin in the longitudinal plane, placed approximately at axle level.

2. From the initial position, the rotation can be limited to the direction towards the front of the vehicle.

3. Both kingpins are allowed to rotate independently.

4. The wheels are connected by a track rod.

5. The steering geometry in the initial position satisfies

$$|\sigma n| = |\tau r|, \quad n \geq 0, r \geq 0, \sigma \geq 0, \tau \leq 0, \tag{2.32a}$$

   providing independent self-centring for each wheel, or

$$\tau n < \sigma r, \quad n \geq 0, r \geq 0, \sigma \geq 0, \tag{2.32b}$$

   for self-centring via the interaction of the wheels.

Given these properties, steering to the left can be obtained by rotating the kingpin of the left-hand wheel towards the direction of travel while the right-hand kingpin remains non-rotated. In analogy, rotating the right-hand kingpin steers to the right. Hence, the rotation is always at the wheel that steers to the outside. The system thus exploits the effect of a decreasing caster on the torque of the lateral tyre forces. The caster angle is utilized as a primary input, with an interrelation to the caster offset. The conditions on the geometry in the initial position guarantee both that this interrelation supports the steering and that the geometry is self-centring, see Section 2.3.1. For a rear-axle steering, a negative caster angle provides the advantage of a camber that improves the cornering stability. The caster degree of freedom is already required in state-of-the-art systems that allow a stable self-steering during reverse travel, as illustrated in Fig. 2.1. To change the direction of travel, both kingpins need to be co-rotated towards the old direction of travel, thus creating a positive caster for the new
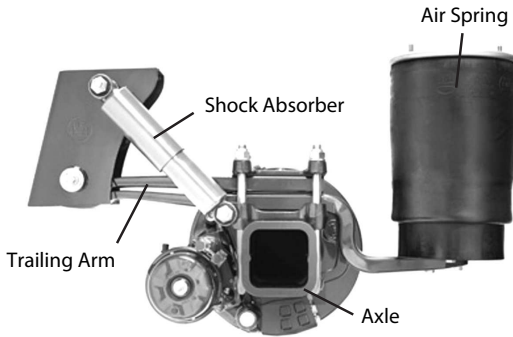
Figure 2.13: State-of-the-art semi-trailer suspension. *Image courtesy BPW Bergische Achsen KG. Source: Alberding et al. (in press), ©IEEE.*

direction of travel. For the steering control proposed, the only additional requirement towards the reverse-travel problem is to rotate the casters of the left- and the right-hand wheel independently of each other.

2.4 Conservation of Energy

The previous section analyses a variable geometry and investigates the way in which it can be used to control the steering angle. The approach introduced is based on the potential energy of the steering system. As mentioned, the downside of this approach is obvious: If potential energy is lost during steering, it must be gained when the steering is returned to the initial position. In the worst case, this energy must be provided by an actuation where the mechanism would require the same power as a command steer system. However, there is only little dissipation during steering. It might be feasible to conserve most of the potential energy within the system, leaving a minimal demand for actuation energy. This section investigates this issue.

2.4.1 Steering Mechanism

Figure 2.13 shows a state-of-the-art semi-trailer suspension. In this setup, by design the axle enables the trailing arms to absorb any torsion, impeding an independent caster variation. Hence, if the suspension is not to be changed, any implementation requires a rotational degree of freedom between kingpin and axle. A re-design of the existing suspension, in particular the use of an independent wheel suspension, obviously promises opportunities to find an economically more competitive solution. Such an optimized design is beyond the scope of this work, however.
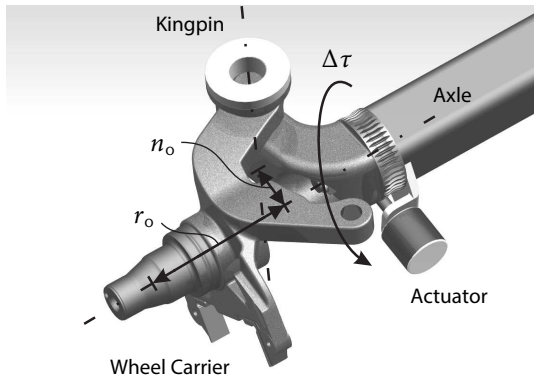
Figure 2.14: Preliminary steering mechanism. *Source: Alberding et al. (in press), ©IEEE.*

Embedded in the state-of-the-art suspension, the preliminary steering mechanism shown in Fig. 2.14 is considered for the following analysis. The analysis can be adapted to any other steering mechanism.

The mechanism is designed to satisfy all conditions suggested at the end of the previous section. Thus, the left-hand kingpin is rotated towards the direction of travel to steer to the left, while the right-hand kingpin is rotated to steer to the right. Hence, the rotation is always at the wheel that steers to the outside. For that purpose, a revolute joint is placed between the axle beam and the kingpin. A low-power actuator, such as a DC motor or a pneumatic cylinder, allows the rotation to be influenced. This actuation is also used to co-rotate both kingpins for a change of the direction of travel.

The axis of rotation intersects the wheel in its centre. Hence, at a steering angle of zero the joint does not experience any load torque of the lateral and vertical tyre forces. Alternatively, the joint could be placed slightly towards the rear. The vertical wheel forces would thus generate a torque that stabilizes the initial position.

A non-zero steering angle moves the contact point of the vertical wheel forces out of the vertical plane through the axis of rotation, causing these forces to create a load torque. A negative caster angle leads to a steering to the outside, while a steering to the outside leads to a torque in the joint in the negative caster direction. The system has a positive feedback, an increase of the steering angle is supported, while a decrease is opposed.

To balance the load torque and to conserve the potential energy within the system, the design includes a spring-like element in the joint with characteristics that are yet to be defined.

Such a spring-like element should act with respect to the relative rotation of both

kingpins, allowing the zero position of the spring to change with the direction of travel. During cornering, it is recommendable to lock the non-rotated joint of the wheel that steers to the inside to bind one end of the spring to the axle. For this purpose, the rotational degree of freedom should incorporate a locking mechanism or self-locking properties.

Braking forces generate a torque that is directed to change the caster of both wheels in the negative direction. If the non-rotated joint is locked, braking is thus a disturbance that increases the steering angle. Assuming the maximum negative caster to be sufficiently limited, the steering remains stable. The following analysis considers the undisturbed system of free rolling tyres.

The initial geometry of the system is assumed to have self-centring properties as discussed in Section 2.3.1. Furthermore, a possible additional spring-like centring device attached to the kingpin is incorporated.

Attention should be paid to the negative caster of the rotated kingpin in its maximum position. This must not exceed the positive caster of the non-rotated kingpin. Otherwise it is almost inevitable that the torque due to the lateral wheel forces changes its sign, rendering the system unstable. Since the pneumatic trail always offsets the caster in the positive direction, assuming moderate side-slip, it is possible to design the maximum negative caster smaller than the positive caster for both directions of travel.

The mechanism can be parametrized by the wheel-centre caster offset in the initial position n_o, the wheel-centre kingpin offset in the initial position r_o, the caster angle in the initial position τ_o, and the kingpin inclination in the initial position σ_o. The joint angle is the deviation of the caster angle from the initial position in the negative direction, denoted by $\Delta\tau$. Hence, a positive value of $\Delta\tau$ is associated to a positive steering angle. For these definitions, the characteristics of the steering geometry are given as functions of $\Delta\tau$ by

$$\tau(\Delta\tau) = \tau_o - \Delta\tau, \tag{2.33a}$$

$$n(\Delta\tau) = \frac{n_o \cos\tau_o + \rho \sin(\tau_o - \Delta\tau)}{\cos(\tau_o - \Delta\tau)}, \tag{2.33b}$$

$$\sigma(\Delta\tau) = \arctan\left(\frac{\tan(\sigma_o) \cdot \cos(\tau_o)}{\cos(\tau_o - \Delta\tau)}\right), \tag{2.33c}$$

$$r(\Delta\tau) = r_o + (n_o \sin(\Delta\tau) - \rho) \cdot \tan(\sigma(\Delta\tau)). \tag{2.33d}$$

The steering angle is further split in two parts

$$\delta = \delta_o + \Delta\delta, \tag{2.34}$$

where δ_o denotes the steering angle with zero side-slip, i.e., the steering angle of an idealized self-steering.

2.4.2 Side-Slip Angle

Before addressing the steering mechanism, a relationship between $\Delta\delta$ and the cornering forces needs to be derived.

For a single-track model of a three-axle semi-trailer, the torque balance about the fifth wheel coupling at the steady state of the vehicle is given by

$$2C_{\alpha,1}a_1\alpha_1^* + 2C_{\alpha,2}a_2\alpha_2^* + 2C_\alpha a\alpha^* = lma_y. \tag{2.35}$$

The side-slip angles of the non-steering axles are denoted by α_i, $i = 1, 2$, while the cornering stiffness is represented by $C_{\alpha,i}$. The steering axle has a distance a to the fifth wheel. For the non-steering axles, this distance is denoted by a_i. The distance between the fifth wheel and the centre of gravity of the trailer is represented by l, the articulation angle by Γ, the radius of curvature by R, the lateral acceleration at the centre of gravity of the trailer by a_y and the trailer mass by m.

The geometric parametrization is illustrated in Fig. 2.15. Since it is related to the vehicle, the derivation uses the mutual sign convention for both wheels denoted by an asterisk, see Section 2.1.2.

The side-slip angles, the steering angles δ_o^*, $\Delta\delta^*$, and the articulation angle are assumed to be small.

This leads to the relationships

$$\alpha_i^* = \frac{a_i}{R} - \Gamma, \tag{2.36a}$$

$$\alpha^* = \frac{a}{R} - \Gamma - \delta_o^* - \Delta\delta^*. \tag{2.36b}$$

By definition in Eq. (2.34) the side-slip angle of the steering axle is zero for $\Delta\delta = 0$. Using Eqs. (2.35) and (2.36), this leads to
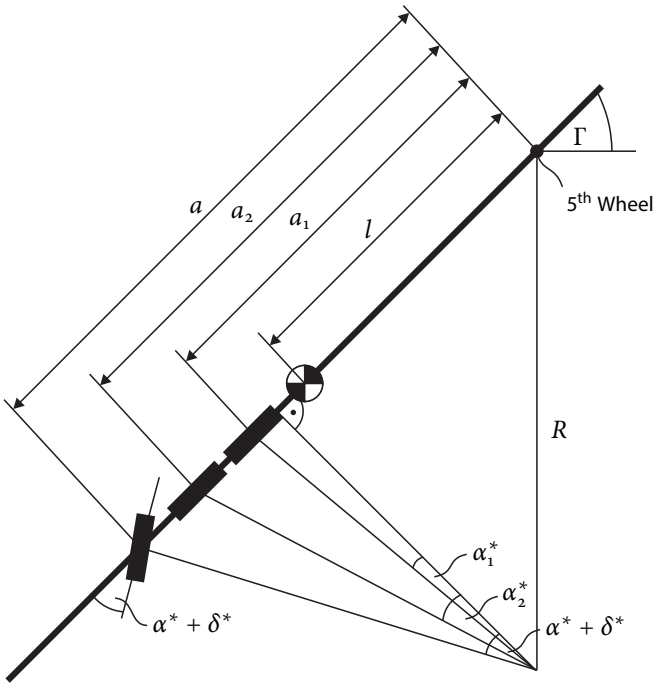
$$\delta_o^* = \left(\frac{a(2C_{\alpha,1}a_1 + 2C_{\alpha,2}a_2)}{2C_{\alpha,1}a_1^2 + 2C_{\alpha,2}a_2^2 - lma_yR} - 1 \right)\Gamma_o, \tag{2.37}$$

where Γ_o denotes the articulation angle at steering angle δ_o^*. Again using Eqs. (2.35) and (2.36), it is related to an articulation angle Γ with non-zero α^* by

$$\Gamma_o = \Gamma - \frac{C_\alpha a}{C_{\alpha,1}a_1 + C_{\alpha,2}a_2}\alpha^*. \tag{2.38}$$

Combining Eqs. (2.35) to (2.38) yields

$$\alpha^* = -k_\alpha\Delta\delta^*, \quad k_\alpha := \frac{C_{\alpha,1}a_1 + C_{\alpha,2}a_2}{C_{\alpha,1}a_1 + C_{\alpha,2}a_2 + C_\alpha a}. \tag{2.39}$$

Figure 2.15: Geometric parametrization of the single track model. *Source: Alberding et al. (in press), ©IEEE.*

Assuming equal cornering coefficients and loads for the three axles, the value of k_α only depends on the geometry

$$k_\alpha = \frac{a_1 + a_2}{a_1 + a_2 + a}.$$

(2.40)

A change of the mutual sign convention to the individual sign convention leads for the right-hand wheel to a sign change of all variables marked by an asterisk. Since both sides of Eq. (2.39) contain such a factor, it can be transformed to the individual convention without any changes,

$$\alpha = -k_\alpha \Delta\delta.$$

(2.41)

Hence, for a positive caster, the steady-state side-slip angle of the steering axle creates a steering torque that opposes the steering difference $\Delta\delta$. This spring-like behaviour is intuitively reasonable, since steering and vehicle always return to the self-steering state when an additional steering torque is withdrawn.

2.4.3 Linear Analysis

As discussed in Section 2.2, the tyre forces are modelled to attack in two contact points. The cornering force $\mathbf{F}_{y,\alpha}$ attacks in C, while the vertical force $\mathbf{F}_z$ and the camber thrust $\mathbf{F}_{y,\gamma}$ attack in N.

$$\mathbf{F}_C^F = \begin{pmatrix} 0 \\ F_{y,\alpha} \\ 0 \end{pmatrix}, \quad \mathbf{F}_C^I = \mathbf{R}_{IF}\mathbf{F}_C^F, \quad \mathbf{F}_C^B = \mathbf{R}_{IB}^{\mathrm{T}}\mathbf{F}_C^I,$$

(2.42a)

$$\mathbf{F}_N^F = \begin{pmatrix} 0 \\ F_{y,\gamma} \\ F_z \end{pmatrix}, \quad \mathbf{F}_N^I = \mathbf{R}_{IF}\mathbf{F}_N^F, \quad \mathbf{F}_N^B = \mathbf{R}_{IB}^{\mathrm{T}}\mathbf{F}_N^I.$$

(2.42b)

The vectors to the contact points $\mathbf{r}_C$ and $\mathbf{r}_N$ are given by Eq. (2.22).

The resulting torque about the kingpin axis is

$$
\begin{aligned}
M_{\delta,F} &= \mathbf{z}_B^{B^{\mathrm{T}}} \left(\mathbf{r}_C^B \times \mathbf{F}_C^B \right) + \mathbf{z}_B^{B^{\mathrm{T}}} \left(\mathbf{r}_N^B \times \mathbf{F}_N^B \right) \\
&= \det \left(\mathbf{z}_B^B \quad \mathbf{r}_C^B \quad \mathbf{F}_C^B \right) + \det \left(\mathbf{z}_B^B \quad \mathbf{r}_N^B \quad \mathbf{F}_N^B \right).
\end{aligned}
$$

(2.43)

The mechanism is designed such that for a steering angle of zero the joint axis intersects the rim centre plane in the wheel centre. Naming the wheel centre for a steering angle zero J,

$$\mathbf{r}_J^I = \begin{pmatrix} -n \\ r \\ \rho \end{pmatrix},$$

(2.44)

the joint torque is given by

$$M_{\tau,F} = \det\begin{pmatrix} \mathbf{y}_I^I & \mathbf{r}_C^I - \mathbf{r}_J^I & \mathbf{F}_C^I \end{pmatrix} + \det\begin{pmatrix} \mathbf{y}_I^I & \mathbf{r}_N^I - \mathbf{r}_J^I & \mathbf{F}_N^I \end{pmatrix}, \tag{2.45}$$

where $M_{\tau,F}$ is defined positive in the direction of a positive value of $\Delta\tau$, i.e., a negative value of τ.

A centring device with load-dependent stiffness $c_\delta F_z$, $c_\delta \geq 0$ is assumed to be mounted at the kingpin. Further, a torsional spring-like element with load-dependent stiffness $c_\tau F_z$, $c_\tau > 0$ is assumed to be acting in the revolute joint. The torque of this element is zero for $\Delta\tau = 0$.

As discussed in Section 2.3, due to the caster reduction, it is preferable to rotate only the kingpin of the wheel that steers to the outside. In the following analysis, the joint angle $\Delta\tau$, the joint torque M_τ, the vertical force F_z, and the sign convention are related to this wheel. As introduced in Section 2.1.2, the steering angle and the torque M_δ are defined positive for steering to the outside and negative for steering to the inside. Due to the track rod, the torques of both kingpins are combined to a mutual torque M_δ, its sign convention chosen with respect to the wheel with the rotated kingpin. The steering angles of both wheels are assumed to be identical.

The load transfer depends on both steering angle and speed. Since the latter effect cannot be included in the spring design, the load transfer is not taken into account. The vertical force on the wheel with the non-rotated kingpin is assumed to be identical to the vertical force of the wheel with the rotated kingpin.

Equations (2.33), (2.34), (2.43) and (2.45) yield $M_{\delta,F}$ and $M_{\tau,F}$. The total torque M_δ about the kingpin and the total joint torque M_τ are the sums of the torques due to the tyre forces and the torques due to the spring-like elements.

Assuming small angles $\Delta\tau, \Delta\delta, \delta_o, \tau_o, \sigma_o$, the torques in the kingpin and the joint can be formulated using a first-order Taylor approximation,

$$M_\delta(\Delta\tau, \Delta\delta, \delta_o) = -2\theta F_z \Delta\delta - 2c_\delta F_z \delta_o + r_o F_z \Delta\tau, \tag{2.46a}$$
$$M_\tau(\Delta\tau, \Delta\delta, \delta_o) = r_o F_z \Delta\delta + r_o F_z \delta_o - c_\tau F_z \Delta\tau, \tag{2.46b}$$

where the constant $\theta > 0$ is introduced to simplify the notation, defined by

$$\theta := (n_o + n_R)k_\alpha C_{\alpha,o} + c_\delta. \tag{2.47}$$

The constant $k_\alpha > 0$ was defined in Eq. (2.40). As expected, the cornering forces create a torque about the kingpin via the caster that opposes the desired steering. The vertical force balances this torque with a lever arm determined by r_o. The load torque in the revolute joint arises due to the wheel centre showing a longitudinal offset towards the axle as the steering angle increases. Since this load torque is also determined by r_o, it clearly cannot be avoided without losing the steering torque at the kingpin. Similarly to a gear ratio, r_o balances the load torque and the required range of rotation.
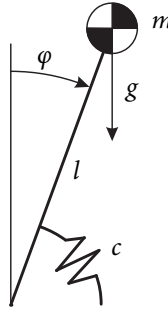
Figure 2.16: Inverted pendulum. *Source: Alberding et al. (in press), ©IEEE.*

The steady state steering angle is determined by the equilibrium of M_δ. Hence, the relationship between steering angle and joint angle is given by

$$\Delta\delta(\Delta\tau, \delta_o) = \frac{r_o}{2\theta}\Delta\tau - \frac{c_\delta}{\theta}\delta_o. \tag{2.48}$$

Since $\theta > 0$, a positive value of $\Delta\tau$ is associated with a positive value of $\Delta\delta$. As expected, a change of the caster angle in the negative direction creates a steering to the outside.

The spring-like element in the revolute joint is intended to maintain M_τ in an equilibrium. This idea can be illustrated by the analogy of an inverted pendulum, as shown in Fig. 2.16. There, an equilibrium of the linearized torque balance

$$c\varphi = mgl \sin\varphi \approx mgl\varphi \tag{2.49a}$$

can be maintained by a spring

$$c = mgl. \tag{2.49b}$$

Under idealized assumptions, in any position of the pendulum close to the upright position the gravitation is balanced by the spring and the pendulum remains at rest. This result is confirmed by the energy balance

$$\frac{1}{2}mgl\varphi^2 = mgl(1 - \cos\varphi) \approx \frac{1}{2}mgl\varphi^2. \tag{2.49c}$$

This idea can be extended to the nonlinear case and to large pendulum angles by designing a nonlinear spring.

For now, the value of δ_o is assumed to be zero. Analogously to the inverted pendulum, the equilibrium thus can be achieved by designing the spring

$$c_\tau = \frac{r_o^2}{2\theta}. \tag{2.50}$$

Hence, under the assumptions made, for every $\Delta\tau$ there exists a $\Delta\delta$ such that both kingpin and joint are in an equilibrium. No external torque is required to maintain this position. In this idealized setup, the steering angle can be changed by rotating the joint without any opposing torque, while the wheels experience significant cornering forces. The only premise is a spring-like element in the revolute joint with the spring constant of Eq. (2.50).

This result can be confirmed by the energy balance. Potential energy is released by the height change and stored in the spring-like elements and the spring-like behaviour of steering and vehicle. The latter was discussed in Section 2.4.2. If no further actuation energy is required, the energy balance in the steady state must be

$$\theta F_z \Delta\delta^2 + \frac{1}{2} c_\tau F_z \Delta\tau^2 = E_{\text{pot},2}(\Delta\delta, \Delta\tau), \tag{2.51}$$

where $E_{\text{pot},2}$ denotes the total potential energy of both wheels, see Eq. (2.29). Using Eqs. (2.48) and (2.50), this equation yields

$$E_{\text{pot},2}(\Delta\delta, \Delta\tau) = -r_\text{o} F_z \Delta\delta \Delta\tau, \tag{2.52}$$

equating the second order Taylor approximation of $E_{\text{pot},2}$ using Eqs. (2.23) and (2.24).

The energy is distributed equally on vehicle state and the spring, with $\frac{1}{2} r_\text{o} \Delta\delta \Delta\tau$ each. Without the spring, this amount of energy would be required to return the steering to its initial position. Exactly the same amount of energy would be needed by a command steer system to obtain $\Delta\delta$.

The interaction between the two wheels is not necessary to obtain an equilibrium. For a single wheel, the main difference is the fact that the terms with $\Delta\delta$ and δ_o in M_δ, Eq. (2.46), are halved. This doubles the ratio that determines $\Delta\delta(\Delta\tau)$, Eq. (2.48), and the spring constant, Eq. (2.50). The torque M_τ is not affected, not for $\delta_\text{o} \neq 0$ either, as discussed in the next paragraph. The energy is still distributed equally on the vehicle state and the spring at $\frac{1}{2} r_\text{o} \Delta\delta \Delta\tau$ each.

The previous analysis considered a simplified case. It assumes that the vehicle initially travels straight ahead, i.e. $\delta_\text{o} = 0$. Now, this assumption is abandoned. For a torque equilibrium in the kingpin and the spring constant Eq. (2.50), the load torque in the revolute joint follows by

$$M_\tau(\delta_\text{o}) = r_\text{o} \left(1 - \frac{c_\delta}{\theta} \right) F_z \delta_\text{o}. \tag{2.53}$$

Hence, for a non-zero value of δ_o, the joint no longer is in an equilibrium. For positive values of n_o and r_o, this torque has the sign of δ_o. Hence, it is directed to further increase the joint angle. This effect supports to obtain a larger steering angle. However, for a smaller steering angle, this torque would have to be compensated by an actuation. There is a fundamental difference towards command steer: the load torque increases

with δ_o, the initial state of the steering, and does not depend on $\Delta\delta$, the final state of the steering. For a command steer approach, these roles are reversed.

Equation (2.37) shows that at low speed δ_o is proportional to the articulation angle, under the assumption that the latter is small. Also, the desired steering angle of command steer systems is typically chosen to be proportional to the articulation angle (Jujnovich & Cebon 2002). Hence, such command steer behaviour could be obtained by maintaining a constant ratio between δ_o and $\Delta\delta$

$$\delta_\mathrm{o} = k_\delta \Delta\delta, \tag{2.54}$$

where k_δ is determined by Eq. (2.37) and the control law for the desired steering angle. The steering angle of self-steering thus is amplified by the factor k_a,

$$\delta = k_a \delta_\mathrm{o}, \quad k_a = k_\delta^{-1} + 1. \tag{2.55}$$

These considerations can be used to take the spring design described above one step further. Equation (2.54) leads to

$$\Delta\delta(\Delta\tau) = \frac{r_\mathrm{o}}{2(\theta + k_\delta c_\delta)} \Delta\tau, \tag{2.56}$$

resulting in a spring

$$c_\tau = \frac{r_\mathrm{o}^2(1 + k_\delta)}{2(\theta + k_\delta c_\delta)}. \tag{2.57}$$

Both are generalizations of Eqs. (2.48) and (2.50). The case $\delta_\mathrm{o} = 0$ is included by choosing $k_\delta = 0$. Non-zero values of k_δ show one significant difference from Eqs. (2.48) and (2.50), where it was possible to obtain arbitrary values of $\Delta\delta$ without any load torque as long as $\delta_\mathrm{o} = 0$ holds. For a spring designed for non-zero k_δ, there is only a single equilibrium, which is associated with $\Delta\delta = k_\delta^{-1}\delta_\mathrm{o}$.

Using Eq. (2.48), the value of $\Delta\tau$ for which Eq. (2.54) holds is given by

$$\Delta\tau_\mathrm{ref}(\delta_\mathrm{o}) = \frac{2(k_\delta^{-1}\theta + c_\delta)}{r_\mathrm{o}} \delta_\mathrm{o}. \tag{2.58}$$

Without actuation or locking and assuming the rotation to be damped, the joint dynamics are described by

$$J\Delta\ddot{\tau} = M_\tau(\Delta\tau, \Delta\delta, \delta_\mathrm{o}) - D\Delta\dot{\tau}, \tag{2.59}$$

where J denotes the moment of inertia of the joint and D the damping coefficient. Assuming the kingpin dynamics to be quasi-static and combining Eqs. (2.46), (2.48), (2.57) and (2.59) yields the error dynamics

$$\begin{pmatrix} \Delta\dot{\tilde{\tau}} \\ \Delta\ddot{\tilde{\tau}} \end{pmatrix} = \begin{pmatrix} 0 & 1 \\ -\frac{r_\mathrm{o}^2 k_\delta(\theta - c_\delta)F_z}{2J\theta(\theta + k_\delta c_\delta)} & -DJ^{-1} \end{pmatrix} \begin{pmatrix} \Delta\tilde{\tau} \\ \Delta\dot{\tilde{\tau}} \end{pmatrix}, \tag{2.60}$$

where $\Delta\tilde{\tau} = \Delta\tau_{\mathrm{ref}} - \Delta\tau$ denotes the control error. For $k_\delta > 0$, the eigenvalues of the system matrix are in the left half plane and the error dynamics are asymptotically stable. The spring Eq. (2.57) acts as a mechanical controller, attracting the steering to Eq. (2.54).

Combining Eqs. (2.55) and (2.56) can be used to determine the required maximum joint angle $\Delta\tau_{\max}$ for a given maximum steering angle $\delta_{\max}$ and a desired steering amplification k_a

$$\Delta\tau_{\max} = \frac{2\left(\theta(k_a - 1) + c_\delta\right)}{r_{\mathrm{o}} k_a} \delta_{\max}. \tag{2.61}$$

As discussed in Section 2.4.4, in the nonlinear case the steering angle shows a convex growth, see Eq. (2.65). Hence, Eq. (2.61) is a conservative estimate that provides an upper bound for the required range of rotation.

2.4.4 Nonlinear Analysis

In the previous section first-order Taylor approximations were used for the analysis and to introduce the spring design. Due to the nonlinear nature of the system, the linear springs Eq. (2.50) or Eq. (2.57) generally are suitable only for small steering angles. A spring design suitable for the complete steering range needs to take the nonlinearities of the plant into account, even if a spring with linear characteristics is to be utilized.

The idea to maintain an equilibrium such as Eq. (2.54) can be extended to the nonlinear case. A numerical approach is used to obtain the nonlinear spring characteristics, which proved to be more effective than an analytic solution of higher-order Taylor approximations.

To study the behaviour of the system, consider the second-order Taylor approximations with respect to $\Delta\tau$, $\Delta\delta$, δ_{o}, τ_{o}, σ_{o},

$$M_\delta(\Delta\tau, \Delta\delta, \delta_{\mathrm{o}}) = -2\left(\xi\Delta\delta + \xi_{\mathrm{o}}\delta_{\mathrm{o}}\right) F_z + \left(r_{\mathrm{o}} + \eta\Delta\delta + \eta_{\mathrm{o}}\delta_{\mathrm{o}}\right) F_z \Delta\tau, \tag{2.62a}$$

$$M_\tau(\Delta\tau, \Delta\delta, \delta_{\mathrm{o}}) = \left(r_{\mathrm{o}} + \zeta\Delta\delta + \zeta_{\mathrm{o}}\delta_{\mathrm{o}}\right)\left(\Delta\delta + \delta_{\mathrm{o}}\right) F_z - c_\tau F_z \Delta\tau, \tag{2.62b}$$

where

$$\xi_{\mathrm{o}} := c_\delta + \eta_{\mathrm{o}}\tau_{\mathrm{o}} + r_{\mathrm{o}}\sigma_{\mathrm{o}}, \qquad\qquad \xi := \theta + \eta\tau_{\mathrm{o}} + r_{\mathrm{o}}\sigma_{\mathrm{o}}, \tag{2.63a}$$

$$\eta_{\mathrm{o}} := n_{\mathrm{o}}\left(k_\gamma C_{\alpha,\mathrm{o}} - 1\right), \qquad\qquad \eta := \eta_{\mathrm{o}} + \kappa, \tag{2.63b}$$

$$\zeta_{\mathrm{o}} := -\frac{1}{2} n_{\mathrm{o}}, \qquad\qquad\qquad \zeta := \zeta_{\mathrm{o}} + \kappa, \tag{2.63c}$$

$$\kappa := k_\alpha C_{\alpha,\mathrm{o}}\left(\rho + \frac{F_{z,\mathrm{o}}}{c_y}\right). \tag{2.63d}$$

The constant θ was defined in Eq. (2.47).

Considering the steering angle relationship Eq. (2.54) and defining

$$\tilde{\xi} := \xi + k_\delta \xi_o, \quad \tilde{\eta} := \eta + k_\delta \eta_o, \quad \tilde{\zeta} := \zeta + k_\delta \zeta_o, \tag{2.64}$$

the equilibrium of Eq. (2.62a) yields

$$\Delta\delta(\Delta\tau) = \frac{r_o \Delta\tau}{2\tilde{\xi} - \tilde{\eta}\Delta\tau}, \tag{2.65}$$

determining via Eq. (2.62b) the joint torque

$$M_\tau(\Delta\tau) = (1 + k_\delta)\frac{r_o \Delta\tau}{2\tilde{\xi} - \tilde{\eta}\Delta\tau}F_z\left(r_o + \tilde{\zeta}\frac{r_o \Delta\tau}{2\tilde{\xi} - \tilde{\eta}\Delta\tau}\right) - c_\tau \Delta\tau F_z. \tag{2.66}$$

For $c_\tau = 0$, both the steering angle, Eq. (2.65), and the joint torque, Eq. (2.66), show a convex growth towards a singularity at

$$\Delta\tau = \frac{2\tilde{\xi}}{\tilde{\eta}}. \tag{2.67}$$

As discussed in Section 2.3.2, the torque due to the vertical forces is directed to amplify the steering angle. As its counterpart, the torque due to the lateral forces is directed to restore the self-steering angle δ_o. The caster-based steering mechanism was designed to maximize its impact by both increasing the former and decreasing the latter. Simplified, the singularity Eq. (2.67) is related to the effect of the increasingly negative caster of the rotated kingpin exceeding the effect of the positive caster of the non-rotated kingpin. As introduced in Section 2.4.1, without spring or actuation, the steering mechanism would possess a positive feedback, attracting the steering towards the singularity.

Extending the approach presented in Section 2.4.3 to the nonlinear case prevents the instability of the system. Figure 2.17 shows the nonlinear spring designed to stabilize the steering in the equilibrium Eq. (2.54) for an exemplary case and its least-squares linear approximation. Due to the convex growth of the joint torque, the nonlinear spring characteristics are always progressive. The curvature is mainly influenced by the geometry.

Hence, a linear spring is generally too stiff for small angles and too soft for large angles. To guarantee a unique stable equilibrium, the joint torque must always change to the negative direction for an increasing joint angle. Since a linear spring is too soft for large angles, in this region the torque changes to the positive direction, creating a second, unstable equilibrium. As illustrated in Fig. 2.18 for the least-squares approximation shown in Fig. 2.17, without actuation this can lead to a hysteresis in the steering behaviour. As the value of δ_o increases, $\Delta\tau$ grows rapidly to its maximum when the
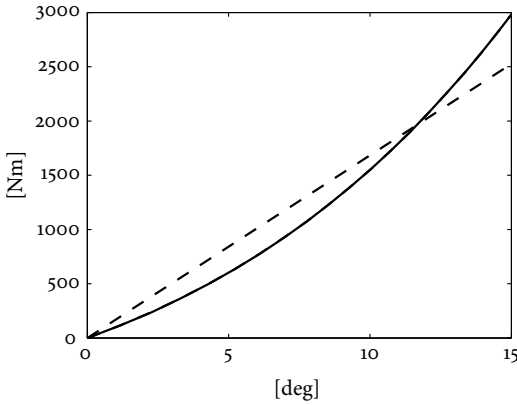
Figure 2.17: Spring characteristics for a steering geometry $n_o = 150\,\text{mm}$, $r_o = 300\,\text{mm}$, $\tau_o = -5°$, $\sigma_o = 10°$, a steering amplification $k_a = 2$, and an axle load of 9000 kg. The dashed line shows a least-squares linear approximation. *Source: Alberding et al. (in press), ©IEEE.*
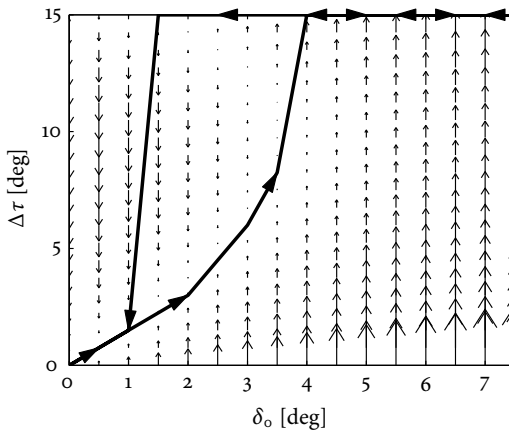
Figure 2.18: Example for a hysteresis due to spring linearity. The bold line shows $\Delta\tau$ as δ_o is first increased, then decreased. The vertical arrows represent the direction and magnitude of the joint torque. *Source: Alberding et al. (in press), ©IEEE.*

spring is too soft, but as δ_0 decreases, $\Delta\tau$ returns from the maximum significantly later. If the maximum joint angle is greater than the unstable equilibrium for $\delta_0 = 0$, the joint can even be confined in the unstable region and remain in the maximum.

Based on these considerations, the use of a linear spring offers both challenges and opportunities. Clearly, the design must guarantee that the joint returns from the maximum at an appropriate steering angle. This requires the spring to be sufficiently stiff. However, an overly stiff spring can impede the joint from leaving the initial position. If for a given geometry no compromise can be found, the range of the joint angle must be reduced or the return supported by an actuation. So far, the spring design was intended to maintain a constant ratio between δ_0 and $\Delta\delta$, Eq. (2.54). Designed properly, the hysteresis behaviour, Fig. 2.18, can provide an alternative. It adds a constant offset to the steering angle when δ_0 reaches the switch-on point. The switching points are determined by the spring constant, the magnitude of the offset by the maximum joint angle. The transition can be influenced by the damping properties of the joint. Compared to the constant ratio, this approach is generally more robust towards changing vehicle parameters and disturbances and shows a better centring behaviour.

2.4.5 Conclusion

The appeal of conventional self-steering is the fact that it does not require any actuation, i.e. the steering is passive. On the downside, the steering angle thus is unchangeably defined as a function of the radius of curvature and vehicle speed, as shown in Eq. (2.37). This function cannot be influenced by the design of the suspension, except for a centring device at the kingpin that could be used to diminish the steering angle.

The approach described yields a form of generalized self-steering. In contrast to conventional self-steering, the steering angle function in form of the relationship between δ_0 and $\Delta\delta$, e.g. Eq. (2.54), can be chosen freely during the design process. In particular, it can be used to obtain a self-steering behaviour that amplifies the steering angle of conventional self-steering, resembling the behaviour of command steer and reducing the low-speed off-tracking of the vehicle. If the revolute joints incorporate a locking mechanism, the system could be switched between conventional and amplified self-steering.

The amplified steering behaviour is passive and does not require any actuation forces. It allows an actuation to be used to influence the steering selectively. The required actuation torque thus is not a function of the side-slip as it is for command steer. Instead, it increases with the deviation from the passive amplified behaviour that is defined by the characteristics of the spring-like element. The passive behaviour takes the role of a feed-forward controller, lowering the requirements on the control authority of the actuators. Therefore, a much smaller actuation than in command steer can be sufficient.

In theory, progressive characteristics allow the self-steering angle to be amplified by

a constant factor without any actuation forces. A design of linear characteristics must consider the possible instability and hysteresis. If necessary, these can be handled by actuation or be intentionally used to obtain a constant offset to the self-steering angle instead of the constant factor.

The spring stiffness was assumed to be load-dependent. If this is not feasible, the passive steering amplification decreases with the load.

As mentioned in Chapter 1, self-steering improves the performance at lower speeds. At higher speeds, it degrades the performance since it cannot resist the lateral acceleration. Since the variable geometry discussed takes advantage of the self-steering principle, it inherits these properties. At higher speeds, an actuation would have to counteract the self-steering effect, which would pervert the idea of the approach. Therefore, the use of the steering best remains confined to low speeds, since it is less suited to improve the high speed performance.

Carrying the line of thought developed even further, the steering could be influenced by adjustable spring characteristics. Increasing and decreasing the spring stiffness moves the equilibrium of the system, such that the steering amplification can be changed. The steering angle thus is completely controllable without any further actuation. Furthermore, the necessary adaptation to the loaded mass is included. This can be seen as the most consequent implementation of the ideas developed here. Existing ideas for adjustable torsion springs (Ahn 2007), possibly even replacing the axle beam, or the variable characteristics of the existing air suspension might be promising starting points for a mechanical design of this approach.

2.5 Simulation Results

To test the concept described above, this work utilizes a detailed and validated multibody simulation environment of a tractor semi-trailer combination. The tractor is controlled by a virtual driver that follows a pre-defined track and speed profile. The steering system has been implemented in multiple versions that differ in the choice of actuation, spring design, steering geometry, and vehicle parametrization. The steering control system uses realistic sensor configurations and signals from the semi-trailer only, the configuration depends on the choice of actuation. All versions have been tested in various situations and manoeuvres, both during forward and reverse travel. Also the effects of sensor or actuator failures on the vehicle safety have been studied.

One of the main results of this work is an approach to passively amplify the steering angle of conventional self-steering, designed to resemble the steering behaviour of command steer without any actuation. To validate this result, the simulations presented in this section utilize a steering system integrated in the existing suspension by the preliminary design discussed in Section 2.4.1. The spring is chosen progressive to obtain a constant amplification factor; the alternative of a linear spring and the result-

Table 2.1: Parameters of the Simulation

Caster angle τ_o	10°
Wheel-centre caster offset n_o	0 mm
Kingpin inclination σ_o	10°
Wheel-centre kingpin offset r_o	282 mm
Joint rear shift	10 mm
Steering angle δ	−20° to 20°
Joint angle $\Delta\tau$	0° to 20°
Steering amplification k_a	2.5
Centring stiffness $c_\delta F_z$	2580 N m rad^{-1}
Axle load	9000 kg

ing hysteresis behaviour are shown in Fig. 2.18. To match the spring characteristics to both forward and reverse travel, the steering geometry is designed symmetrically, i.e., the wheel-centre caster offset is zero and the caster angle in the initial position half the range of rotation. A positive kingpin inclination is included to obtain self-centring, see Eq. (2.32b). Pneumatic cylinders are used to rotate the kingpins into their position for reverse travel. To return to the forward position, the joints are placed slightly towards the rear. The vertical wheel forces thus generate a constant offset on the joint torque that stabilizes the forward position. To maintain the symmetry, the cylinder pressure is defined such as to generate an offset of identical amplitude into the opposite direction. The parameters of the design are summarized in Table 2.1.

For the scope of this work, the most important result is the performance of the steering system, namely the ability of the steering angle to follow its reference. The generation of this reference, which relates the steering angle to the self-steering angle and a desired vehicle trajectory, is independent from the steering system. An example is introduced briefly in the following. To minimize off-tracking, Odhams et al. (2011) propose to steer such that the rear of the trailer follows the fifth wheel. Using Fig. 2.15 and Eqs. (2.35) to (2.40) and following the approach of Section 3.2.1, in steady state this behaviour requires the steering angle

$$\delta^* = \frac{1}{aC_\alpha L}\Big(aC_\alpha(2a - L) + a_1C_{\alpha,1}(2a_1 - L) + a_2C_{\alpha,2}(2a_2 - L)\Big)\Gamma - \frac{lm}{2aC_\alpha}a_y, \quad (2.68)$$

where L denotes the distance from the trailer rear to the fifth wheel. The asterisk refers to the sign convention, see Section 2.1.2. Assuming low speed and equal cornering stiffnesses among the tyres, combining Eqs. (2.37) to (2.39), (2.55) and (2.68) yields the desired steering amplification

$$k_a = \frac{\lambda_1 + \lambda_2}{\lambda_1 + \lambda_3}, \quad (2.69)$$

where

$$\lambda_1 := \frac{a}{a + a_1 + a_2}, \tag{2.70a}$$

$$\lambda_2 := \frac{a_1^2 + a_2^2}{a_1(a - a_1) + a_2(a - a_2)}, \tag{2.70b}$$

$$\lambda_3 := \frac{aL}{a(2a - L) + a_1(2a_1 - L) + a_2(2a_2 - L)}, \tag{2.70c}$$

which is only depending on the vehicle dimensions. The parameters of the vehicle simulated lead to the desired steering amplification $k_a = 2.5$. According to Eq. (2.61), for the given vehicle parameters the maximum joint angle of 20° is expected to be sufficiently large to maintain this steering amplification over the full steering range.

Figures 2.19 and 2.20 show the simulation results for passing a roundabout with an outer radius of 18 m and an inner radius of 12 m at 10 km/h during forward travel. The spring successfully maintains the desired steering amplification and resembles the command steer behaviour without requiring any actuation energy. The multi-body simulation thus validates the model of Section 2.1 and the analysis of Sections 2.3 and 2.4.

Figures 2.21 and 2.22 show the simulation results for passing a roundabout with an outer radius of 28 m and an inner radius of 22 m at 10 km/h during reverse travel. Despite the differences in the dynamics of forward and reverse travel, the steering is successfully amplified. The system with a constant progressive spring without any auxiliary actuation shows to be less robust during reverse travel than during forward travel. Systems with a linear spring, an adjustable spring stiffness, or a further actuation improve the robustness significantly and are less sensitive towards variations of parameters of the vehicle.

As intended, the amplified steering significantly reduces the off-tracking of the vehicle and improves the low-speed performance. Figure 2.23 demonstrates this benefit in manoeuvrability compared to both conventional self-steering and a non-steering axle. The simulation scenario is steady state cornering with an outer radius of 12.5 m. European legislation requires the inner radius of the ring covered by the vehicle during this manoeuvre to be at least 5.3 m. The non-steering vehicle is designed for this requirement and takes 5.3 m, the self-steering vehicle reduces the off-tracking and reaches 5.9 m, while the vehicle with amplified steering shows 6.5 m. Hence, compared to self-steering, the amplified steering doubles the off-tracking reduction. It is limited by the maximum steering angle and can only reach a steering amplification by a factor of 2 instead of the desired 2.5. Extending steering and joint ranges can further improve the performance.
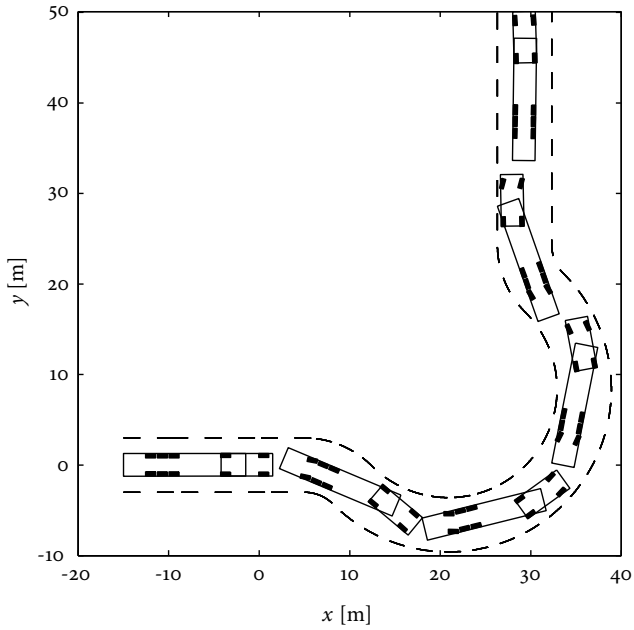
Figure 2.19: Simulation scenario forward travel. Passing a roundabout with an outer radius of 18 m and an inner radius of 12 m at 10 km/h. *Source: Alberding et al. (in press), ©IEEE.*
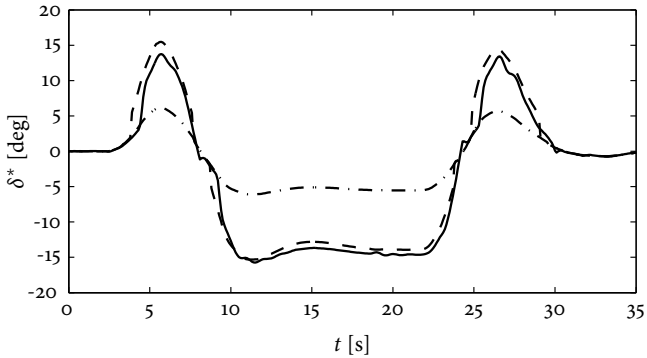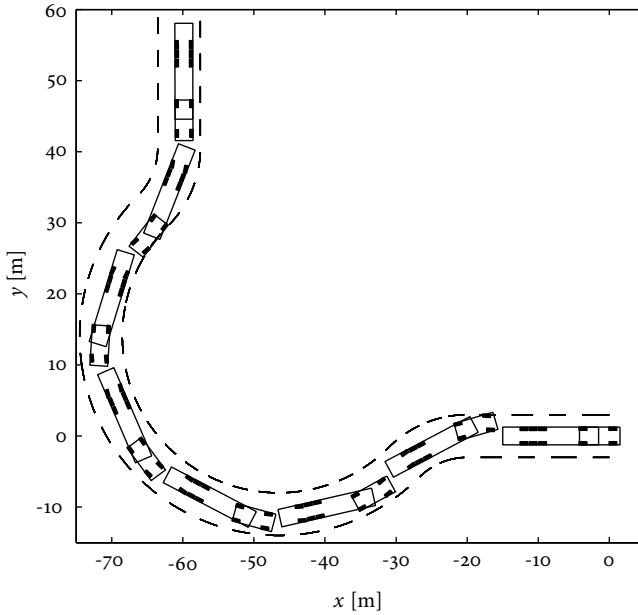
(a) Steering angle. Solid: steering angle δ^*, dashed: desired steering angle $k_a\delta_o^*$, dash-dotted: estimated self-steering angle δ_o^*. The asterisk denotes the sign convention, see Section 2.1.2.
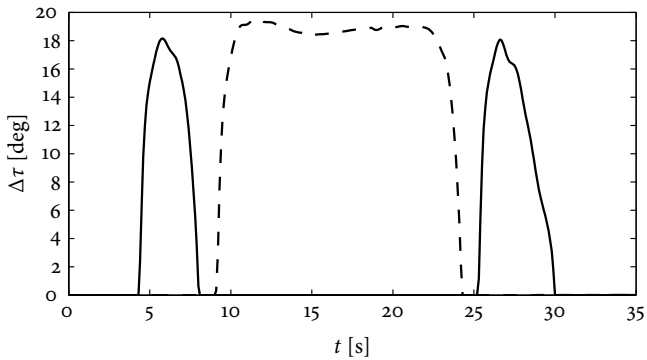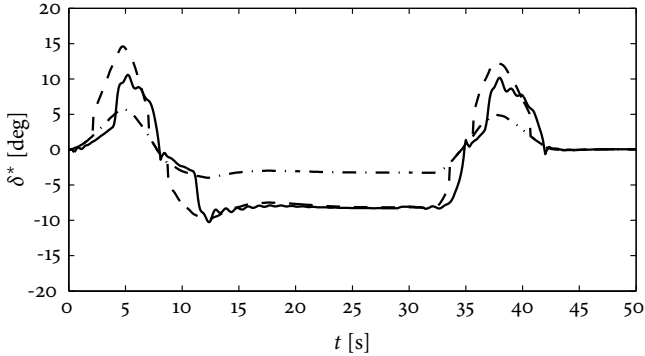

(b) Joint angle. Solid: left-hand joint $\Delta\tau_l$, dashed: right-hand joint $\Delta\tau_r$.

Figure 2.20: Simulation results forward travel. *Source: Alberding et al. (in press), ©IEEE.*

Figure 2.21: Simulation scenario reverse travel. Passing a roundabout with an outer radius of 28 m and an inner radius of 22 m at 10 km/h. *Source: Alberding et al. (in press), ©IEEE.*
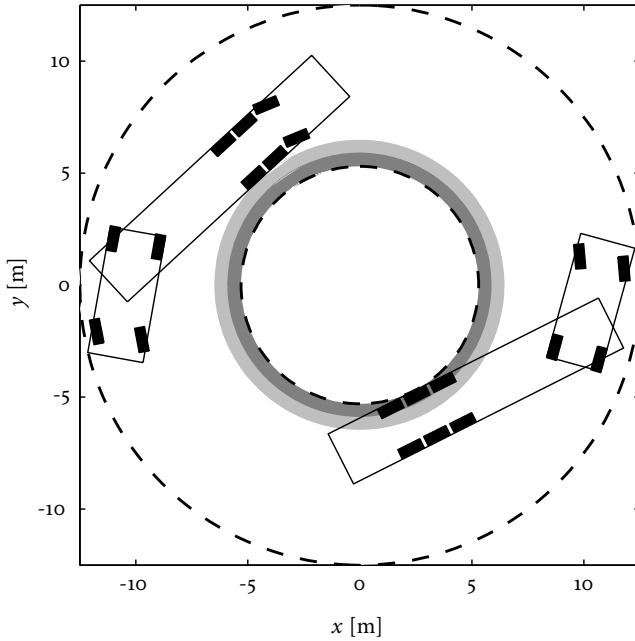
(a) Steering angle. Solid: steering angle δ^*, dashed: desired steering angle $k_a\delta_o^*$, dash-dotted: estimated self-steering angle δ_o^*. The asterisk denotes the sign convention, see Section 2.1.2.
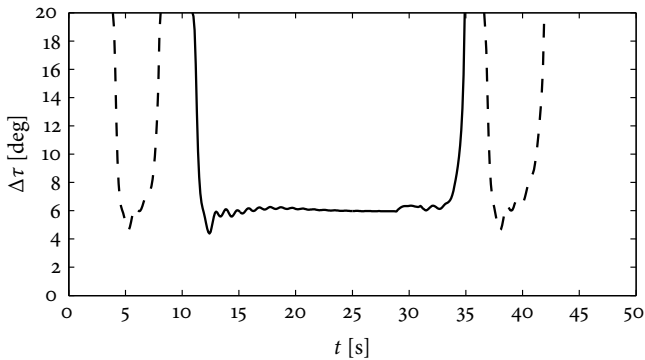
(b) Joint angle. Solid: right-hand joint $\Delta\tau_r$, dashed: left-hand joint $\Delta\tau_l$; left and right related to the reverse direction of travel.

Figure 2.22: Simulation results reverse travel. *Source: Alberding et al. (in press), ©IEEE.*

Figure 2.23: Off-tracking reduction. Legislative limits are indicated by the dashed lines. The steering angle is saturated at 20°. The light and dark grey surfaces show the additional spaces required by a self-steering and non-steering vehicle. *Source: Alberding et al. (in press), ©IEEE.*

2.6 Vehicle Experiments

This section presents the set-up and experimental results of a functional demonstrator. The objective of the experiments is to investigate the technical feasibility rather than to obtain an optimized design or an optimized performance. Therefore, the demonstrator is based on a standard production self-steering axle to minimize the implementational effort. The disadvantages of the existing suspension for the design process have been discussed above. The use of a standard production axle introduces additional performance limitations due to a steering geometry that is asymmetrical with respect to the caster and that is not optimized for the steering system discussed.

The mechanical design of the demonstrator has been carried out by a project partner and was not part of this work.

As shown in Fig. 2.24, the set-up is similar to the preliminary mechanism described in Section 2.4.1 and the model used in the simulations described in Section 2.5. The parameters of the design are summarized in Table 2.2. Rotational joints are placed between the kingpins and the axle body. A linear torsional spring is placed inside the axle and connects both kingpins. To use the steering during reverse travel, two single-acting 30” pneumatic cylinders co-rotate the kingpins into the direction of the negative caster. Each of the cylinders can generate a torque of approximately 2000 N m. To return the joints to the initial position during forward travel, the joints are placed 2 cm to the rear, providing a lever arm to the vertical tyre forces. At nominal load, this design results in a torque of approximately 500 N m in each joint, plus the torque due to the return springs of the cylinders.

The rotation of the joints is limited to the range between 0° to 20° by mechanical stops. In the 0° and 20° positions, the joints can be locked using pneumatic cylinders. To avoid jamming, during forward travel the lock should be disengaged as long as the tyre contact point is ahead of the joint, i.e. at a steering angle of less than approximately 5°. During reverse travel, the lock can only be disengaged with the cylinder for reverse travel being active.

Both wheel carriers are connected by a track rod. Since a single-sided kingpin rotation inclines the track rod, the standard production steering lock mechanism is removed. The track rod is not designed to avoid a force generation due to the inclination, which might affect the variable geometry.

The steering angle is limited to 15°. To facilitate the steering, the centring stiffness of the kingpins is reduced to 580 N m rad^{-1}. Due to the choice of the components, the nominal axle load is limited to 5000 kg. To free installation space, no braking cylinders are included.

The geometry of the standard production self-steering axle used as a basis for the demonstrator has a caster angle τ_o of 0°, a wheel-centre caster offset n_o of 147 mm, a kingpin inclination σ_o of 10°, and a wheel-centre kingpin offset r_o of 282 mm. Since
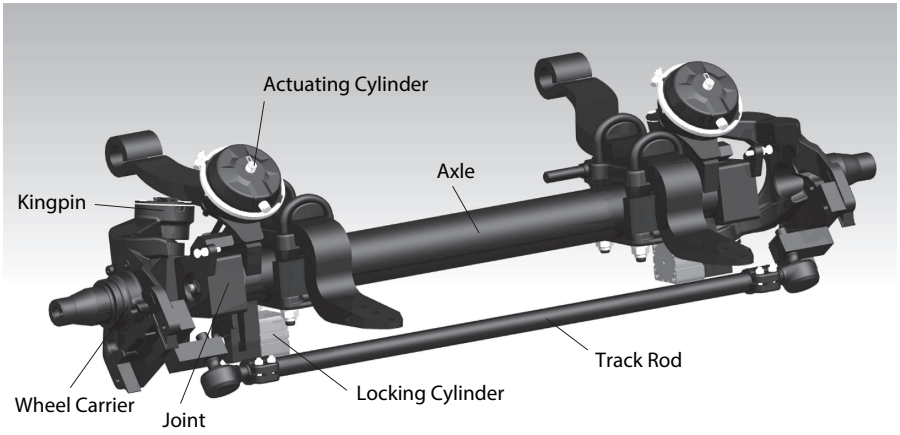
(a) CAD rendering.
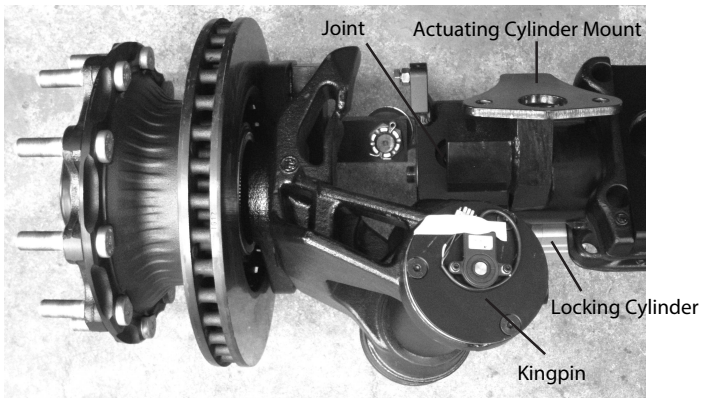
(b) Photographic image.

Figure 2.24: Functional demonstrator.

Table 2.2: Parameters of the demonstrator design

|	
Caster angle τ_o	$-10°$
Wheel-centre caster offset n_o	147 mm
Kingpin inclination σ_o	10°
Wheel-centre kingpin offset r_o	282 mm
Joint rear shift	20 mm
Steering angle δ	$-15°$ to $15°$
Joint angle $\Delta\tau$	0° to 20°
Stiffness of the torsional spring $c_\tau F_z$	6732.3 N m rad^{-1}
Centring stiffness $c_\delta F_z$	580 N m rad^{-1}
Nominal axle load	5000 kg

the caster angle of the demonstrator is variable, τ_o can be designed at a different value. Due to the significant wheel-centre caster offset, the geometries in the initial positions of forward and reverse travel are not identical. This asymmetry of the steering geometry causes the steering behaviour to change with the direction of travel. The design of the spring stiffness must take into account both directions of travel. Furthermore, the fact that the negative caster of the kingpin rotated during cornering must never exceed the positive caster of the non-rotated kingpin must be considered as well, otherwise the steering becomes unstable.

For the given geometry, since only the design parameters spring stiffness and caster angle τ_o are available, compromises in the steering performance have to be accepted to permit a stable steering in both directions of travel. The spring stiffness is chosen at 6732.3 N m rad^{-1}, the caster angle τ_o is $-10°$. As shown in the simulation results depicted in Figs. 2.25 and 2.26, this design is expected to generate a substantial steering amplification at reverse travel, but only a minor amplification at forward travel. In both simulations, the scenario is a roundabout of 15 m radius at a vehicle speed of 10 km/h, while the simulation environment is the multi-body simulation used in Section 2.5.

The control logic of the system is illustrated in Fig. 2.27. The actuators of the system are the two pneumatic cylinders that rotate the kingpins into the position for reverse travel and the two pneumatic cylinders that control the joint locks. The lock operation is monitored by magnetic sensors. The joint rotation is measured by string potentiometers, while the steering angle is measured by magnetic sensors at the kingpins. The direction of travel is determined by the activity of the reversing light. The experimental vehicle is furthermore equipped with a kingpin sensor to measure the articulation angle. The desired direction of steering is determined based on the steering and articulation angle measurements. During forward travel, the left lock is opened to steer to the left and the right lock to steer to the right. During reverse travel, the
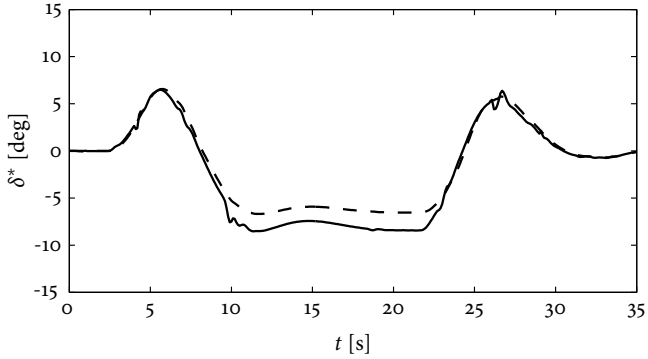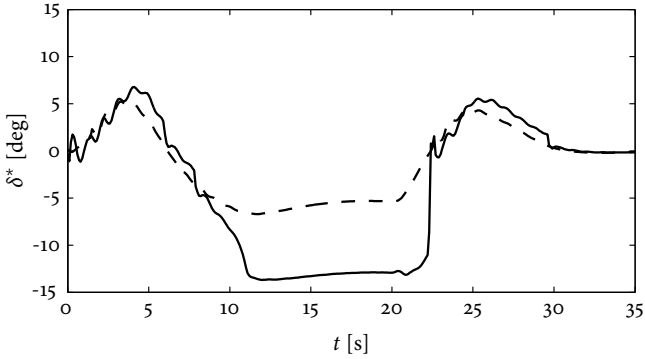
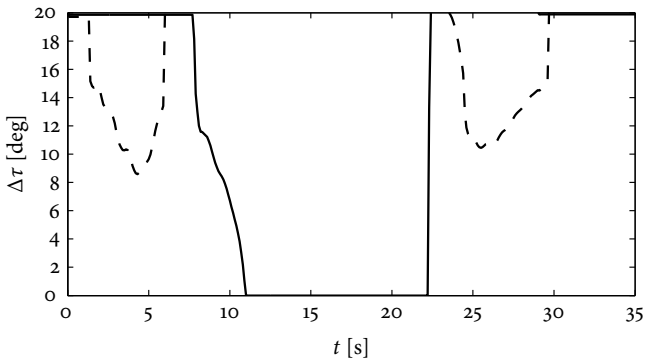**(a)** Steering angle. Solid: steering angle δ^*, dashed: estimated self-steering angle δ_o^*.
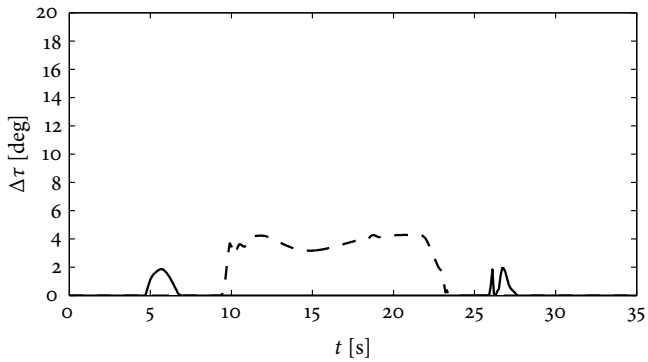
(b) Joint angle. Solid: left-hand joint $\Delta\tau_l$, dashed: right-hand joint $\Delta\tau_r$.

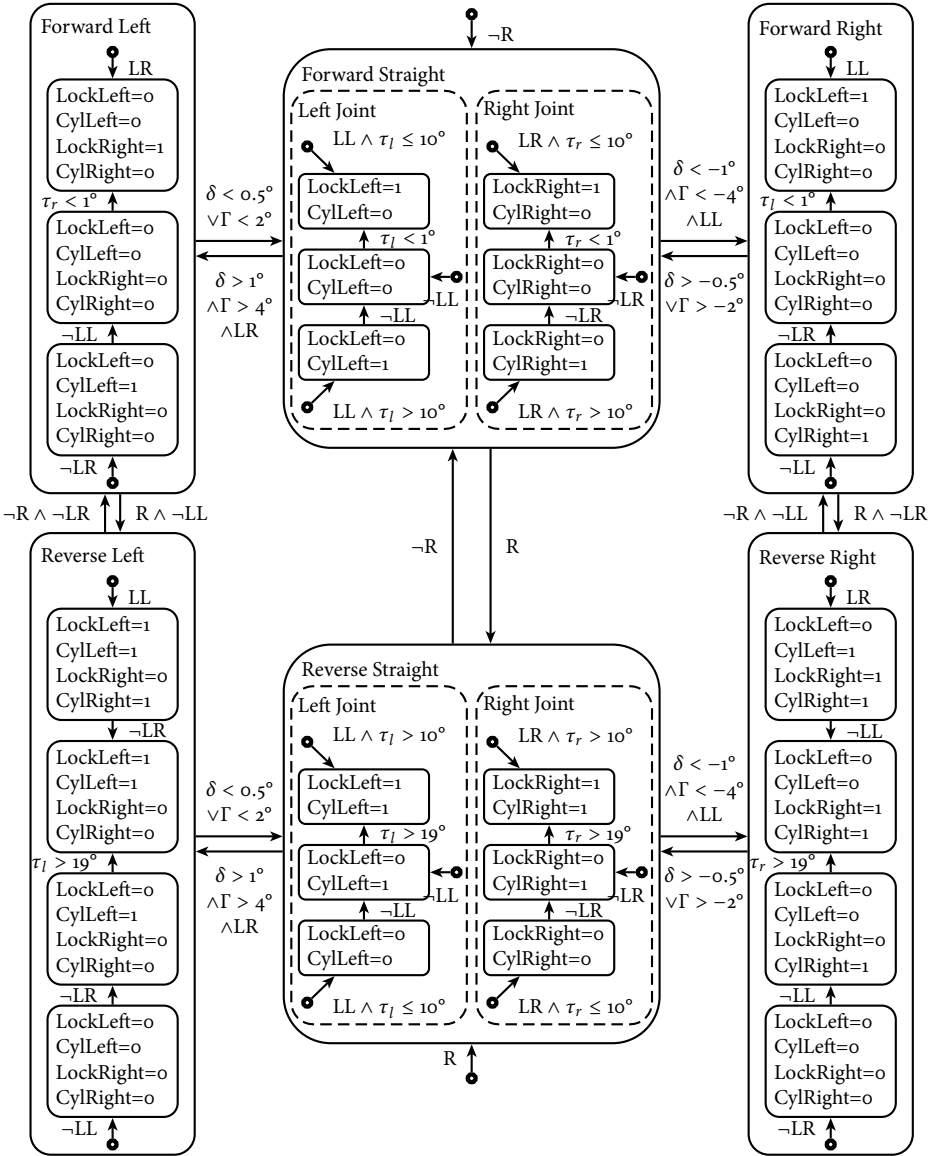**Figure 2.25:** Simulation results forward travel.

(a) Steering angle. Solid: steering angle δ^*, dashed: estimated self-steering angle δ_o^*.

(b) Joint angle. Solid: left-hand joint $\Delta\tau_l$, dashed: right-hand joint $\Delta\tau_r$.

Figure 2.26: Simulation results reverse travel.

Figure 2.27: Control system. Inputs: LL (left lock engaged), LR (right lock engaged), R (reversing light active), τ_l (joint angle left), τ_r (joint angle right), δ (steer angle), Γ (articulation angle). Outputs: LockLeft (engage left lock), LockRight (engage right lock), CylLeft (activate left cylinder), CylRight (activate right cylinder). Deviant from Section 2.1.2, left and right are always defined with respect to forward travel.

right lock is opened to steer to the left and the left lock to steer to the right.

In the experiments, the demonstrator showed an excessive friction in the rotational joints that limits the function of the system. The bearings, in size limited by the standard production axle, show to be too small to withstand the weight of the vehicle. The pneumatic cylinders are sufficiently powerful to overcome the friction and to rotate the kingpins into the reverse-travel position. However, the displacement of the joints towards the tyre contact points does not return the kingpins to the forward-travel position. Thus, the friction torque in each joint is at least 500 N m and less than 2000 N m. The problem could be solved by a revised design of the demonstrator. To the date of this report, such a new demonstrator is not available. Therefore, the experimental results of the existing demonstrator are presented, though due to the excessive friction the conclusiveness of these results is limited.
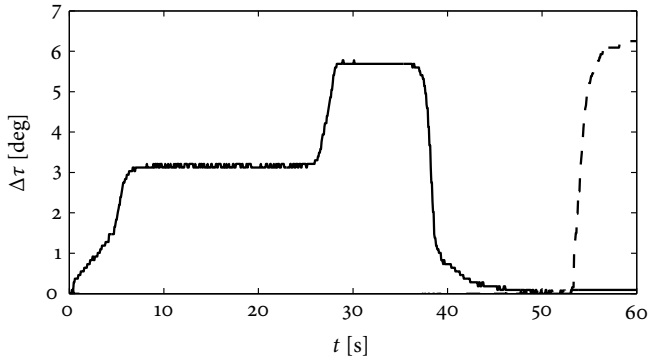
Figure 2.28 shows experimental results during forward travel. Despite showing effects of the friction, the experiments indicate the correctness of the analysis and support the technical feasibility of the approach. As expected, the joint angle increases when a wheel steers to the outside and decreases when the steering returns. The rotation of the left-hand joint starts with the vehicle steering to the left at $t =$0 s, but stops at 3° due to the friction. The friction is overcome and the joint angle increases to 6° at $t =$27 s when the driver changes the direction and the load transfer begins to shift. The rotation returns with the steering at $t =$38 s. The rotation of the right-hand joint is delayed due to the friction and does not start with the vehicle steering to the right at $t =$38 s. Though, the joint moves directly to 6° at $t =$54 s once the torque due to the steering is sufficiently large to overcome the friction. Both when the right-hand joint rotates from 0° to 6° at $t =$54 s and when the left-hand joint returns from 6° to 0° at $t =$38 s, the steering angle rapidly changes by 3° to the right. This behaviour confirms the expected steering amplification. The levels of the joint angles and the steering amplification match the simulation, see Fig. 2.25. As discussed above, the steering amplification during forward travel is designed much smaller than the amplification during reverse travel due to the design constraints of the standard production axle. It could be increased substantially by an optimized design.

Figure 2.29 shows experimental results during reverse travel. The steering amplification during reverse travel is designed to be much higher than during forward travel and the joint is expected to rotate over the complete range, see Fig. 2.26. As for forward travel, the joint angle increases when a wheel steers to the outside. However, the amplitude is much smaller than anticipated. The excessive friction of the demonstrator is the most likely explanation for this limitation. The rotation into the reverse-travel position raises the axle body, in all probability increasing the load on the bearings compared to the forward-travel position.

The experiments presented support the theoretical results of this work. Future work should revise the bearing design of the demonstrator and repeat the experiments to allow a detailed analysis.
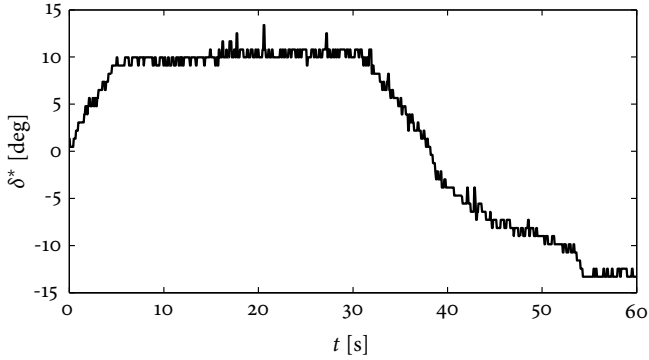
(a) Steering angle.

(b) Joint angle. Solid: left-hand joint $\Delta\tau_l$, dashed: right-hand joint $\Delta\tau_r$.

Figure 2.28: Experimental results forward travel. The joint angle increases when a wheel steers to the outside and decreases when the steering returns. Both when the right-hand joint rotates at $t =54$ s and when the left-hand joint returns at $t =38$ s, the steering angle rapidly changes to the right.
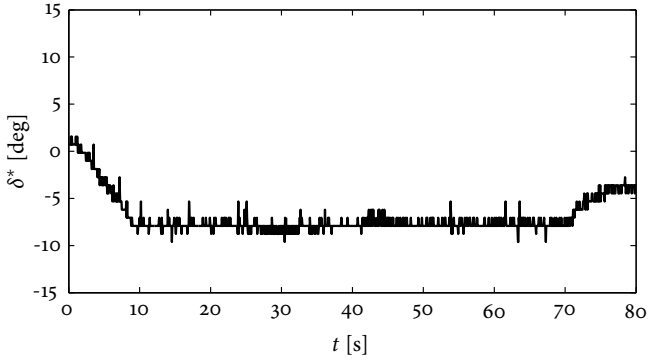
(a) Steering angle.

(b) Joint angle. Solid: left-hand joint $\Delta\tau_l$, dashed: right-hand joint $\Delta\tau_r$.
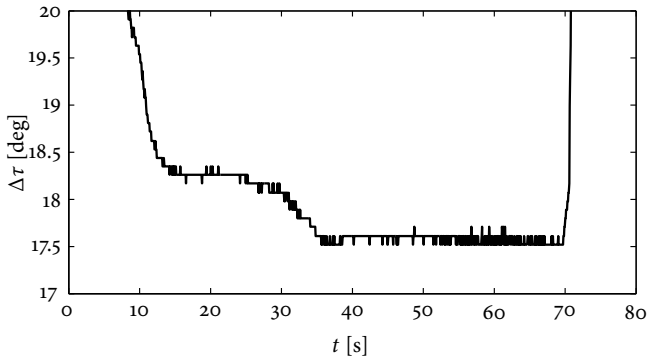
Figure 2.29: Experimental results reverse travel. As for forward travel, the joint angle increases when a wheel steers to the outside. The excessive friction in the joints of the demonstrator limits the function of the system, the amplitude of the rotation is much smaller than anticipated.

Steering Control of a Semi-Trailer in Reverse Travel

This chapter is based on the author's manuscript for the paper:

Alberding, M., Vivaldelli, M., Sager, F. & Onder, C. (2013), Steering control of a semi-trailer in reverse travel, Manuscript submitted for publication.

The autonomous steering of a tractor with one or more passive trailers during reverse travel has been studied comprehensively (Tanaka & Sano 1994, Kong & Kosko 1992, Altafini, Speranzon & Wahlberg 2001, Matsushita & Murukami 2008, Morales, Martínez, Mandow & García-Cerezo 2013). Less attention has been paid to automatic trailer steering with the tractor steering controlled by a human driver. The majority of commercial command-steer systems control the steering angle proportionally to the articulation angle, both during forward and reverse travel. Some allow a remote control by the driver. Percy & Spark (2013) extend this approach by requiring the driver only to provide a curvature reference by remote control and assigning the steering control of a B-double truck-trailer to an automatic controller.

This work takes a novel approach to the problem. The objective is to optimally assist a human driver to reverse a tractor semi-trailer combination. The trailer steering is to be based on the driver's steering actions on the tractor, without a remote control or any other additional driver input.

This chapter is organized as follows. Section 3.1 derives a time-variant linear model

of the system dynamics. The model is validated using measurement data from vehicle experiments. Based on the model, a state estimator in the form of a discrete-time Kalman filter is designed. The feasibility to estimate the tractor steering and the articulation angle at various speeds is investigated. Section 3.2 presents the control system, which is the main result of this chapter. In Section 3.3, the controller is tested using a validated multi-body simulation model. The system is compared to a conventional controller design that steers proportionally to the articulation angle.

3.1 Modelling

The controller design is based on a simplified linear model of the vehicle dynamics of the tractor semi-trailer combination, similar to the model presented by Sampson & Cebon (2003). Figure 3.1 illustrates the variables and parameters of the model. In contrast to the previous chapter, all variables are defined in a right-handed coordinate system and the distinction between single wheel and vehicle using an asterisk is omitted. The model describes both the dynamics of forward and reverse travel. This work assumes a single steerable axle on the semi-trailer. The model and the control design can be extended to multiple steerable axles.

The derivation of the control-oriented model is based on the following simplifying assumptions:

1. Tractor and semi-trailer are rigid bodies.

2. The tyres of an axle are represented by a single tyre at the centre of the axle (single-track model).

3. The tyre side-slip angles are small and the lateral tyre force characteristics are linear, $F_y = -C_\alpha \alpha$.

4. The steering angles, the articulation angle, and the vehicle side-slip angles are small.

5. The longitudinal speed is constant and equal for tractor and trailer, and the lateral speed is small.

6. The influence of the pitch and roll motion on the lateral dynamics are neglected.

7. The tractor has a single rear axle with twin tyres.

8. The semi-trailer has three axles, of which the rearmost is steerable.

Figure 3.1: Definition of vehicle variables and parameters. *Source: Alberding et al. (2013).*

Balancing the lateral forces and the yaw moments of the semi-trailer and the tractor yields

$$mv_x(\dot{\psi} + \dot{\beta}) = 2F_{y,1} + 2F_{y,2} + 2F_y + F_{y,C}, \tag{3.1}$$

$$J_z\ddot{\psi} = -2d_1F_{y,1} - 2d_2F_{y,2} - 2dF_y + lF_{y,C}, \tag{3.2}$$

$$m_Tv_x(\dot{\psi}_T + \dot{\beta}_T) = 2F_{y,F} + 4F_{y,R} - F_{y,C}, \tag{3.3}$$

$$J_{z,T}\ddot{\psi}_T = 2d_FF_{y,F} - 4d_RF_{y,R} + l_TF_{y,C}, \tag{3.4}$$

where m denotes the trailer mass, m_T the tractor mass, J_z the yaw inertia of the trailer, and $J_{z,T}$ the yaw inertia of the tractor.

The velocities of the tractor and the semi-trailer have to match at the fifth wheel coupling,

$$\psi + \beta + \frac{l}{v_x}\dot{\psi} = \psi_T + \beta_T - \frac{l_T}{v_x}\dot{\psi}_T, \tag{3.5}$$

where the time derivative is given by

$$\dot{\psi} - \dot{\psi}_T = -\frac{l}{v_x}\ddot{\psi} - \dot{\beta} - \frac{l_T}{v_x}\ddot{\psi}_T + \dot{\beta}_T. \tag{3.6}$$

Based on the assumptions made, the tyre side-slip angles are determined by

$$\alpha_1 = \beta - \frac{d_1}{v_x}\dot{\psi}, \qquad \alpha_2 = \beta - \frac{d_2}{v_x}\dot{\psi}, \tag{3.7a}$$

$$\alpha = \beta - \frac{d}{v_x}\dot{\psi} - \delta, \qquad \alpha_F = \beta_T + \frac{d_F}{v_x}\dot{\psi}_T - \delta_T, \tag{3.7b}$$

$$\alpha_R = \beta_T - \frac{d_R}{v_x}\dot{\psi}_T. \tag{3.7c}$$

Combining Eq. (3.7) and Eqs. (3.3) to (3.6) yields

$$mv_x(\dot{\psi} + \dot{\beta}) = Y_{\dot{\psi}}\dot{\psi} + Y_{\beta}\beta + Y_{\delta}\delta + F_{y,C}, \tag{3.8}$$

$$J_z\ddot{\psi} = N_{\dot{\psi}}\dot{\psi} + N_{\beta}\beta + N_{\delta}\delta + lF_{y,C}, \tag{3.9}$$

$$m_Tv_x(\dot{\psi}_T + \dot{\beta}_T) = Y_{\dot{\psi},T}\dot{\psi}_T + Y_{\beta,T}\beta_T + Y_{\delta,T}\delta_T - F_{y,C}, \tag{3.10}$$

$$J_{z,T}\ddot{\psi}_T = N_{\dot{\psi},T}\dot{\psi}_T + N_{\beta,T}\beta_T + N_{\delta,T}\delta_T + l_TF_{y,C}. \tag{3.11}$$

where the partial derivatives of the lateral forces and the yaw moments are given by

$$Y_{\dot\psi} = \frac{2}{v_x} \operatorname{sign}(v_x) \left(C_{\alpha,1} d_1 + C_{\alpha,2} d_2 + C_\alpha d \right), \tag{3.12a}$$

$$Y_\beta = -2 \operatorname{sign}(v_x) \left(C_{\alpha,1} + C_{\alpha,2} + C_\alpha \right), \quad Y_\delta = 2 \operatorname{sign}(v_x) C_\alpha, \tag{3.12b}$$

$$N_{\dot\psi} = -\frac{2}{v_x} \operatorname{sign}(v_x) \left(C_{\alpha,1} d_1^2 + C_{\alpha,2} d_2^2 + C_\alpha d^2 \right), \quad N_\beta = v_x Y_{\dot\psi}, \tag{3.12c}$$

$$N_\delta = -d Y_\delta, \quad Y_{\dot\psi,T} = -\frac{2}{v_x} \operatorname{sign}(v_x) \left(C_{\alpha,F} d_F - 2 C_{\alpha,R} d_R \right), \tag{3.12d}$$

$$Y_{\beta,T} = -2 \operatorname{sign}(v_x) \left(C_{\alpha,F} + 2 C_{\alpha,R} \right), \quad Y_{\delta,T} = 2 \operatorname{sign}(v_x) C_{\alpha,F}, \tag{3.12e}$$

$$N_{\dot\psi,T} = -\frac{2}{v_x} \operatorname{sign}(v_x) \left(C_{\alpha,F} d_F^2 + 2 C_{\alpha,R} d_R^2 \right), \quad N_{\beta,T} = v_x Y_{\dot\psi,T}, \tag{3.12f}$$

$$N_{\delta,T} = d_F Y_{\delta,T}. \tag{3.12g}$$

The direction of travel changes the direction of the lateral forces, switching the signs of the partial derivatives.

Combining Eqs. (3.6), (3.8), (3.9) and (3.11) and using Eq. (3.10) to eliminate $F_{y,C}$ yields the continuous-time system

$$\dot{\mathbf{x}} = \mathbf{A}\mathbf{x} + \mathbf{B}\delta + \mathbf{B}_T \delta_T, \tag{3.13}$$

where the state is defined as

$$\mathbf{x} = \begin{pmatrix} \dot\psi \\ \beta \\ \dot\psi_T \\ \beta_T \end{pmatrix} \tag{3.14}$$

and the system matrices are given by

$$\mathbf{M} = \begin{pmatrix} -\frac{l}{v_x} & -1 & -\frac{l_T}{v_x} & 1 \\ 0 & m v_x & 0 & m_T v_x \\ J_z & 0 & 0 & l m_T v_x \\ 0 & 0 & J_{z,T} & l_T m_T v_x \end{pmatrix}, \tag{3.15}$$

$$\mathbf{A} = \mathbf{M}^{-1} \begin{pmatrix} 1 & 0 & -1 & 0 \\ Y_{\dot\psi} - m v_x & Y_\beta & Y_{\dot\psi,T} - m_T v_x & Y_{\beta,T} \\ N_{\dot\psi} & N_\beta & l(Y_{\dot\psi,T} - m_T v_x) & l Y_{\beta,T} \\ 0 & 0 & N_{\dot\psi,T} + l_T(Y_{\dot\psi,T} - m_T v_x) & N_{\beta,T} + l_T Y_{\beta,T} \\ 0 & 0 & 0 & 0 \end{pmatrix}, \tag{3.16}$$

$$\mathbf{B} = \mathbf{M}^{-1} \begin{pmatrix} 0 \\ Y_\delta \\ N_\delta \\ 0 \end{pmatrix}, \quad \mathbf{B}_T = \mathbf{M}^{-1} \begin{pmatrix} 0 \\ Y_{\delta,T} \\ l Y_{\delta,T} \\ N_{\delta,T} + l_T Y_{\delta,T} \end{pmatrix}. \tag{3.17}$$

From a control perspective, the semi-trailer steering angle δ is the control input and the tractor steering angle δ_T is a disturbance on the system. Using

$$\Gamma = \psi - \psi_T \tag{3.18}$$

and Eq. (3.5), the articulation angle can be determined from the state by

$$\Gamma = \mathbf{C}_\Gamma \mathbf{x}, \qquad \mathbf{C}_\Gamma = \begin{pmatrix} -\frac{l}{v_x} & -1 & -\frac{l_T}{v_x} & 1 \end{pmatrix} \tag{3.19}$$

and the semi-trailer yaw rate by

$$\dot{\psi} = \mathbf{C}_{\dot{\psi}} \mathbf{x}, \qquad \mathbf{C}_{\dot{\psi}} = \begin{pmatrix} 1 & 0 & 0 & 0 \end{pmatrix}. \tag{3.20}$$

The system matrices are time-variant as a function of vehicle speed, direction of travel, and load. Knowledge about the vehicle speed can be obtained from the Anti-lock Braking System (ABS) wheel speed sensors, about the direction of travel from the reversing light, and about the load from the air spring pressure. Assuming the tractor mass to be constant and using the air spring pressure characteristics to calculate the total axle load of the semi-trailer m_A from a pressure measurement, the tyre loads can be approximately determined by

$$F_z = \frac{1}{6} m_A g, \tag{3.21}$$

$$F_{z,F} = \frac{1}{2} m_T g \frac{d_R}{d_F + d_R}, \tag{3.22}$$

$$F_{z,R} = \frac{1}{4} m_T g \frac{d_F}{d_F + d_R} + \frac{1}{4} m_A g \frac{d_2}{l + l_T - d_R}, \tag{3.23}$$

$$m = m_A \left(1 + \frac{d_2}{l + l_T - d_R} \right), \tag{3.24}$$

yielding the cornering stiffness parameters

$$C_\alpha = C_{\alpha,1} = C_{\alpha,2} = C_{\alpha,0} F_z, \tag{3.25}$$

$$C_{\alpha,F} = C_{\alpha,0} F_{z,F}, \tag{3.26}$$

$$C_{\alpha,R} = C_{\alpha,0} F_{z,R} \tag{3.27}$$

and the inertia parameters

$$J_{z,T} = \frac{1}{12} m_T \left(X_T^2 + Y_T^2 \right), \tag{3.28}$$

$$J_z = \frac{1}{12} m \left(X^2 + Y^2 \right), \tag{3.29}$$

Table 3.1: Vehicle parameters

d_1	0.4 m
d_2	1.7 m
d	3 m
d_F	1 m
d_R	2.6 m
a_1	6.4 m
a_2	7.7 m
a_F	3 m
a_R	0.6 m
a	9 m
l	6 m
l_T	2 m
X	13.5 m
X_T	5.7 m
Y	2.5 m
Y_T	2.5 m
L	12 m
m_T	8182 kg
$C_{\alpha,0}$	250,000 N rad^{-1}/33,000 N

where X and Y denote the length and width of the semi-trailer and X_T and Y_T are the length and width of the tractor, respectively. All other parameters are assumed to be constant and are derived from a nominal vehicle, see Table 3.1. Alternatively, parameter estimation techniques could be used (Cheng & Cebon 2011).

Amending the state Eq. (3.14) by the tractor steering angle,

$$\mathbf{z} = \begin{pmatrix} \mathbf{x} \\ \delta_T \end{pmatrix}, \tag{3.30}$$

and assuming the tractor steering to be a slowly changing disturbance, $\dot{\delta}_T = 0$, the dynamics of the system can be described by the extended system

$$\dot{\mathbf{z}} = \mathcal{A}\mathbf{z} + \mathcal{B}\delta, \tag{3.31}$$

$$\mathcal{M} = \begin{pmatrix} \mathbf{M} & \mathbf{0} \\ \mathbf{0} & 1 \end{pmatrix}, \tag{3.32}$$

$$\mathcal{A} = \mathcal{M}^{-1} \begin{pmatrix} \mathbf{A} & \mathbf{B}_T \\ \mathbf{0} & \mathbf{0} \end{pmatrix}, \tag{3.33}$$

$$\mathcal{B} = \mathcal{M}^{-1} \begin{pmatrix} \mathbf{B} \\ \mathbf{0} \end{pmatrix}, \tag{3.34}$$

where $\mathbf{0}$ denotes a zero matrix. Assuming a yaw rate measurement on the semi-trailer to be available,

$$y = \mathcal{C}\mathbf{z}, \qquad \mathcal{C} = \begin{pmatrix} 1 & 0 & 0 & 0 & 0 \end{pmatrix}, \tag{3.35}$$

for any non-zero vehicle speed the system $(\mathcal{A}, \mathcal{C})$ becomes completely observable. Hence, by state estimation, the model can be used to determine the tractor steering angle

$$\delta_T = \mathcal{C}_{\delta,T}\mathbf{z}, \qquad \mathcal{C}_{\delta,T} = \begin{pmatrix} 0 & 0 & 0 & 0 & 1 \end{pmatrix} \tag{3.36}$$

and, in analogy to Eq. (3.19), the articulation angle

$$\Gamma = \mathcal{C}_\Gamma\mathbf{z}, \qquad \mathcal{C}_\Gamma = \begin{pmatrix} -\frac{l}{v_x} & -1 & -\frac{l_T}{v_x} & 1 & 0 \end{pmatrix}. \tag{3.37}$$

An estimation of the tractor steering can be of interest since such a measurement commonly is not accessible on the trailer, see Section 3.2. An estimation of the articulation angle keeps a sensor from being required at the fifth wheel. Despite their technical simplicity, to date such sensors still are rather costly. However, an estimator is based on the information provided by the dynamic behaviour of the system, and it requires a sufficient vehicle motion, expressed by the loss of observability for zero speed. Thus, the accuracy of the estimation must be expected to decrease at low speeds.

For the design of a discrete-time Kalman filter, the continuous-time system can be expressed in discrete time by using the forward Euler method,

$$\mathbf{z}_{k+1} = \mathcal{A}_k \mathbf{z}_k + \mathcal{B}_k \delta_k, \qquad \mathcal{A}_k = \mathcal{A} t_s + \mathbf{I}, \qquad \mathcal{B}_k = \mathcal{B} t_s, \qquad (3.38)$$

where t_s denotes the Electronic Control Unit (ECU) sampling time and $\mathbf{I}$ the identity matrix. The sampling is assumed to be sufficiently fast. In a time step, the estimator initially calculates the system matrices $\mathcal{A}_{k-1}$ and $\mathcal{B}_{k-1}$ based on the vehicle speed, direction of travel, and suspension pressure. The prediction

$$\hat{\mathbf{z}}_k^- = \mathcal{A}_{k-1}\hat{\mathbf{z}}_{k-1} + \mathcal{B}_{k-1}\delta_{k-1}, \qquad (3.39)$$

$$\mathbf{P}_k^- = \mathcal{A}_{k-1}\mathbf{P}_{k-1}\mathcal{A}_{k-1}^{\mathrm{T}} + \mathbf{Q} \qquad (3.40)$$

and the correction

$$\mathbf{K}_k = \mathbf{P}_k^- \mathcal{C}^{\mathrm{T}}(\mathcal{C}\mathbf{P}_k^- \mathcal{C}^{\mathrm{T}} + R)^{-1}, \qquad (3.41)$$

$$\hat{\mathbf{z}}_k = \hat{\mathbf{z}}_k^- + \mathbf{K}_k(\dot{\psi}_k - \mathcal{C}\hat{\mathbf{z}}_k^-), \qquad (3.42)$$

$$\mathbf{P}_k = (\mathbf{I} - \mathbf{K}_k \mathcal{C})\mathbf{P}_k^- \qquad (3.43)$$

follow, where $\mathbf{K}_k$ denotes the Kalman gain, $\mathbf{P}_k$ the error covariance, $\mathbf{Q}$ the process noise covariance, and R the measurement noise covariance (Welch & Bishop 1995). The covariances $\mathbf{Q}$ and R are assumed to be constant. From the state estimate $\hat{\mathbf{z}}$, the tractor steering angle and the articulation angle can be determined using Eqs. (3.36) and (3.37). To avoid the singularity at zero vehicle speed, the estimation can be deactivated for speeds of less than 1 km/h.

Figures 3.2 and 3.3 show measurement data obtained from vehicle experiments as well as those from the model Eqs. (3.12a) to (3.29) using the measured tractor steering as input and the estimation Eqs. (3.30) to (3.43) based on the measured semi-trailer yaw rate. The experimental vehicle has a total mass of 28,480 kg and a total load at the semi-trailer axles of 15,640 kg. The semi-trailer is non-steering, the rearmost axle is lifted. The model uses parameters of a nominal vehicle that have not been adapted to the experimental vehicle.

Figure 3.2 shows the results during forward driving at medium and high speeds. The validity of the model is demonstrated and shows a low sensitivity to the parametrization. The estimation of both articulation and tractor steering is sufficiently accurate. Only at high articulation angles of over 40°, the performance decreases due the tyre saturation not being taken into account in the mathematical model.

Figure 3.3 shows the results at low speeds, both during forward and reverse travel. The model holds for both directions of travel. Compared to medium and high speeds, the estimator performance is decreased. Partly, this can be attributed to the low resolution of the speed measurement available of only 1 km/h. Since speed variations cannot
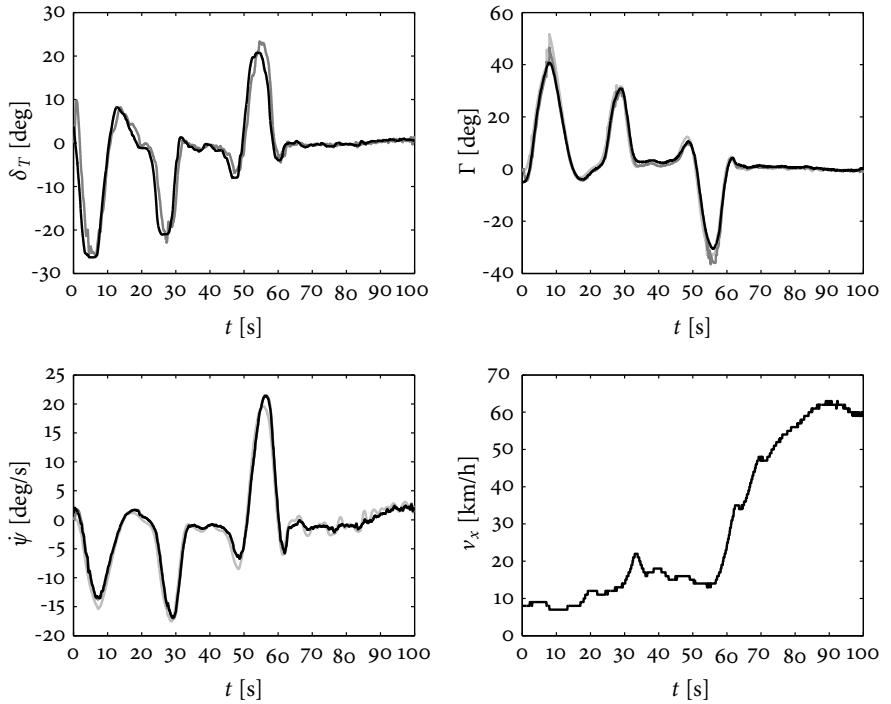
Figure 3.2: Model validation and estimator results for medium and high speeds. Black: measurement, dark grey: estimate, light grey: model. The model is valid, estimation at medium and high speeds is feasible. *Source: Alberding et al. (2013).*
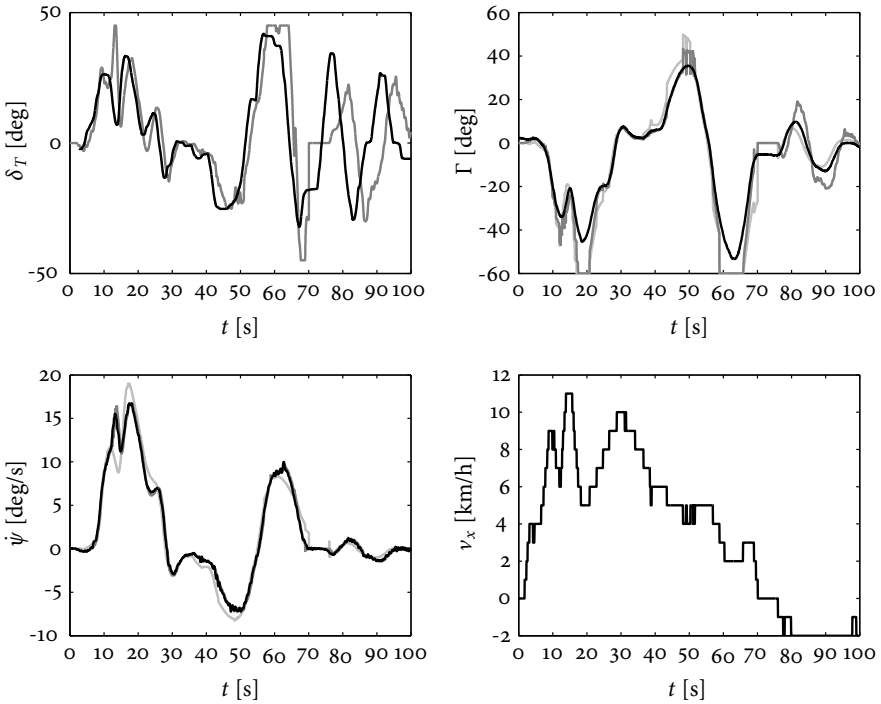
Figure 3.3: Model validation and estimator results for low speeds. Black: measurement, dark grey: estimate, light grey: model. The model holds for both forward and reverse travel. In contrast to medium and high speeds, a reliable estimation is not feasible. *Source: Alberding et al. (2013).*
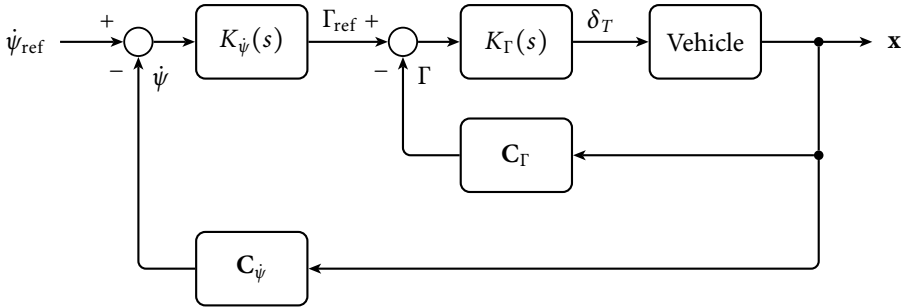
Figure 3.4: Abstraction of a driver's behaviour during reverse travel as a cascade control loop. The outer controller $K_{\dot{\psi}}(s)$ is directed at the yaw rate, the inner controller $K_\Gamma(s)$ at the articulation angle. *Source: Alberding et al. (2013).*

be sensed, any variation of the yaw rate is mistakenly attributed to the cornering motion, generating incorrect estimates. However, even with an increased resolution, the loss of observability at zero speed does not allow a reliable estimation of the tractor steering at walking speed.

3.2 Controller Design

The dynamics of forward travel are asymptotically stable. All eigenvalues of the system matrix Eq. (3.16) are in the left-half plane. For any tractor steering action, the semi-trailer tyre forces steer the articulation angle to an equilibrium, similarly to a caster-based self-steering.

The dynamics of reverse travel are unstable. The system matrix Eq. (3.16) has eigenvalues in the right-half plane. With the analogy of a negative caster, the semi-trailer tyre forces introduce a positive feedback that destabilizes the articulation angle.

For the driver, reverse travel is therefore a challenging task. During forward travel, the driver steering controls the tractor yaw rate, while the trailer yaw rate follows. During reverse travel, in a form of cascade control, the driver steering needs to control the articulation angle, which controls the trailer yaw rate. This abstraction of the driver's behaviour in the terms of control theory is illustrated in Fig. 3.4.

The typical behaviour of a human driver is shown in Fig. 3.5. With the vehicle initially in an unstable equilibrium, the driver needs to counter-steer opposite to the desired direction of cornering. The articulation is thus forced to leave the unstable equilibrium into the desired direction. Once the articulation starts to increase, the driver needs to change the direction of steering to compensate the instability. Once the trailer yaw rate matches the driver's demand, it can be maintained by stabilizing the articulation angle in a new unstable equilibrium.
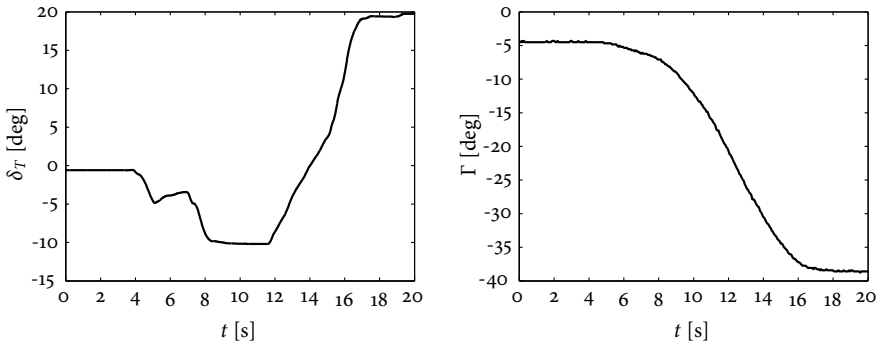
Figure 3.5: Reverse travel steering of a human driver in vehicle experiments. Between $t = 0$ s and $t = 4$ s, the vehicle is in the initial unstable equilibrium. Between $t = 4$ s and $t = 12$ s, the driver counter-steers to initiate the transition. Between $t = 12$ s and $t = 16$ s, the driver increasingly compensates the instability. Between $t = 16$ s and $t = 20$ s, the driver stabilizes the articulation angle in the new unstable equilibrium. *Source: Alberding et al. (2013).*

The steering task can thus be divided into a stabilization in an unstable equilibrium and a set-point change that destabilizes the vehicle into a desired direction. To support the driver in the former case, a semi-trailer steering needs to stabilize the articulation. To support the latter, the control action needs to be the exact opposite, destabilizing the articulation and assisting the transition to a new set-point.

Based on these considerations, the control design of this work is split in two modes of operation. First, a steady-state controller stabilizes the vehicle and maintains the yaw rate and articulation angle, which relieves the driver from this task. In practice, this mode can be useful particularly during straight-ahead travel. Second, a transient controller supports any set-point change initiated by the driver, which minimizes the steering effort at the tractor and allows faster transitions. In addition, both modes of operation are intended to minimize the vehicle off-tracking, decreasing the space required for a given manoeuvre.

3.2.1 Steady-State Control

A given yaw rate can be maintained by various combinations of articulation angle, tractor steering, and trailer steering. The steady state of the vehicle thus depends on the semi-trailer steering. The design of a steady-state steering controller therefore needs to define a desired steady state first.

The majority of active semi-trailer steering systems control the steering angle proportionally to the articulation angle (Jujnovich & Cebon 2002). The control objective is the reduction of tyre wear and off-tracking. To minimize the off-tracking during
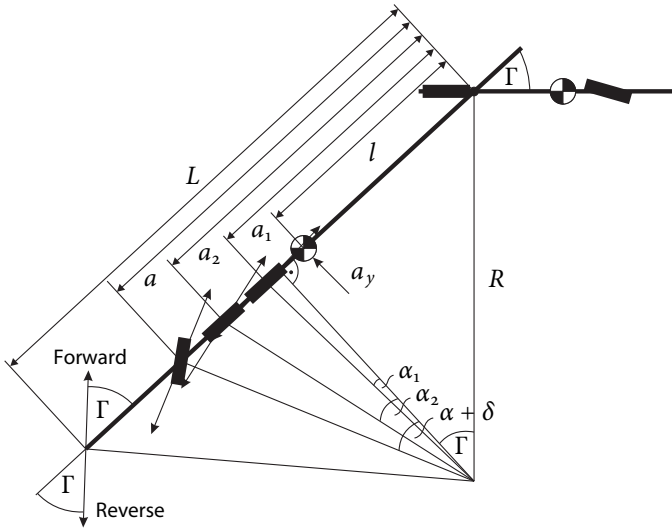
Figure 3.6: Steady-state cornering. *Source: Alberding et al. (2013).*

forward driving, Odhams et al. (2011) suggest to steer such that the rear of the vehicle tracks the path of the fifth wheel. This objective is adopted in this work to define the desired steady state.

The steady-state situation of the rear tracking the fifth wheel is illustrated in Fig. 3.6 for both forward and reverse travel. Neglecting the side-slip of the tractor at the fifth wheel and assuming that the tyre side-slip angles, the steering angle, and the articulation angle are small, the tyre side-slip angles are given by

$$\alpha_1 = \frac{2a_1 - L}{L}\Gamma, \tag{3.44}$$

$$\alpha_2 = \frac{2a_2 - L}{L}\Gamma, \tag{3.45}$$

$$\alpha = \frac{2a - L}{L}\Gamma - \delta. \tag{3.46}$$

The torque balance about the fifth wheel yields

$$2a_1 C_{\alpha,1}\alpha_1 + 2a_2 C_{\alpha,2}\alpha_2 + 2a C_\alpha \alpha - \text{sign}(v_x)lma_y = 0. \tag{3.47}$$

The lateral acceleration at the centre of gravity of the semi-trailer can be approximated by

$$a_y = \frac{v_x^2}{R} = 2\frac{v_x^2}{L}\Gamma. \tag{3.48}$$

Using Eqs. (3.44), (3.45) and (3.48), the torque balance Eq. (3.47) can be solved for the side-slip angle of the steering axle that is required to balance the torque of the non-steering axles and the lateral acceleration,

$$\alpha = -\frac{a_1 C_{\alpha,1}(2a_1 - L) + a_2 C_{\alpha,2}(2a_2 - L) - \text{sign}(v_x)lmv_x^2}{aC_\alpha L}\Gamma. \tag{3.49}$$

Combining Eqs. (3.46) and (3.49) yields the steering angle in the steady state as a linear function of the articulation angle

$$\delta = k_f\Gamma, \tag{3.50}$$

where the time-variant gain k_f is a function of speed and load,

$$k_f = \frac{aC_\alpha(2a - L) + a_1 C_{\alpha,1}(2a_1 - L) + a_2 C_{\alpha,2}(2a_2 - L) - \text{sign}(v_x)lmv_x^2}{aC_\alpha L}. \tag{3.51a}$$

Assuming the cornering stiffness at all trailer axles to be equal and the speed to be small, the gain is time-invariant and determined by the geometry only,

$$k_f = \frac{a(2a - L) + a_1(2a_1 - L) + a_2(2a_2 - L)}{aL}. \tag{3.51b}$$

Using Eqs. (3.13), (3.19) and (3.50), the steady state for a given tractor steering can be determined from

$$(\mathbf{A} + \mathbf{B}k_f\mathbf{C}_\Gamma)\mathbf{x} + \mathbf{B}_T\delta_T = \mathbf{0}. \tag{3.52}$$

Again using Eq. (3.19), this leads to the steady-state articulation angle for a given tractor steering

$$\Gamma = k_r\delta_T, \qquad k_r = -\mathbf{C}_\Gamma(\mathbf{A} + \mathbf{B}k_f\mathbf{C}_\Gamma)^{-1}\mathbf{B}_T. \tag{3.53}$$

Equations (3.50) and (3.53) can be used to design a two-degree-of-freedom controller to stabilize the steady state

$$\delta = k_f\Gamma_{\text{ref}} + k_b(\Gamma_{\text{ref}} - \Gamma), \tag{3.54}$$

where

$$\Gamma_{\text{ref}} = k_r\delta_T. \tag{3.55}$$

In this controller, k_r, Eq. (3.53), determines the steady state for the given tractor steering, which is used to define the articulation angle reference Γ_{ref}. The gain k_f, Eq. (3.51), is a feedforward controller designed to track the reference. The gain $k_b > 0$ is a feedback gain introduced to reject disturbances and to stabilize the system in the unstable equilibrium. Figure 3.7 illustrates the control architecture.
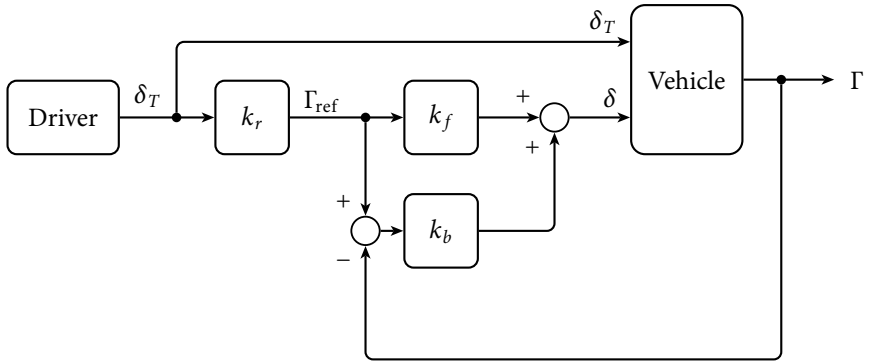
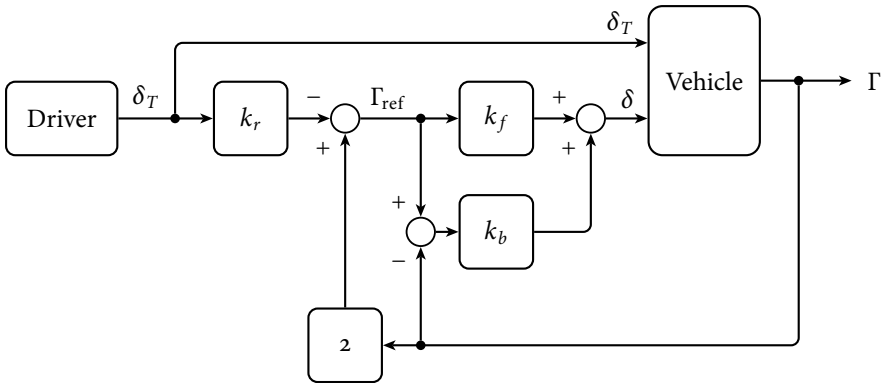**Figure 3.7:** Steady-state control. *Source: Alberding et al. (2013).*

Figure 3.8: Transient control. *Source: Alberding et al. (2013).*

3.2.2 Control during Transients

In the transient case, the driver intends to destabilize the vehicle and to leave the equilibrium. In theory, this could be achieved using the steady-state controller if the driver steers the vehicle like a single-unit vehicle. By steering into the direction of the desired yaw motion, the tractor steering would define the steady-state reference Eq. (3.55) for the articulation and the trailer steering. However, such tractor steering would push the articulation into the wrong direction. To compensate this effect, the trailer steering would need to have a higher control authority on the articulation than the tractor. In practice, this is not feasible.

As discussed in the beginning of this section, the driver instead needs to countersteer in the opposite direction of the desired articulation to initiate a transition. Thus,

the steady-state reference Eq. (3.55) cannot be applied. The actual reference demanded by the driver is in the exact opposite direction. This situation can be formulated into a reference definition by subtracting the difference between the steady-state articulation and the actual articulation from the actual articulation,

$$\Gamma_{\mathrm{ref}} = \Gamma - (k_r \delta_T - \Gamma) = 2\Gamma - k_r \delta_T, \tag{3.56}$$

yielding a control problem that destabilizes the articulation from its equilibria and thus supports a transition initiated by the driver. The stabilizing reference obtained by adding the difference yields the steady-state reference Eq. (3.55)

$$\Gamma_{\mathrm{ref}} = \Gamma + (k_r \delta_T - \Gamma) = k_r \delta_T. \tag{3.57}$$

The reference Eq. (3.56) can be passed to the two-degree-of-freedom controller Eq. (3.54). The feedback gain k_b can be chosen different from the steady-state controller. That control structure is shown in Fig. 3.8.

3.2.3 Integration

In principle, the transient controller could be used without being complemented by a steady-state control system. The inherent difficulty is the fact that the controller supports any deviation from an equilibrium, be it in or against the driver's interest. The vehicle would thus show a good response to the driver's actions, but it would also be difficult to stabilize.

This work thus proposes to switch the control action between the destabilizing transient mode and the stabilizing steady-state mode. The resulting control system is illustrated in Fig. 3.9.
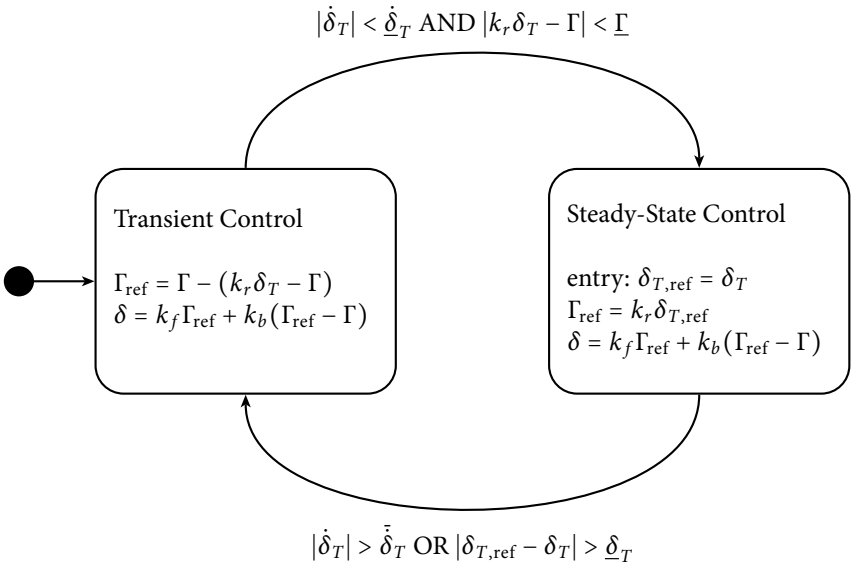
The steady-state controller determines the articulation reference Eq. (3.55) based on the tractor steering at the entry into the mode. This approach prevents an increased resistance if the driver changes the steering angle. Basing the reference on the actual steering angle would allow the driver to perform minor changes in the set-point. However, as discussed above, against the driver's intuitions such steering would need to be non-counter-steering like in a single-unit vehicle and would be very limited in range.

The switching is determined by the driver's actions and the vehicle's proximity to an equilibrium. The steady-state controller is activated if the tractor steering is almost constant,

$$|\dot{\delta}_T| < \underline{\dot{\delta}}_T, \tag{3.58a}$$

and if the vehicle is close to an equilibrium,

$$|k_r \delta_T - \Gamma| < \underline{\Gamma}. \tag{3.58b}$$

$$|\dot{\delta}_T| < \underline{\dot{\delta}}_T \text{ AND } |k_r\delta_T - \Gamma| < \underline{\Gamma}$$

Transient Control

$$\Gamma_{\text{ref}} = \Gamma - (k_r\delta_T - \Gamma)$$
$$\delta = k_f\Gamma_{\text{ref}} + k_b(\Gamma_{\text{ref}} - \Gamma)$$

Steady-State Control

entry: $\delta_{T,\text{ref}} = \delta_T$
$$\Gamma_{\text{ref}} = k_r\delta_{T,\text{ref}}$$
$$\delta = k_f\Gamma_{\text{ref}} + k_b(\Gamma_{\text{ref}} - \Gamma)$$

$$|\dot{\delta}_T| > \bar{\dot{\delta}}_T \text{ OR } |\delta_{T,\text{ref}} - \delta_T| > \underline{\delta}_T$$

Figure 3.9: Integrated control system. *Source: Alberding et al. (2013).*

The constants $\underline{\dot{\delta}}_T > 0$ and $\underline{\Gamma} > 0$ are thresholds on the time derivative of the tractor steering and the articulation angle, respectively.

The transient controller is activated if the tractor steering changes at a minimum rate,

$$|\dot{\delta}_T| > \bar{\dot{\delta}}_T, \tag{3.59a}$$

or if the tractor steering angle deviates too much from its value at the entry into the steady-state control mode,

$$|\delta_{T,\text{ref}} - \delta_T| > \underline{\delta}_T. \tag{3.59b}$$

Again, $\underline{\delta}_T > 0$ and $\bar{\dot{\delta}}_T > 0$ are suitable thresholds on the steering angle and its time derivative.

The controller thus requires information on the articulation angle, the driver steering angle, the time derivative of the driver steering, the vehicle speed, the direction of travel, and the suspension pressure. Speed and pressure measurements are commonly available and can be accessed on the semi-trailer Controller Area Network (CAN) bus. The direction of travel can be determined by the reversing light activity.

Sensors for the articulation angle are commercially available and are standard equipment in state-of-the-art electronically controlled semi-trailer steering systems. Information on the driver steering angle and its time derivative can be obtained from a steering wheel encoder. These signals are commonly available on a tractor in the CAN bus standard SAE J1939. The driver steering information needs to be made accessible on the semi-trailer to be processed by the steering control unit. Standards for the CAN bus communication between tractor and trailer are defined by ISO 11992. To date, these standards have been focused on the requirements of the Electronic Braking System (EBS), whereas the tractor steering generally is not included. This omission can be expected to change with a future amendment of the ISO 11992 standard. On present-day vehicles, the tractor steering measurement is not easily accessible from the trailer. As discussed in Section 3.1, an estimation of the tractor steering is feasible, but only at medium and high speeds. At walking speeds, which is within the intended operational region of the controller, a measurement cannot be avoided.
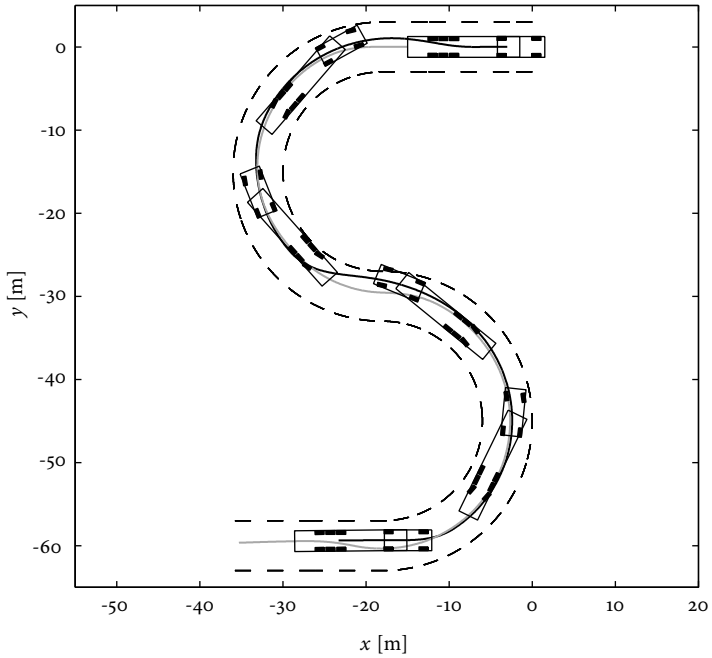
3.3 Simulation Results

The control system is tested using a detailed and validated multi-body simulation model of a tractor semi-trailer combination.

The human driver is simulated by a cascade controller, similarly to the approach described by Pradalier & Usher (2008) and the structure shown in Fig. 3.4. The outer controller is a proportional feedback gain on the lateral displacement from a predefined track with preview, generating a reference for the articulation angle. The inner controller tracks this reference using a two-degree-of-freedom architecture. A proportional feedback gain is complemented by a feedforward-like part based on Eq. (3.53),

$$\delta_T = k_r^{-1}\Gamma. \tag{3.60}$$

The controller takes into account limitations of the human senses by a threshold on the articulation control error (Macadam 2010). In addition to the steering, the driver controller maintains a pre-defined speed by using the throttle and the brakes of the vehicle.

The measured signals are the articulation angle, the tractor steering angle, the trailer speed, the direction of travel, and the summarized load of the trailer axles. The latter can be determined by the suspension pressure. The time derivative of the tractor steering is obtained by discrete-time numerical differentiation and a Finite Impulse Response (FIR) filter. All measurement data are subject to noise, resolution, and sampling properties based on common standard production sensors. Both trailer and tractor steering are subject to actuator limitations in terms of angle and rate. The low-level control dynamics of the trailer steering are represented by a low-pass filter. The control algorithm is operated at 200 Hz.
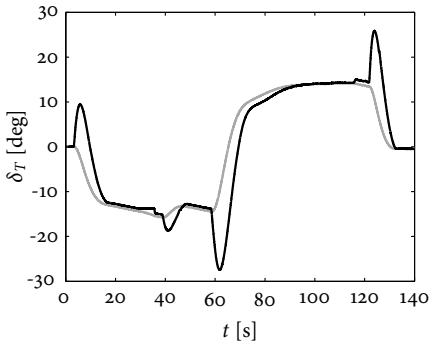
Figure 3.10: Simulation results for a conventional control system, steering proportionally to the articulation angle. The black solid line shows the path of the fifth wheel, the light line the path of the vehicle rear. *Source: Alberding et al. (2013).*
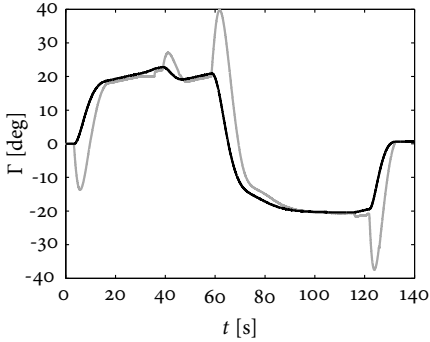
(a) Articulation angle. Black: measurement, light: model-based equilibrium associated to the tractor steering measurement, Eq. (3.53).
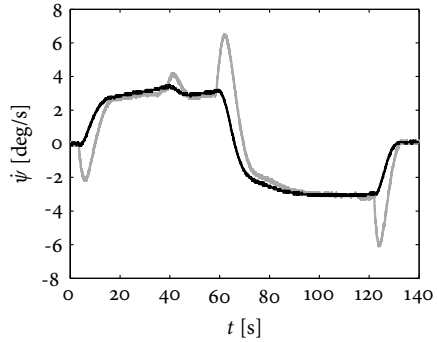
(b) Yaw rate. Black: semi-trailer measurement, light: tractor measurement.

(c) Tractor steering angle. Black: measurement, light: model-based value to maintain the articulation, Eq. (3.60).

(d) Semi-trailer steering angle.

Figure 3.11: Simulation results for a conventional control system, steering proportionally to the articulation angle. *Source: Alberding et al. (2013).*

Figure 3.12: Simulation results for the steering control of this work. The black solid line shows the path of the fifth wheel, the light line the path of the vehicle rear. *Source: Alberding et al. (2013).*
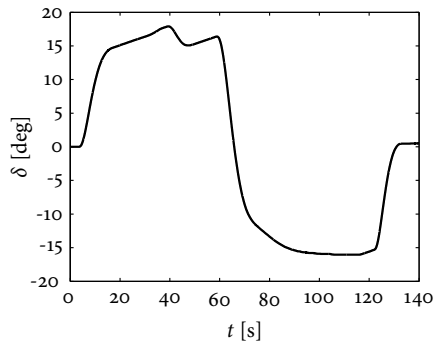
(a) Articulation angle. Black: measurement, light: model-based equilibrium associated to the tractor steering measurement, Eq. (3.53).

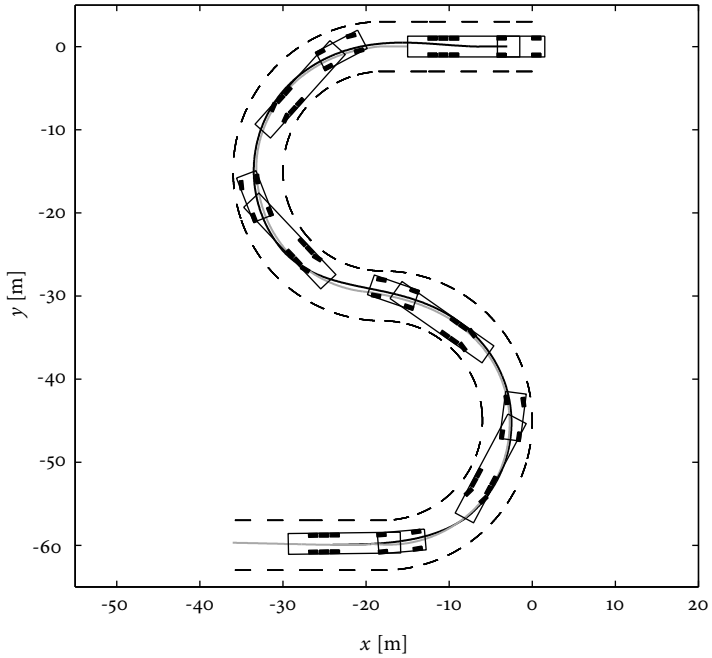**(b)** Yaw rate. Black: semi-trailer measurement, light: tractor measurement.
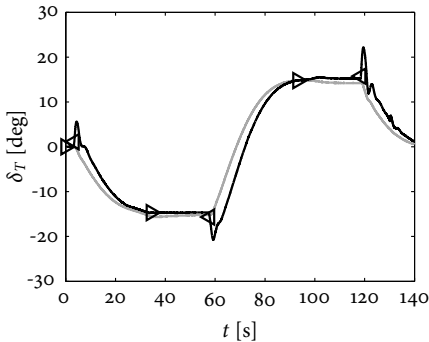
(c) Tractor steering angle. Black: measurement, light: model-based value to maintain the articulation, Eq. (3.60).
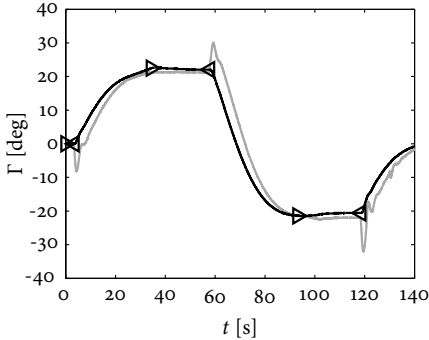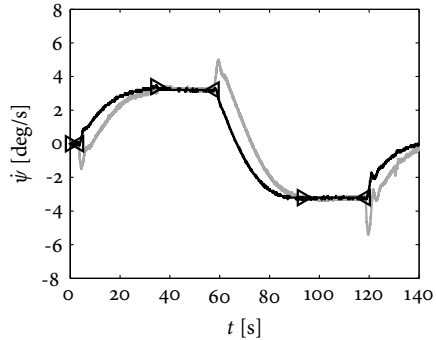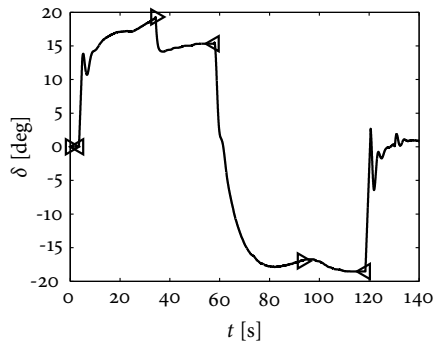
(d) Semi-trailer steering angle.

Figure 3.13: Simulation results for the steering controller developed in this work. In the intervals between the black triangles, the steady-state control is active. *Source: Alberding et al. (2013).*

The simulation scenario is an S-shaped double curve with a radius of 15 m at a speed of 3 km/h. The vehicle carries a load of 27,500 kg, yielding an axle load of 9000 kg at the trailer.

Figures 3.10 and 3.11 show the simulation results using a conventional control approach, steering proportionally to the articulation angle. The gain is obtained from Eq. (3.51), which eliminates the vehicle off-tracking in the steady state. The transients during entering, the change of direction, and leaving the curve show a significant off-tracking of up to 1.5 m. To initiate a transition, the driver needs to counter-steer up to 14°. In the steady state of the first curve, the driver needs to take a corrective action to stabilize the vehicle.

Figures 3.12 and 3.13 show the simulation results using the steering controller developed in this work. The off-tracking is eliminated in both the steady state and in the transient. The good transient behaviour can be attributed to the fast response of the trailer steering, which changes its sign ahead of the articulation angle. The counter-steering of the driver takes values of up to 6°, which is a reduction by more than 50 % compared to the conventional steering. The control system successfully detects the steady states and stabilizes the vehicle without any interventions by the driver. The automatic steering reduction between t =40 s and t =60 s resembles the shape of the manual correction by the driver in the conventional control scenario. With a precision of less than 1.5°, the model-based determination of the steady-state articulation proves to be sufficiently accurate.

4

Conclusions

This chapter is based on the author's manuscripts for the papers:

Alberding, M., Onder, C., Sager, F. & Guzzella, L. (in press), 'Variable caster steering', *IEEE Transactions on Vehicular Technology*. ©IEEE

Alberding, M., Vivaldelli, M., Sager, F. & Onder, C. (2013), Steering control of a semi-trailer in reverse travel, Manuscript submitted for publication.

The objective of this work was to contribute to two aspects of the steering of semi-trailers. First, the steering mechanism, second, the steering control.

4.1 Steering Mechanism

Chapter 2 presented the research on the steering mechanism and analysed the feasibility of improving the steering behaviour of a trailer self-steering system using a variable steering geometry.

The motivation was to overcome the performance limitations of passive trailer self-steering systems, without introducing any expensive high-power actuation hardware. The final objective was to realize a low-cost system that reaches the same performance levels as directly actuated steering systems, including the capability of reverse-travel steering and the controllability of the steering angle.

The caster angle has been identified as the most effective parameter in the steering geometry to control the steering. The only additional requirement compared to state-

of-the-art mechanisms that allow self-steering during reverse travel is to rotate the casters of both wheels independently. For a change of the direction of travel, both rotations need to be parallel to generate a positive caster. To influence the steering angle, they need to change opposite to each other. It is preferable, but not required, to adjust only the caster of the wheel that steers to the outside and to leave the second kingpin in its initial position.

Without a high-power actuation, the rotation can be obtained passively by introducing a spring-like element. The design of both linear and progressive springs has been discussed. The result is a passive steering system that amplifies the steering angle of conventional self-steering without any actuation, resembling the steering behaviour of directly actuated command steer systems and improving the low-speed performance of the vehicle. A locking mechanism can be used to allow a switching between amplified and conventional self-steering.

This passive steering amplification does not require any actuation forces. Optionally, a low-power electric or pneumatic actuation can be introduced to influence the steering selectively.

In a most consequent implementation of the ideas developed, the steering angle can be rendered completely controllable without any further actuation by a spring with adjustable stiffness.

The approach proposed can be translated into many different mechanical designs. Under the aspect of technical feasibility, the analysis of this work introduced a preliminary steering mechanism that is integrated into a state-of-the-art suspension. In such suspensions, the axle by design impedes an independent caster change. Thus, a re-design of the suspension, in particular the use of an independent wheel suspension, promises opportunities to find an economically more competitive solution.

The concept has been successfully validated in a multi-body simulation environment, both during forward and reverse travel. A steering amplification has been shown to substantially improve the low-speed performance compared to conventional self-steering. The technical feasibility has been investigated in vehicle experiments using a simple demonstrator based on a standard production self-steering axle.

In its present form, the approach has mainly three limitations and challenges for an optimized design. First, since it takes advantage of the self-steering principle, it inherits its insufficient high-speed performance. Second, braking forces generate a disturbance that is directed to increase the steering angle. Third, if the spring stiffness is not adjustable, the passive steering amplification decreases with the mass loaded.

This work provided a description of the system structure, a comprehensive assessment of its properties and limitations using simulation experiments, and an investigation of the technical feasibility in first vehicle experiments. Future work should continue to test the steering in vehicle experiments and develop an optimized mechanical design. Furthermore, possible applications beyond trailer steering should be investigated, such as non-driven pusher and tag truck axles.

4.2 Steering Control

Chapter 3 presented the research on steering control and introduced a novel approach for the steering control of a semi-trailer in reverse travel, with the objective to optimally assist a human driver.

The control system presented operates in two modes which are activated based on the driver's steering actions at the tractor, namely one to stabilize the articulation angle and one to change it. The objective is to obtain a fast response to a change of direction as well as a good stability during straight-ahead travel and constant cornering.

The control system was tested using a validated multi-body simulation model. Compared to a conventional control approach that steers proportionally to the articulation angle, both the off-tracking of the vehicle in the transient and the steering effort of the driver were reduced substantially. The system requires information on the articulation angle, the tractor steering angle, the time derivative of the tractor steering, the vehicle speed, the reversing light, and the semi-trailer suspension pressure. The control algorithm is computationally efficient and suitable for low-cost automotive electronic control units.

For the control design, a time-variant linear model of the vehicle dynamics was derived. The model was validated using measurement data obtained from vehicle experiments. Based on the model, a state estimator in the form of a discrete-time Kalman filter was designed and used to estimate the tractor steering and the articulation angle. It was tested using measurement data obtained from vehicle experiments, providing good results at medium and high speeds. At walking speeds, the experiments showed that a reliable estimation is not feasible. For the controller developed in this work, the need for measurements of the tractor steering and the articulation angle thus cannot be avoided. Since to date, by default a tractor steering measurement is not accessible from the trailer, this requirement is an obstacle for the implementation of this controller. The inclusion of the tractor steering measurement in a future amendment of the ISO 11992 standard for the CAN communication between the tractor and the trailer would solve this problem.

Future work is to test the control system in vehicle experiments. Based on the results of these experiments and the feedback provided by the test drivers, the detection of and the response to the driver's intentions can be refined. The tyre saturation could be included in the model. Finally, a more detailed nonlinear model and more advanced estimation techniques could investigate an approach to reliably estimate the tractor steering at walking speeds.

Bibliography

Ahn, C.-S. (2007), 'A stabilizer having adjustable rigidity', Patent KR100767511B B1.

Aïoun, F., Heniche, A. & Bourlès, H. (1994), Maximally-diagonal solution to the inverse LQR problem, *in* 'Proc. Conf. on Decision and Control', Lake Buena Vista, FL, USA.

Alberding, M., Onder, C., Sager, F. & Guzzella, L. (in press), 'Variable caster steering', *IEEE Transactions on Vehicular Technology*.

Alberding, M., Vivaldelli, M., Sager, F. & Onder, C. (2013), Steering control of a semi-trailer in reverse travel. Manuscript submitted for publication.

Altafini, C., Speranzon, A. & Wahlberg, B. (2001), 'A feedback control scheme for reversing a truck and trailer vehicle', *IEEE Transactions on Robotics and Automation* **17**(6), 915–922.

Aurell, J. & Edlund, S. (1989), 'The influence of steered axles on the dynamic stability of heavy vehicles', *SAE Technical Paper 892498*.

Bushnell, L., Tilbury, D. & Sastry, S. (1995), 'Steering three-input nonholonomic systems: The fire truck example', *The International Journal of Robotics Research* **14**(4), 366–381.

Chalin, T. (2001), 'Reversible caster steerable suspension system', Patent US6182984 B1.

Chen, B. & Peng, H. (2005), 'Rollover warning for articulated heavy vehicles based on a time-to-rollover metric', *Transactions of the ASME–Journal of Dynamic Systems, Measurement, and Control* **127**, 406–414.

Chen, C. & Tomizuka, M. (2000), 'Lateral control of commercial heavy vehicles', *Vehicle System Dynamics* **33**(6), 391–420.

Chen, H. & Velinsky, S. (1992), 'Designing articulated vehicles for low-speed maneuverability', *Journal of Transportation Engineering* **118**(5), 711–728.

Cheng, C. & Cebon, D. (2008), 'Improving roll stability of articulated heavy vehicles using active semi-trailer steering', *Vehicle System Dynamics* **46**(sup1), 373–388.

Cheng, C. & Cebon, D. (2011), 'Parameter and state estimation for articulated heavy vehicles', *Vehicle System Dynamics* **49**(1–2), 399–418.

Cheng, C., Roebuck, R., Odhams, A. & Cebon, D. (2011), 'High-speed optimal steering of a tractor-semitrailer', *Vehicle System Dynamics* **49**(49), 561–593.

Clark, S. K., ed. (1981), *Mechanics of Pneumatic Tires*, U.S. Department of Transportation, National Highway Traffic Safety Administration.

Cole, D., Pick, A. & Odhams, A. (2006), 'Predictive and linear quadratic methods for potential application to modelling driver steering control', *Vehicle System Dynamics* **44**(3), 259–284.

Coleman, B. & Sweatman, P. (2002), Steerable axles to improve productivity and access, Technical report, National Road Transport Commission, Melbourne, Australia.

Dahlberg, E. (2001), Commercial Vehicle Stability – Focusing on Rollover, PhD thesis, KTH Stockholm, Sweden.

Dahlberg, E. & Stensson, A. (2006), 'The dynamic rollover threshold – a heavy truck sensitivity study', *Int. Journal of Vehicle Design* **40**(1–3), 228–251.

Evers, W.-J., Besselink, I., Teerhuis, A. & Nijmeijer, H. (2011), 'On the achievable performance using variable geometry active secondary suspension systems in commercial vehicles', *Vehicle System Dynamics* **49**(10), 1553–1573.

Fancher, P., Ervin, R., Winkler, C. & Gillespie, T. (1986), A factbook of the mechanical properties of the components for single-unit and articulated heavy trucks, Technical Report UMTRI-86-12, University of Michigan Transportation Research Institute, Ann Arbor, MI, USA.

Fancher, P. & Mathew, A. (1987), A vehicle dynamics handbook for single-unit and articulated heavy trucks, Technical Report UMTRI-87-27, University of Michigan Transportation Research Institute, Ann Arbor, MI, USA.

Fancher, P. & Winkler, C. (2007), 'Directional performance issues in evaluation and design of articulated heavy vehicles', *Vehicle System Dynamics* **45**(7–8), 607–647.

Fletcher, C., Manzie, C. & Good, M. (2006), Trailer steering: An Australian research perspective and application for by-wire control, *in* 'Proc. 9th International Symposium on Heavy Vehicle Weights and Dimensions', University Park, PA, USA.

Fu, T.-T. & Cebon, D. (2003), 'Economic evaluation and the design of vehicle suspensions', *Int. J. of Vehicle Design* **31**(2), 125–161.

Gaspar, P., Szaszi, I. & Bokor, J. (2005), 'Reconfigurable control structure to prevent the rollover of heavy vehicles', *Control Engineering Practice* **13**(6), 699–711.

Gonzales-Cantos, A. & Ollero, A. (2009), 'Backing-up maneuvers of autonomous tractor-trailer vehicles using the qualitative theory of nonlinear dynamical systems', *International Journal of Robotics Research* **28**(1), 49–65.

Goodarzi, A., Oloomi, E. & Esmailzadeh, E. (2011), 'Design and analysis of an intelligent controller for active geometry suspension systems', *Vehicle System Dynamics* **49**(1–2), 333–359.

Gottschalk, M. & Jablonski, K. (2001), 'Self-steering, caster-adjustable suspension system', Patent US6293570 B1.

Heißing, B., Ersoy, M. & Gies, S., eds (2011), *Fahrwerkhandbuch*, Vieweg+Teubner.

Hirschberg, W., Rill, G. & Weinfurter, H. (2007), 'Tire model TMeasy', *Vehicle System Dynamics* **45**(sup1), 101–119.

Hoepke, E. & Breuer, S., eds (2006), *Nutzfahrzeugtechnik*, Vieweg+Teubner.

Hussain, K., Stein, W. & Day, A. (2005), 'Modelling commercial vehicle handling and rolling stability', *Proc. IMechE Part K: J. Multi-body Dynamics* **219**, 357–369.

Hyun, D. & Langari, R. (2003), 'Modeling to predict rollover threat of tractor-semitrailers', *Vehicle System Dynamics* **39**(6), 401–414.

Imine, H., Fridman, L. & Madani, T. (2012), 'Steering control for rollover avoidance of heavy vehicles', *IEEE Transactions on Vehicular Technology* **61**(8), 3499–3509.

Isermann, R., ed. (2006), *Fahrdynamik-Regelung*, Vieweg+Teubner.

Ivanov, R. & Liubenov, S. (1995), 'Possibilities for reduction of tyre wear through the design parameters of the steering axle', *Proc. IMechE Part D: J. Automobile Engineering* **209**(2), 111–115.

Jazar, R., Subic, A. & Zhang, N. (2012), 'Kinematics of a smart variable caster mechanism of a vehicle steerable wheel', *Vehicle System Dynamics* **50**(12), 1861–1875.

Jeppesen, B. & Cebon, D. (2009), 'Application of observer-based fault detection in vehicle roll control', *Vehicle System Dynamics* **47**(4), 465–495.

Jujnovich, B. & Cebon, D. (2002), Comparative performance of semi-trailer steering systems, *in* 'Proc. 7th International Symposium on Heavy Vehicle Weights and Dimensions', Delft, The Netherlands.

Jujnovich, B. & Cebon, D. (2013), 'Path-following steering control for articulated vehicles', *Transactions of the ASME–Journal of Dynamic Systems, Measurement, and Control* **135**, 031006.

Kalman, R. (1960), 'A new approach to linear filtering and prediction problems', *Transactions of the ASME–Journal of Basic Engineering* **82**(Series D), 35–45.

Kharrazi, S., Lidberg, M., Lingman, P., Svensson, J.-I. & Dela, N. (2008), 'The effectiveness of rear axle steering on the yaw stability and responsiveness of a heavy truck', *Vehicle System Dynamics* **46**(1), 365–372.

Kiencke, U. & Nielsen, L. (2000), *Automotive Control Systems*, Springer.

Knight, I., Robinson, T., Robinson, B., Barlow, T., McCrae, I., Odhams, A., Roebuck, R. & Cheng, C. (2010), The likely effects of permitting longer semi-trailers in the UK: vehicle specification performance and safety, Technical Report PPR526, Transport Research Laboratory, UK.

Kong, S. & Kosko, B. (1992), 'Adaptive fuzzy-systems for backing up a truck-and-trailer', *IEEE Transactions on Neural Networks* **3**(2), 211–223.

LeBlanc, P., El-Gindy, M. & Woodrooffe, J. (1989), 'Self-steering axles: Theory and practice', *SAE Technical Paper 891633*.

Lee, S., Lee, U. & Han, C. (2001), 'Enhancement of vehicle handling characteristics by suspension kinematic control', *Proc. IMechE Part D: J. Automobile Engineering* **215**(2), 197–216.

Lee, U., Lee, S., Han, C., Hedrick, K. & Català, A. (2008), 'Active geometry control suspension system for the enhancement of vehicle stability', *Proc. IMechE Part D: J. Automobile Engineering* **222**(6), 979–988.

Lin, R. & Cebon, D. (1996), 'Active roll control of articulated vehicles', *Vehicle System Dynamics* **26**(1), 17–43.

Macadam, C. (2010), 'Understanding and modeling the human driver', *Vehicle System Dynamics* **40**(1–3), 101–134.

Martínez, J., Morales, J., Mandow, A. & García-Cerezo, A. (2008), 'Steering limitations for a vehicle pulling passive trailers', *IEEE Transactions on Control Systems Technology* **16**(4), 809–818.

Matschinsky, W. (2007), *Radführungen der Straßenfahrzeuge*, Springer.

Matsushita, K. & Murukami, T. (2008), 'Nonholonomic equivalent disturbance based backward motion control of tractor-trailer with virtual steering', *IEEE Transactions on Industrial Electronics* **55**(1), 280–287.

Miege, A. & Cebon, D. (2005*a*), 'Active roll control of an experimental articulated vehicle', *Proc. IMechE Part D: J. Automobile Engineering* **219**(6), 791–806.

Miege, A. & Cebon, D. (2005*b*), 'Optimal roll control of an articulated heavy vehicle: theory and model validation', *Vehicle System Dynamics* **43**(12), 867–884.

Mitschke, M. & Wallentowitz, H., eds (2004), *Dynamik der Kraftfahrzeuge*, Springer.

Moon, K.-H., Lee, S.-H., Chang, S., Mok, J.-K. & Park, T.-W. (2009), 'Method for control of steering angles for articulated vehicles using virtual rigid axles', *International Journal of Automotive Technology* **10**(4), 441–449.

Morales, J., Martínez, J., Mandow, A. & García-Cerezo, A. (2013), 'Steering the last trailer as a virtual tractor for reversing vehicles with passive on- and off-axle hitches', *IEEE Transactions on Industrial Electronics* **60**(12), 5729–5736.

Németh, B. & Gáspár, P. (2011), Enhancement of vehicle stability based on variable geometry suspension and robust LPV control, *in* 'Proc. IEEE/ASME International Conference on Advanced Intelligent Mechatronics', Budapest, Hungary.

Ochner, P. (1959), 'Der Einfluß von Nachlauf, Spreizung, Sturz und Vorspur auf die Kinematik von Achsschenkellenkungen', *Deutsche Kraftfahrtforschung und Straßenverkehrstechnik* **123**, 1–29.

Odenthal, D., Bünte, T. & Ackermann, J. (1999), Nonlinear steering and braking control for vehicle rollover avoidance, *in* 'Proc. European Control Conference', Karlsruhe, Germany.

Odhams, A., Roebuck, R., Cebon, D. & Winkler, C. (2008), 'Dynamic safety of active trailer steering systems', *Proc. IMechE Part K: J. Multi-body Dynamics* **222**(4), 367–380.

Odhams, A., Roebuck, R., Jujnovich, B. & Cebon, D. (2011), 'Active steering of a tractor–semi-trailer', *Proc. IMechE Part D: J. Automobile Engineering* **225**(7), 847–869.

Pacejka, H. B. (2006), *Tire and Vehicle Dynamics*, Elsevier.

Palkovics, L. & El-Gindy, M. (1996), 'Examination of different control strategies of heavy-vehicle performance', *Transactions of the ASME–Journal of Dynamic Systems, Measurement, and Control* **118**, 459–498.

Palkovics, L. & Fries, A. (2001), 'Intelligent electronic systems in commercial vehicles for enhanced traffic safety', *Vehicle System Dynamics* **35**(4–5), 227–289.

Percy, A. & Spark, I. (2013), 'A numerical control algorithm for a b-double truck-trailer with steerable trailer wheels and active hitch angles', *Proc. IMechE Part D: J. Automobile Engineering* **227**(6), 899–904.

Popp, K. & Schiehlen, W. (2010), *Ground Vehicle Dynamics*, Springer.

Pradalier, C. & Usher, K. (2008), 'Robust trajectory tracking for a reversing tractor trailer', *Journal of Field Robotics* **25**(6–7), 378–399.

Provencher, Y. (1989), The effect of undercarriage configuration on tractor-trailer performance, Technical report, Forest Engineering Research Institute of Canada, Pointe Claire, Quebec, Canada.

Qu, Q. & Zu, J. (2008), 'On steering control of commercial three-axle vehicle', *Transactions of the ASME–Journal of Dynamic Systems, Measurement, and Control* **130**, 021010.

Rangavajhula, K. & Tsao, H.-S. (2007), 'Active trailer steering control of an articulated system with a tractor and three full trailers for tractor-track following', *Int. J. Heavy Vehicle Systems* **14**(3), 271–293.

Rödönyi, G., Gáspár, P. & Bokor, J. (2011), 'The emergency steering of a heavy truck by front-wheel braking', *Int. J. Heavy Vehicle Systems* **18**(2), 135–160.

Reimpell, J. & Betzler, J. (2005), *Fahrwerktechnik: Grundlagen*, Vogel.

Rhein, B. (2005), *Fahrwerksysteme gezogener Fahrzeuge*, sv corporate media.

Roebuck, R., Cebon, D., Jeppesen, B. & Haque, J. (2005), 'A systems approach to controlled heavy vehicle suspensions', *Int. J. Heavy Vehicle Systems* **12**(3), 169–192.

Ryu, J.-C., Agrawal, S. & Franch, J. (2008), 'Motion planning and control of a tractor with a steerable trailer using differential flatness', *Journal of Computational and Nonlinear Dynamics* **3**(3), 031003.

Salaani, M. (2009), 'The application of understeer gradient in stability analysis of articulated vehicles', *Int. J. Heavy Vehicle Systems* **16**(1–2), 3–25.

Sampei, M., Tamura, T., Kobayashi, T. & Shibui, N. (1995), 'Arbitrary path tracking control of articulated vehicles using nonlinear control theory', *IEEE Transactions on Control Systems Technology* **3**(1), 125–131.

Sampson, D. (2000), Active Roll Control of Articulated Heavy Vehicles, PhD thesis, Cambridge University, UK.

Sampson, D. & Cebon, D. (2003), 'Achievable roll stability of heavy road vehicles', *Proc. IMechE Part D: J. Automobile Engineering* **217**(4), 269–287.

Sankar, S., Rakheja, S. & Piché, A. (1991), 'Directional dynamics of a tractor-semitrailer with self- and forced-steering axles', *SAE Technical Paper 912686*.

Segel, L., Ervin, R. D. & Fancher, P. S. (1981), *The Mechanics of Heavy-Duty Trucks and Truck Combinations*, International Association for Vehicle Design.

Sharp, R., Casanova, D. & Symonds, P. (2000), 'A mathematical model for driver steering control, with design, tuning and performance results', *Vehicle System Dynamics* **33**(5), 289–326.

Stone, E. & Cebon, D. (2010), 'Control of semi-active anti-roll systems on heavy vehicles', *Vehicle System Dynamics* **48**(10), 1215–1243.

Tanaka, K., Kenji, Y. & Hiroshi, O. (2009), 'Sensor reduction for backing-up control of a vehicle with triple trailers', *IEEE Transactions on Industrial Electronics* **56**(2), 497–509.

Tanaka, K., Kosaki, T. & Wang, H. (1998), 'Backing control problem of a mobile robot with multiple trailers: Fuzzy modeling and lmi-based design', *IEEE Transactions on Systems, Man, and Cybernetics* **28**(3), 329–337.

Tanaka, K. & Sano, M. (1994), 'A robust stabilization problem of fuzzy control-systems and its application to backing up control of a truck-trailer', *IEEE Transactions on Fuzzy Systems* **2**(2), 119–134.

Tanaka, K., Taniguchi, T. & Wang, H. (1997), 'Fuzzy controller and observer design for backing control of a trailer-truck', *Engineering Applications of Artificial Intelligence* **10**(5), 441–452.

Tilbury, D., Sørdalen, O., Bushnell, L. & Sastry, S. (1995), 'A multisteering trailer system: Conversion into chained form using dynamic feedback', *IEEE Transactions on Robotics and Automation* **11**(6), 807–818.

Walsh, G., Tilbury, D. & Sastry, S. (1994), 'Stabilization of trajectories for systems with nonholonomic constraints', *IEEE Transactions on Automatic Control* **39**(1), 216–222.

Wang, Y. & Cartmell, M. (1998), 'Trajectory generation for a four wheel steering tractor-trailer system: A two-step method', *Robotica* **16**(4), 381–386.

Watanabe, Y. & Sharp, R. (1999), 'Mechanical and control design of a variable geometry active suspension system', *Vehicle System Dynamics* **32**(1), 217–235.

Welch, G. & Bishop, G. (1995), An introduction to the kalman filter, Technical Report TR 95-041, University of North Carolina at Chapel Hill, Chapel Hill, NC, USA.

Wideberg, J. & Dahlberg, E. (2009), 'A comparative study of legislation and stability measures of heavy articulated vehicles in different regions', *Int. J. Heavy Vehicle Systems* **16**(3), 354–361.

Williams, D. (2010), 'Handling benefits of steering a third axle', *Proc. IMechE Part D: J. Automobile Engineering* **224**(D12), 1501–1511.

Williams, D. (2011), 'On the equivalent wheelbase of a three-axle vehicle', *Vehicle System Dynamics* **49**(9), 1521–1532.

Wong, J. Y. (2008), *Theory of Ground Vehicles*, John Wiley.

Wu, D. & Hai, J. (2003), 'Analysis of dynamic lateral response for multi-axle-steering tractor and trailer', *Int. J. Heavy Vehicle Systems* **10**(4), 281–294.

Yu, H., Güvenç, L. & Özgüner, U. (2008), 'Heavy duty vehicle rollover detection and active roll control', *Vehicle System Dynamics* **46**(6), 451–470.

Zobel, D. (2003), 'Trajectory segmentation for the autonomous control of backward motion for truck and trailer', *IEEE Transactions on Intelligent Transportation Systems* **4**(2), 59–66.